IN VIVO DETECTION OF RETAINED GADOLINIUM IN BONE BY X-RAY FLUORESCENCE

IN VIVO DETECTION OF RETAINED GADOLINIUM IN BONE BY X-RAY FLUORESCENCE FOLLOWING ADMINISTRATION OF GADOLINIUM-BASED CONTRAST AGENTS USED IN MRI

By

MICHELLE L. LORD,
B.Sc.

A Thesis
Submitted to the School of Graduate Studies
in Partial Fulfillment of the Requirements
for the Degree
Doctor of Philosophy

McMaster University

DOCTOR OF PHILOSOPHY (2019) McMaster University
(Medical Physics) Hamilton, Ontario

TITLE: In vivo detection of retained gadolinium in bone by x-ray fluorescence following administration of gadolinium-based contrast agents used in MRI

AUTHOR: Michelle L. Lord, (University of Western Ontario)

SUPERVISOR: Dr. David Chettle, Dr. Fiona McNeill

NUMBER OF PAGES: xvi, 138

Abstract

Gadolinium-based contrast agents (GBCAs) have been used in hospitals worldwide for the past three decades to increase contrast for magnetic resonance imaging (MRI), thus allowing for more accurate diagnoses. When first developed, GBCA complexes were thought to be completely stable, and excreted from the body within hours. However, GBCAs have since been shown to deposit in organs such as bone, suggesting complex dissociation. GBCA safety has now become one of the biggest concerns in the field of radiology, with the clinical implications of retained Gd remaining unknown. A non-invasive technique to measure retained Gd in the body would allow for investigation of the potential negative health effects of GBCAs.

In this thesis, the technique of x-ray fluorescence (XRF) to detect retained gadolinium (Gd) in bone following the administration of GBCAs is investigated. The research employs a series of bone phantom measurements to determine the feasibility of using an XRF-based detection system to perform non-invasive *in vivo* measurements of Gd in human tibia bones. Minimum detection limits (MDLs) of the XRF detection system are calculated to assess the feasibility of performing a human measurement in a realistic time. Through these experiments, the XRF detection system developed in this thesis work is deemed feasible for human measurements of Gd in bone.

The second half of this thesis work involves performing the first non-invasive measurements of Gd in bone in a small population: 11 exposed individuals who had previously received GBCA, and 11 controls. The result of this work is promising, as the XRF system is successful in measuring Gd in bone *in vivo*. Additionally, the Gd bone concentration of the exposed group is significantly higher than the control group. Following this small pilot study, additional measurements are conducted on individuals self-reporting symptoms of Gd toxicity. Gd concentrations in bone and urine are compared for three groups: symptomatic exposed, non-symptomatic exposed, and control. The concentration of Gd in bone and urine for the symptomatic exposed group is significantly higher. However, there is no correlation between the amount of Gd in bone and urine, suggesting a secondary storage site for Gd in the body, other than bone.

Preface

This is a "sandwich" thesis based on the papers published during my PhD. Chapter 1 serves as both a clinical and technical introduction, where key concepts are discussed to allow the reader to understand the published papers presented in this thesis. Chapter 2 provides supplementary information for the experimental methods that were not included in the published papers due to journal length restrictions. In this chapter, detailed protocol and calculations are explained to assist those wanting to replicate the work completed in this thesis. Chapters 3-7 present the five published papers of this thesis work. Each paper is prefaced with a summary and description of contributions. Lastly, the final chapter of this thesis presents a summary of conclusions from the published papers and incorporates them into a general overview of Gd retention in the body. Additionally, future avenues of research are discussed in this chapter.

Acknowledgements

The past four-and-a-half years of my PhD at McMaster have been a fantastic journey, where I have grown both as a researcher and a person. The work I accomplished in my graduate studies is something I once thought I could never achieve. At the same time, there are a few key people who supported me along the way. Without their encouragement, this thesis would not have been possible.

First off, I would like to extend my gratitude to my two supervisors David Chettle and Fiona McNeill. I could not have asked for more supportive and encouraging supervisors to have by my side. They saw the potential in me that I never saw, and pushed me to transfer from my Masters to PhD. Without their reassurance, this thesis would most likely be for the fulfilment of a Masters degree, rather than a PhD. Thank you to David, who no matter how busy he was, always made time to meet with me and read over my work. Thank you to Fiona, who spent hours with me in the lab trying to troubleshoot equipment that would seem to fix itself simply by her being present. Thank you to my committee Soo Hyun Byun, James Gräfe, and Mike Noseworthy for always making time to meet with me and providing their expertise throughout this thesis work.

Thank you to all of my colleagues in the Radiation Sciences Graduate Program, who made life as a graduate student continuously fun and interesting. To my office mates, who wrapped every single belonging of mine in aluminum foil while I was away at a conference, I forgive you. Thanks to Tony Marrone and Justin Bennett for their technical expertise and daily entertainment, Mike Inskip for his advice and assistance with producing phantoms, and Fiona Ahlang for her administrative help over the past few years.

To my ballet teachers Evgenia and Irina, ballet provided me with an escape from everyday life and provided me with the balance I needed. I am forever grateful for the amazing experience of being in your ballet classes while at McMaster, and will continue dancing for as long as I can.

I would have never reached this point without the encouragement from my family. Thank you to my sisters, Erica and Allison, who have been my personal cheer team throughout this journey. Thank you to my mom and dad who were always there for me and supported every decision I made.

Finally, thank you to the most important person in my life, my husband, Raffi. I am so grateful to have someone in my life who gives me unwavering support and cares for my well-being. Living with a chronic disease that requires attention 24/7 and being in graduate school at the same time is quite challenging, and I could not have done both without your help. I cannot wait to start our lives together!

Contents

List of Figures

Chapter 1

Introduction

1.1 Gadolinium

Gadolinium (Gd) is a silvery-white rare earth metal with an atomic number of 64, and an atomic mass of approximately 157 amu. Gd is classified as a lanthanide, located in period 6 of the periodic table. In nature, Gd is found in oxidized form with an oxidation state of +3, forming Gd(III) compounds with most elements [2,3]. Gd is an excellent neutron absorber, as it has the largest thermal neutron capture cross section of all the stable elements [4]. The large neutron capture cross sections of Gd-157 and Gd-155 enable Gd to be an excellent candidate for detection through neutron activation analysis: a trace element analysis technique that uses neutrons to excite elements present in a bulk sample and detect the resultant radioactive emissions [5–7]. The large neutron capture cross section of Gd also makes it a useful element for neutron radiography [8], and neutron therapy for cancer [9].

Due to its 7 unpaired electrons in the $4f$ orbitals, Gd has strong paramagentic properties, which causes it to alter proton relaxation times when present in tissue during magnetic resonance imaging (MRI) (Figure 1.1) [10]. In MRI for diagnostic purposes, the differentiation of tissues is defined by the difference in relaxation times, either longitudinal relaxation (T1) or transverse relaxation (T2). It is the differences in these relaxation times that create the contrast between healthy and diseased tissue, allowing for more accurate diagnoses with the use of paramagnetic contrast agents

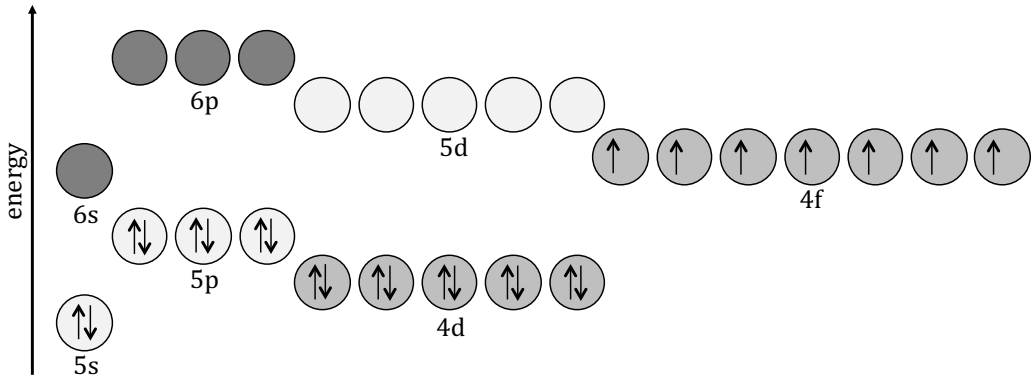

Figure 1.1: Electron configuration of Gd^{3+}. The 7 unpaired electrons in the $4f$ orbitals lead to the strong paramagnetic properties of Gd^{3+}.

such as Gd [11–13]. The paramagentism of Gd has the strongest effect on the T1 relaxation time (longitudinal relaxation), shortening the time of recovery of magnetization along the +z axis after a 90^o radiofrequency pulse is applied. Longitudinal relaxation, also known as spin-lattice relaxation, is the result of interactions between the nuclear magnetic dipoles and dipole-dipole interactions from randomly fluctuating magnetic fields between atoms. The magnetic moment of an unpaired electron is approximately 1000 times stronger than the magnetic moment of a nucleus. Therefore, the addition of 7 unpaired electrons in Gd increases the dipole-dipole interactions in the lattice, leading to a faster rate of relaxation, thus a greater contrast between healthy and diseased tissue. [14, 15]

Alternative paramagnetic elements have been investigated as possible contrast agents for altering relaxation times in MRI. However, many of these elements are not suitable, as they are either toxic *in vivo*, or easily lose their paramagnetic properties through reactions in the body. The ideal contrast agent for MRI should be a compound that is non-toxic, has a strong paramagnetic effect, remains stable in the body, and has a tissue-specific distribution (i.e. accumulates in tumour tissue). As already discussed, the large number of unpaired electrons makes Gd possess the strongest relaxation effect compared to other rare earth elements [16]. However, Gd ions (Gd^{3+}) are highly toxic in the body if in their free form.

Gd^{3+} is a competitive inhibitor with Ca^{2+}, due to their similar atomic radii. This causes Gd^{3+} to hinder important biological components in the body such as voltage-gated calcium channels in cell membranes, which are responsible for contraction of muscle and transmission of nerve impulses [3, 17]. In addition to hindering essential biological processes in the body, Gd^{3+} binds to hydroxides and phosphates in blood and can be taken up by the liver [18]. To prevent toxic effects in the body, free gadolinium is bound to a ligand, such as EDTA (ethylenediaminetetraacetic acid) or DTPA (diethylenetriaminepentaacetic acid), to form a stable chelate. The classes and properties of these chelates will be discussed further in section 1.1.1.

In the case of MRI for diagnostic purposes, the tissue specific distribution of a contrast agent often refers to the extent to which contrast agent accumulates in a tumour. Tumour tissue is physiologically different from healthy tissue with respect to the vasculature. Tumour tissue allows for the permeability of larger molecules compared to healthy tissue, and therefore, will uptake more contrast agent [19].

Since Gd has strong paramagnetic properties, is assumed to be non-toxic and stable in chelate form, and accumulates in tumour tissue, it has been the most widely explored element for improving contrast and image quality for diagnostic MRI. This thesis work focuses on Gd^{3+} bound to ligands to create chelates, which are referred to as gadolinium-based contrast agents (GBCAs). Exploring the safety of GBCAs is the purpose of this thesis work.

1.1.1 Gadolinium-based contrast agents

MRI is a powerful tool in diagnostic imaging because of its ability to create detailed spatial images without the use of ionizing radiation. As mentioned in section 1.1, the contrast between tissues in MRI is created from the differences in relaxation times of protons after a radiofrequency pulse is applied. Therefore, GBCAs are administered to assist in differentiating between healthy and diseased tissue. For T1 weighted images, GBCA accumulated within tumour tissue will cause the relaxation time of the protons in the tumour to shorten, essentially causing the tumour to "light up" on the

acquired image [10].

The effectiveness of GBCAs for diagnoses has driven their widespread use in hospitals world-wide. Since their initial introduction in the early 1980's, GBCAs have been administered in over 450 million doses [20]. When gadolinium was first introduced as a potential contrast agent for MRI, it was incorporated into a chelate ligand to avoid the toxic effects of free Gd. These water-soluable Gd chelates (i.e. GBCAs) were initially thought to be completely stable in the body, and to be excreted in the urine within hours of administration [16,21]. However, early evidence of Gd retention in the body suggested that Gd chelates were not stable, dissociating in the body, rather than being excreted [22, 23].

At the time of this thesis work, there are 9 FDA-approved varieties of GBCAs available for clinical use [20]. Each variety of GBCA can be described by: chelate class (linear or macrocyclic), charge (ionic or non-ionic), and *in vivo* stability (kinetic and thermal). The chelate class describes the molecular structure to which the Gd^{3+} ion is bound. Linear chelate ligands are long organic molecules that wrap around Gd^{3+}, where macrocyclic chelate ligands have a molecular ring which encloses Gd^{3+} in a cage-like structure, creating tighter bonds compared to the linear ligands. The charge of GBCAs is either described as ionic, where the complex has an overall charge, or non-ionic, where the complex is neutral [24–27]

The stability of GBCAs in the human body has been thoroughly investigated in multiple studies, including animal studies [28,29], *in vitro* [30,31], and *in vivo* human studies [32–35]. From these studies, a significant difference in stability was found between GBCAs, suggesting that certain complexes are more likely to dissociate in the body. The stability of a chelate is described by thermal stability: the energy required to break the bonds between Gd^{3+} and the chelate ligand, and kinetic stability: the rate at which GBCAs dissociate [26,36]. In general, macrocyclic GBCAs tend to have higher thermal and kinetic stabilities compared to linear GBCAs [26, 37]. However, differences in stability exist between GBCAs within a class of chelate [34,35,38]. Ionic GBCAs are generally more stable compared to non-ionic. Therefore, ionic macrocyclic

GBCAs tend to be the most stable and non-ionic linear GBCAs tend to be the least stable [39].

The dissociation of Gd^{3+} from the chelate ligand *in vivo* can be triggered by the presence of ions competing to replace Gd^{3+} in the chelate. The process of Gd^{3+} being exchanged for another ion is referred to as transmetallation, and can occur for the competitive cations Zn^{2+}, Cu^{2+}, and Ca^{2+} [40]. Transmetallation has been observed for the lower stability linear GBCAs, and is less likely to occur for macrocyclic GBCAs [40–42]. External factors such as pH can affect transmetallation, making some GBCA complexes less stable in an acidic environment [28, 43, 44].

While the stability of GBCAs is important to reduce any potential toxic effects, one must also take into account the relaxivity, which is the GBCA's ability to shorten T1 relaxation time and increase image contrast. When deciding on which type of GBCA to use, one should aim to optimize the balance of relaxivity and stability, to increase contrast enhancement while decreasing the probability of toxic effects. Macrocyclic GBCAs have standard–low relaxivities, while linear GBCAs have standard–high relaxivites, producing greater contrast between healthy and tumour tissue [45].

Within the first two decades of GBCA use for MRI contrast enhancement, hundreds of studies were performed to investigate the possibility of dissociation of GBCAs *in vivo*, resulting in the release of the toxic Gd^{3+} ion in the body. With the knowledge that dissociation could potentially occur *in vivo*, GBCAs continued to be used without concern, due to their effectiveness in diagnosing diseases such as cancer. It wasn't until 2006, when the first occurrence of nephrogenic systemic fibrosis appeared, that the MRI community began to re-evaluate patient safety and the use of GBCAs.

1.1.2 Nephrogenic Systemic Fibrosis

Nephrogenic systemic fibrosis (NSF) is a painful condition in which the skin hardens due to the formation of plaques, leaving the affected individual with discomfort and limited range of motion. Individuals presenting symptoms of NSF can be treated for

relief of their symptoms, but there is no clear cure for the condition [46]. In 2006, the onset of NSF was linked to the administration of GBCAs in patients with renal disease, as patients presenting symptoms of NSF had recently received contrast for MRI [47]. The presence of NSF in patients with renal disease suggested that GBCAs were not clearing from the body within the expected 2 hours, but rather, dissociating and depositing in the body [47–49]. Patients with renal disease have different pharmokinetics than individuals with normal renal function: GBCAs cannot be excreted from the body at the same rate and remain in the body for 30-120 hours, leading to a higher probability of dissociation and release of free Gd^{3+} ions *in vivo* [47, 50]. The correlation between NSF and GBCA administration in patients with renal disease was supported further when Gd was found to be deposited in the skin of patients with NSF [51, 52].

The occurrence of NSF in patients with renal disease following administration of GBCA for MRI caused the MRI community to consider the potential toxicity of GBCAs seriously. A set of precautions was put in place to prevent NSF, through either immediate dialysis following GBCA administration or complete avoidance of administration prior to an MRI for individuals with renal disease. To my knowledge, the incidence of NSF has completely disappeared, with the last case being reported in 2009, leading to restored confidence in the safety of GBCAs [53]. Gd retention in the body was only thought to be a concern for those with impaired renal function. However, in 2013, Gd was found to be retained in brain of individuals with healthy renal function, raising new questions and concerns regarding the safety of the widely-used GBCAs [54].

1.1.3 Gadolinium retention in humans

Presently, gadolinium retention in humans is a rapidly evolving and highly active area of research. For this reason, it is important to note that the literature reviewed in this thesis is current as of November 2018.

Although the first evidence of Gd retention in individuals with normal renal function occurred in 2004 [23, 32], it was the 2013 report of retained Gd in brain that sparked the intense investigation into the safety of GBCA administration for healthy individuals. Kanda *et al.* published the initial findings of Gd retention in the dentate nucleus and global palidus through unenhanced T1 signal intensity increases in these regions of the brain [54]. Over the past 5 years, the concern for metal toxicity in the brain has motivated numerous peer-reviewed articles investigating the retention of Gd in the brain through T1 signal intensity [20]. In these articles, an overall trend of increase in T1 signal intensity with increasing GBCA dose was established [55–57]. This correlation was then verified using the technique of inductively coupled plasma mass spectrometry (ICP-MS) to measure the Gd concentration in autopsy brain samples [58].

While there has been significant focus on Gd retention in the brain of healthy individuals, a more likely long-term storage site of Gd in the body, and the storage site that this thesis work focuses on, is bone. In a recent study by Murata *et al.*, brain and bone autopsy samples from individuals without renal failure, and who had previously received GBCAs, were measured using ICP-MS. Gd concentrations in bone were approximately 23 times higher than concentrations found in brain tissue, suggesting that a large portion of Gd retained in the body is found in bone [59]. In fact, bone is a natural reservoir for rare earth elements, such as Gd [3]. As mentioned in section 1.1, Gd^{3+} is a competitive inhibitor with Ca^{2+} and is likely to incorporate into bone in the form of Gd salts, such a gadolinium phosphate ($GdPO_4$) [60]. The incorporation of Gd into bone matrix creates a long-term storage site for Gd to release slowly into the body, which explains the increasing severity of NSF over time [61, 62]. Earlier measurements of Gd concentration in bone consisted of performing ICP-MS on femoral heads of patients undergoing hip replacement surgery. These measurements showed unusually high levels of Gd in bone for individuals who had previously received GBCA, with up to 8 years between administration and bone measurement [33, 63].

Clinical implications of Gd retention in brain and bone are largely unknown, as Gd retention in individuals with normal renal function is a fairly recent field of investigation. Currently, we know that for an individual retaining Gd, it is most likely that a large proportion of this Gd will be found in bone. This makes bone an ideal candidate for measuring Gd retention in healthy individuals and investigating any potential clinical implications.

1.1.4 Gadolinium toxicity

In 2016, symptoms of potential Gd toxicity were identified hours to weeks after certain individuals had recieved GBCAs [64]. Semelka *et al.* proposed the term "gadolinium deposition disease" to describe symptoms associated with Gd accumulation in the body, which are essentially less severe symptoms of NSF: headache, bone and joint pain, and skin changes [65]. Multiple case studies have investigated self-reported symptoms associated with GBCA administration in individuals, months to years after receiving GBCAs, while monitoring Gd levels in urine [66], or in skin [67]. All studies concluded that presented symptoms in individuals with normal renal function were most likely associated with toxicity from GBCAs, both linear and macrocyclic, and further investigation is needed to explore the long term clinical implications associated with the use of GBCAs [66–68].

1.1.5 Gadolinium measurements in humans

The recent concern of Gd retention in the body of healthy individuals, as well as reports of Gd toxicity symptoms in certain individuals, has led to the need for a non-invasive, convenient device that can assess retained Gd *in vivo* while investigating the clinical implications of Gd retention. As discussed in section 1.1.3, bone is assumed to be a primary and long-term storage site for Gd. Bone also serves as a convenient measurement location since bones like the forehead or tibia have a thin layer of over-laying tissue. All previous measurements of Gd in bone have been invasive and have involved removing pieces of bone from the body, either from individuals undergoing hip replacement surgery or autopsy samples [33, 59, 63]. ICP-MS has then been used on these removed bone samples to assess concentration. ICP-MS is a highly effective

technique for measuring small concentrations of Gd, but destroys the bone sample in the measurement process. X-ray fluorescence is a non-invasive and non-destructive technique that can be used to measure retained Gd in bone *in vivo*, which is the premise of this thesis work. The following section (1.2) describes the technique of x-ray fluorescence and how it can be applied to measure retained gadolinium in bone.

1.2 Detecting gadolinium by x-ray fluorescence

This section serves as a technical introduction to this thesis work, where the general process of x-ray fluorescence is described, along with the mechanisms of the x-ray fluorescence detection system. Finally, the specifics of x-ray fluorescence for Gd detection are discussed.

1.2.1 X-ray fluorescence

To understand the process of x-ray fluorescence, the system must be broken down into the fundamental particles that have a role in this process, which are photons and electrons. A photon is defined as a discrete emission of electromagnetic radiation. An x-ray is a photon that originates from an electron, and a γ-ray is a photon that originates in a nucleus [69]. The energies of these photons can overlap on the electromagnetic spectrum, leaving the origin as the only way to distinguish x-rays from γ-rays. X-rays and γ-rays can interact with matter either through Compton scattering (inelastic), Rayleigh scattering (elastic), pair production (not of interest in this work due to the high energy threshold of the interaction), or the photoelectric effect, which is the interaction behind the process of x-ray fluorescence [70].

The photoelectric effect

The photoelectric effect, also known as photoelectric absorption, involves a photon (x-ray or γ-ray) interacting with an atom by being "absorbed". In this interaction, the absorbed photon excites an inner shell electron to an energy in which it is ejected (i.e. ionized) from the atom. Ionization of the atom can only occur when the incident photon energy ($h\nu$) is greater than the binding energy of the inner shell electron [71]. The ejected electron will therefore have a kinetic energy given by:

$$E_e = h\nu - E_b \tag{1.1}$$

where E_e is the kinetic energy of the ejected electron, h is the Planck constant, ν is the frequency of the incident photon, and E_b is the binding energy of the inner shell electron. The ionization of the atom leaves a vacancy in the lower energy shell from which the electron was ejected. An electron from a higher energy shell will "fall" to fill the vacancy in the inner shell, releasing an x-ray that is equivalent to the difference in potential energy between the higher and lower energy states (Figure 1.2), or an Auger electron, which will be discussed further in this section [72].

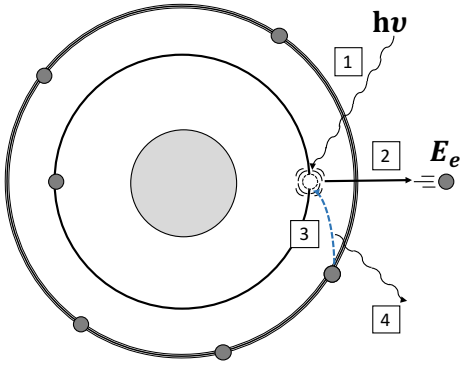

Figure 1.2: Steps of the photoelectric effect in an atom: 1) An incident photon with energy $h\nu$ is absorbed by an atom and excites an inner shell electron, 2) the excited inner electron is ejected from the atom with a kinetic energy of E_e, 3) an electron from a higher energy level fills the vacancy in the inner shell, 4) a characteristic x-ray may be emitted.

The probability of a photon interacting in a medium via the photoelectric effect is described by the photoelectric cross section, which depends on the energy of the incident photon, and the atomic number of the medium:

$$\sigma_{PE} \propto \frac{Z^n}{(h\nu)^{3.5}} \tag{1.2}$$

where σ_{PE} is the photoelectric cross section, Z is atomic number, $h\nu$ is the energy of the incident photon, and n is a number varying between 4 - 5 (the dependence on Z varies with energy) [72].

Characteristic x-rays and x-ray energy levels

The x-ray released by an electron transitioning from a higher energy level to a vacancy in a lower energy level is called a "characteristic x-ray" because the x-ray has an energy that is characteristic to the element from which it is emitted [71]. X-ray levels are often used to describe the initial and final electronic states for the emission of characteristic x-rays. In x-ray level notation, the letters K, L, M denote the primary quantum numbers 1, 2, 3, and a subscript is used to denote the subshell and total angular momentum j [73]. The characteristic x-ray can then be classified by the initial and final x-ray levels of the electron from which it was emitted. For example, when an electron falls from the L shell to the K shell, the characteristic x-ray is called a Kα x-ray. In general, characteristic x-rays are labelled as α, β, or γ based on the number of shells the electron falls [74]. Figure 1.3 shows the basic electron transitions between x-ray levels, resulting in the release of characteristic x-rays. These transitions can be further defined based on the subshell and total angular momentum of the electronic states, which we will see when looking at the transitions for Gd in section 1.2.3.

Auger electrons and fluorescent yield

When a photon interacts with an atom via the photoelectric effect, there is a chance that an electron transitioning from a higher energy level to a lower energy level will transfer its energy to an outer shell electron, which will then be emitted as an Auger electron. This process is known as the Auger effect and is the competing process

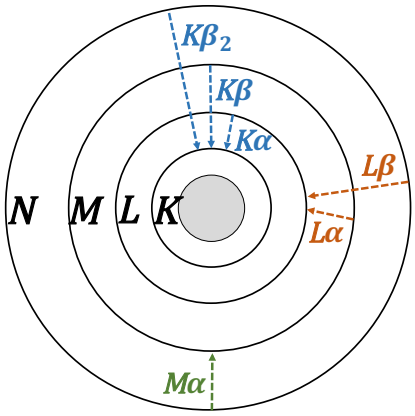

Figure 1.3: Electron transitions from higher to lower energy x-ray levels, resulting in the the release of characteristic x-rays.

for the release of a characteristic x-ray. The release of an Auger electron decreases in probability as the atomic number of the element increases. The fluorescent yield describes the probability of a characteristic x-ray being emitted for each photon absorbed by a specific atom [75].

X-ray fluorescence for trace element analysis

The technique of x-ray fluorescence (XRF) involves bombarding a sample with high energy x-rays or γ-rays, which are absorbed by atoms in the sample through the photoelectric effect. The characteristic x-rays fluoresced from the excited atoms are unique to the elements in the sample and can act as fingerprints, identifying which elements are present.

Following the discovery of x-rays by Roentgen in 1895, the early 20th century consisted of many studies on the properties of x-rays in relation to atomic structure. The use of x-rays to excite and fluoresce samples was taken on as a simple, relatively quick, and non-destructive technique for the analysis of materials, with the first commercial XRF spectrometer becoming available in 1948 [76]. Presently, XRF is used to determine the elemental composition of samples in a variety of fields. Due to its non-

destructive nature, XRF has even been used to analyse pigments in famous art pieces, such as paintings by Vincent Van Gogh [77], as well as archeological samples [78, 79]. Knowing the composition of pigments is valuable from a historical perspective, but also for the purpose of preservation and restoration [80]. XRF is also well suited for measuring elemental composition of the body, and has been used for *in vivo* assessments of numerous elements such a lead [81], cadmium [82], and strontium [83]. As previously mentioned in section 1.1.5, this thesis work focuses on *in vivo* detection of Gd in bone using XRF. The XRF system used to perform the measurements for this thesis will be described in the following section (1.2.2).

1.2.2 X-ray fluorescence detection system

An *in vivo* XRF detection system must consist of 3 features: a sample to be measured, an excitation source to excite the element of interest in the sample, and a detector to detect the characteristic x-rays emitted from the element of interest. The following section describes the properties and mechanisms of the excitation source, and detector used in this thesis work.

Cd-109 Excitation source

To measure Gd in bone using XRF, an 88 keV γ-ray from a cadmium-109 source is used to excite any present Gd. Cd-109 decays to the excited state of Ag-109 through electron capture with a probability of 100%, where an inner shell electron is absorbed into the nucleus and combines with a proton to create a neutron and neutrino. The excited Ag-109 nucleus de-excites to ground state through the emission of an 88 keV γ-ray (3.66%) or the emission of an atomic electron through internal conversion (96.34%) (Figure 1.4). Ag x-rays are produced from both the electron capture of Cd-109 to Ag-109 as well as the internal conversion of Ag-109 since both processes involve removing an inner shell electron, which will then be filled by an electron from a higher energy state. The most common x-rays emitted from electron capture and internal conversion are the Kα1 (22.16 keV), Kα2 (21.99 keV), and Kβs ($\sim$25 keV), although both electron capture and internal conversion can occur for higher energy shells, such as L or M. This source was chosen for its ability to excite gadolinium,

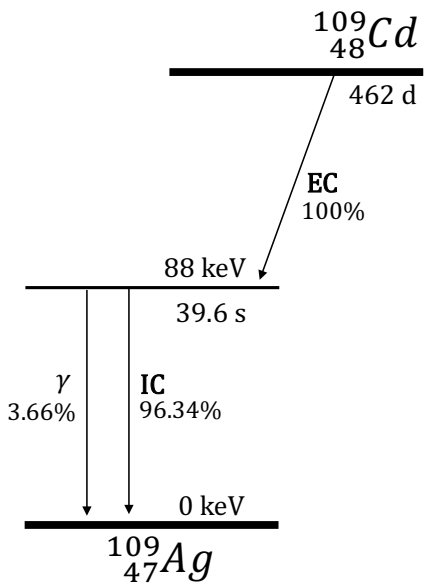

Figure 1.4: The decay scheme for Cd-109, with half lives displayed for each step of the decay. The ground state of Ag-109 is represented by 0 keV.

as well as its availability in point source form. Cd-109 has a relatively long half life of 462.6 days, allowing a Cd-109 point source to be used experimentally for a few years [84].

Properties of high purity germanium detectors

High purity germanium (HPGe) detectors are a type of semiconductor detector. Due to the high density of the solid crystal increasing the attenuation of incident photons, these detectors are efficient in detecting penetrating radiation, such as x-rays and γ-rays. A semiconductor crystal consists of a pure material, such as germanium, in which the energy band gap between the valence and conduction band is small enough to allow some electrons to be thermally excited into the conduction band and conduct [72]. When ionizing radiation strikes a semiconductor crystal in a detector, electrons are excited to the conduction band and leave vacancies in the valence band, creating an equal number of negative and positive charge carriers known as electrons and holes (Figure 1.5). The collection of electron-hole pairs through the application

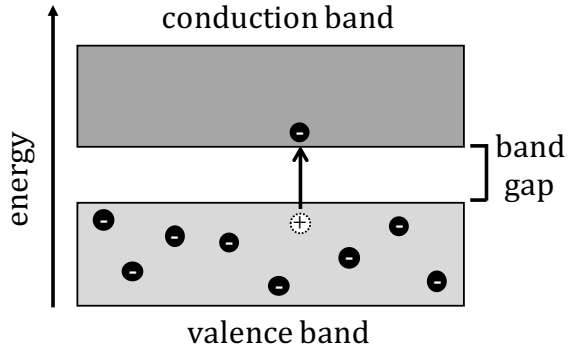

Figure 1.5: The band gap structure of a semiconductor material. With enough thermal energy to overcome the band gap, electrons can be excited to the conduction band.

of a high voltage potential is the basis for detecting radiation events [85]. Semiconductor detectors, especially HPGe, have a small enough band gap that allow them to conduct a significant amount of current at room temperature, due to electrons being thermally excited into the conduction band. This current is known as "leakage current" and creates background noise that lowers the signal-to-noise ratio of radiation events. The probability of excitation is proportional to $e^{-1/T}$, where T is absolute temperature. Therefore, the detector cryostat is regularily filled with liquid nitrogen to lower the probability of excitation, as well as increase the band gap, to prevent the thermal excitation of electrons in the HPGe crystal [86].

To enhance the conductivity of a semiconductor detector, the crystal can be doped with atoms from neighbouring groups on the periodic table. For example, doping a germanium crystal with arsenic introduces impurity atoms with 5 valence electrons. This creates extra electrons in the crystal structure, which have a high probability of being thermally excited into the conduction band. This is called an "n-type" semiconductor. A "p-type" semiconductor can be created by doping the crystal with impurities such as gallium or indium, creating extra holes in the crystal. These extra holes in the crystal structure move like positive charges in the valence band [70].

A p-n junction is a boundary between p-type and n-type semiconductor materials in a single semiconductor crystal. Since p-type semiconductors have extra holes and n-type semiconductors have extra electrons, the gradient in charge carriers will cause the charges to diffuse across the p-n junction. Holes from the p-type semiconductor will migrate towards the n-type semiconductor, and electrons from the n-type semiconductor will migrate towards the p-type semiconductor. The migrated holes will be "filled" by electrons in the n-type semiconductor, and the migrated electrons will fill the holes in the p-type semiconductor, creating a region with fewer charge carriers called the "depletion region". Additionally, this movement of charge carriers across the junction creates an electric field (E) in the depletion region (Figure 1.6) [72].

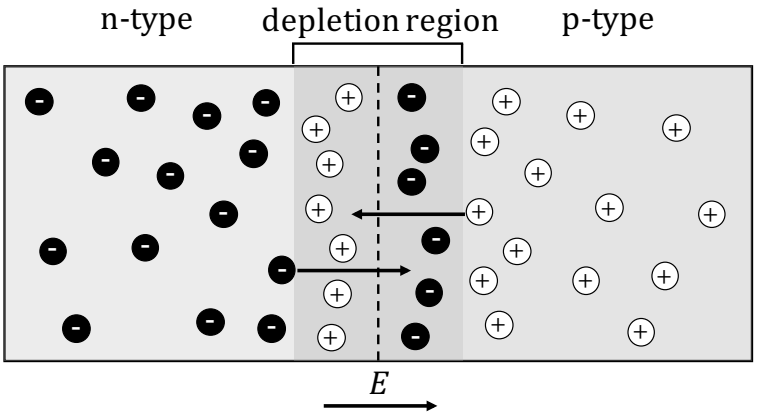

Figure 1.6: A p-n junction formed at the boundary between p-type and n-type semiconductor material. The migration of charge carriers creates a depletion region with a potential V and electric field E.

The potential across the depletion region is described by Poisson's equation:

$$\nabla^2 V = -\frac{\rho}{\epsilon} \tag{1.3}$$

where ρ is the net charge density, and ϵ is the dielectric constant for the semiconductor material. Applying an external high voltage (V_0) to the semiconductor crystal in a reverse bias direction involves connecting a negative terminal to the p-type semiconductor and a positive terminal to the n-type semiconductor. The reverse bias voltage

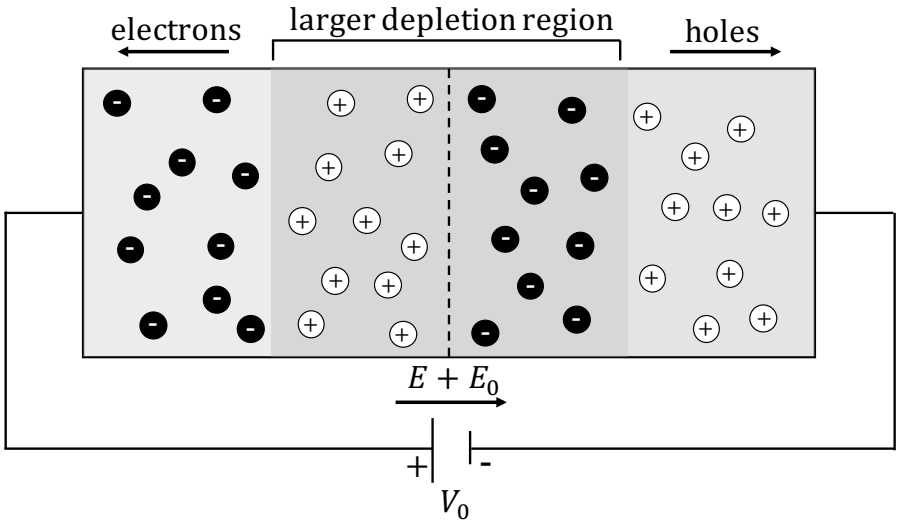

Figure 1.7: A reverse bias voltage of V_0 applied to a p-n junction will cause the charge carriers to move away from the p-n junction, causing the depletion region to become larger and have a stronger electric field of $E + E_0$.

causes the charge carriers to move in a direction away from the p-n junction, which creates a thicker depletion region (Figure 1.7) [87]. The detector configuration used for this thesis work is referred to as "planar", and consists of a cylindrical p-type crystal with an n-type and p-type electrical contact on each flat surface of the crystal. The p-n junction is therefore formed between the p-type crystal and the n-type electrical contact (Figure 1.8). For the planar detector configuration, the thickness of the depletion region can be approximated by:

$$d \simeq \left(\frac{2\epsilon V_0}{eN}\right)^{1/2} \tag{1.4}$$

where V_0 is the applied reverse bias voltage, e is the charge of an electron, N is the net impurty concentration in the crystal, and ϵ is the dielectric constant for the semiconductor material. The depletion region of a p-n junction serves as an effective radiation detector, as the volume has a high resistivity and charges created from ionizing radiation can be collected by the electric field $(E + E_0)$ [72].

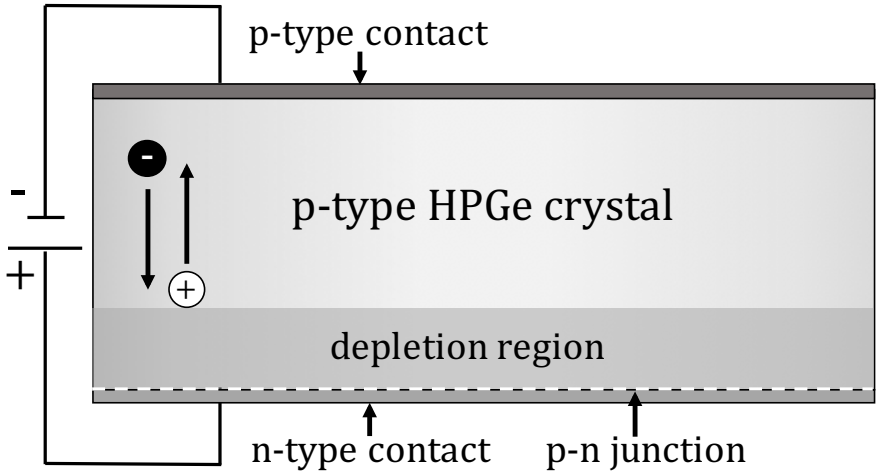

Figure 1.8: Formation of a p-n junction and depletion region in a planar detector configuration, which is used in this thesis work.

HPGe detectors have excellent energy resolution compared to other types of radiation detectors, meaning the measured energy peaks have smaller widths and are more defined on energy spectra. The energy resolution of an HPGe detector is dependent on three factors: variation in the number of charge carriers, variation in the charge carrier collection, and electric noise from detector electronics [72]. The full width half-maximum (FWHM) is the measurement used to quantify the energy resolution of a peak and can be defined as:

$$W_T{}^2 = W_D{}^2 + W_X{}^2 + W_E{}^2 \tag{1.5}$$

where W_D is the peak width from variation in the number of charge carriers, W_X is the peak width from variation in the charge carrier collection, and W_E is the peak width from electronic noise. W_D can be further described by:

$$W_D = 2.355^2 F \omega E_\gamma \tag{1.6}$$

where E_γ is the incident photon energy, ω is the energy required for creating an electron-hole pair, and F is the Fano factor [72]. The Fano factor accounts for the

fact that the observed variation in the number of charge carriers created in semiconductor detectors is smaller than the expected variation in a Poisson model. The Fano factor therefore serves as a correction factor to relate the observed variance to Poisson variance. From equation 1.6 it is apparent that the lower the Fano factor, the higher the energy resolution in a semiconductor detector [88].

Detection process for high purity germanium detectors

The general process of a semiconductor detector involves converting incident photons into electrical signals, which are then processed to determine the energies and intensities of the photons [87]. When an incident photon (x-ray or γ-ray) strikes an HPGe detector, it can undergo a variety of interactions such as Compton scattering, coherent scattering, or the photoelectric effect. However, the event that leads to the detection of a photon is the ionization of an atom, where the incident photon gives up all or a fraction of its energy to the electron. The excited electron will then be ejected from the atom, colliding with other atoms in the detector crystal and creating more ionization events [89]. As previously described, the ionization of an atom leads to the excitation of an electron to the conduction band, leaving a vacancy in the valence band, and in turn creating an electron-hole pair. For an HPGe detector, approximately 3 eV of deposited energy is required to create one electron-hole pair. Thus, the number of electron-hole pairs produced increases proportionally with incident photon energy [90].

Charge carriers produced by ionizing radiation in the depletion region of the detector crystal are swept towards electrodes by the applied electric field, and collected on a feedback capacitor (C_f) in a preamplifier. As charge is collected, the voltage on the feedback capacitor rises. The preamplifier outputs a voltage pulse, which is then analysed along a signal processing chain, resulting in a spectrum of output voltages binned by magnitude. Since the energy of the incident photon is proportional to the number of electron-hole pairs created, this spectrum represents the energies and intensities of the detected photons [89]. The relationship between the magnitude of the voltage pulse and detected photon energy needs to be calibrated by the user

with known calibration sources. During the time in which a pulse is being processed, another event cannot be processed. This is referred to as system "dead time", and causes a loss of information. In general, the lower the system dead time, the less information lost.

Choice of detector for gadolinium bone measurements

The choice of a HPGe detector for *in vivo* measurements of Gd in bone using XRF was due to the superior efficiency and energy resolution of HPGe detectors for the given energy range of interest. For the purposes of Gd measurements, photons need to be detected within the energy range of 40-90 keV. Due to the high atomic number of Ge (Z=32), HPGe detectors have greater linear attenuation for these photon energies compared to other semiconductor detectors such as silicon. A silicon detector crystal has a much lower atomic number than Ge (Z=13), and would have to be very large to detect all radiation events, as more penetrating radiation would pass through the detector crystal without interacting [88]. In addition to the superior linear attenuation, HPGe detectors are able to obtain the largest depletion depth compared to any other semiconductor, increasing the efficiency of photon detection further [72].

As previously described, the energy resolution of a detector refers to the width of the energy peak in the resultant spectrum. The higher the energy resolution, the smaller the peak width, and the easier the peak is to identify and distinguish from other peaks on a spectrum. Semiconductors have superior energy resolution compared to other radiation detector types, with approximately 20-80 times better energy resolution than scintillation detectors [86]. Charge carriers created in semiconductor detectors from incident photons are a direct measurement of photon energy and intensity. Unlike semiconductor detectors, scintillation detectors are not a direct measurement since incident radiation interacts to release light, which is then converted into photoelectrons. The length and inefficiency of the process leads to poor resolution peaks on spectra [90]. An additional factor contributing to the high energy resolution of semiconductor detectors is the fact that many charge carriers are created for a small amount of energy deposited. For example, approximately 1 charge

carrier is created per 3 eV, where approximately 10 photoelectrons are produced per 1 keV in scintillation detectors. The larger number of charge carriers produced per energy results in less statistical variation in signal amplitude, and therefore a narrower peak [85]. The high energy resolution obtained with HPGe detectors allows for the two Gd peaks of interest (Kα1 and Kα2) to be distinguished from each other and properly analysed when performing Gd bone measurements. Therefore, due to the good efficiency and high energy resolution, a HPGe detector was the obvious choice for this thesis work.

1.2.3 Detection of gadolinium in bone

So far, section 1.2 has given a technical background for this thesis work and has described the general process of XRF, as well as the detection system used. However, to understand the detection process of Gd using XRF, we must look at the energies we are measuring. The characteristic x-rays of interest when measuring gadolinium in bone are the Kα1 x-ray (42.996 keV) released from an electron falling from the L_3 shell to the K shell, and the Kα2 x-ray (42.308 keV) released from an electron falling from the L_2 shell to the K shell (Figure 1.9). These are the two most common electron transitions that result from the excitation of Gd and are therefore the most prominent characteristic x-rays. The K-shell fluorescence yield of Gd is 0.94, meaning that the ejection of an K shell electron will cause the release of a characteristic K x-ray approximately 94% of the time [91]. The high fluorescence yield of Gd makes it an excellent candidate for Gd measurements using XRF.

The detection of the Gd K x-rays produced from excitation of Gd in bone follows the general detection process of HPGe detectors described in section 1.2.2: Gd K x-rays strike the HPGe detector crystal, creating charge carriers and leading to an output voltage to be further analysed along a signal processing chain. The tenth value layer (i.e. the distance for 90% photon interaction) of the Gd Kα x-rays in germanium are 8.1 and 8.5 mm. Therefore any HPGe detector crystal with a thickness greater than 8.5 mm will be highly efficient in detecting the Gd Kα x-rays.

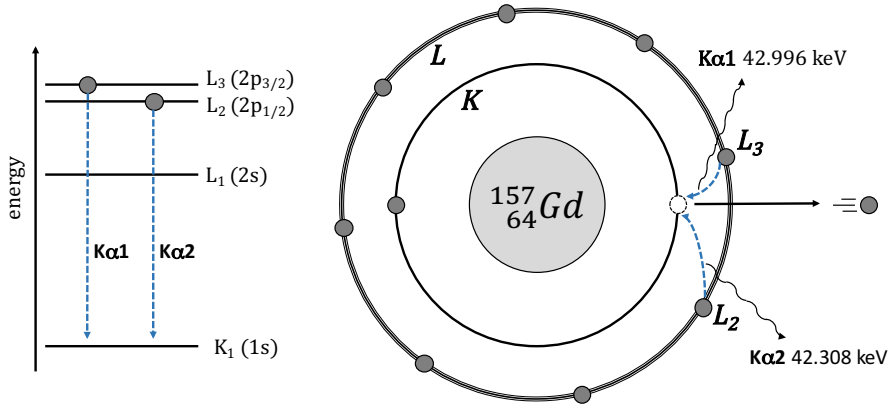

Figure 1.9: The production of Gd characteristic x-rays: Kα1 x-ray (42.996 keV) resulting from a L_3 shell to K shell electronic transition, and Kα2 x-ray (42.308 keV) resulting from a L_2 shell to K shell electronic transition. The subscripts on the L shell represent the subshell (s, p, d etc.) and total angular momentum j (1/2, 3/2, 5/2 etc.).

As discussed in section 1.2.1, in order for an excitation photon to excite an element of interest, the excitation energy must be higher than the binding energy of an inner shell electron. The binding energy for the inner most shell (K shell) can be referred to as the K-edge, and represents a sudden increase in the photoelectric cross section just above the binding energy. Any energy above the K edge has the potential to ionize an electron in the K shell, with energies just above the K edge having the highest probability of ionization [92]. The K-edge for Gd is 50.2 keV, meaning energies just above this value will result in the greatest production of Gd K x-rays [93]. However, the source used in this thesis work has an excitation energy of 88 keV, which is 37.8 keV above the K-edge, and has a photoelectric cross section of 4.061 cm^2/g, compared to the photoelectric cross section of 18.1 cm^2/g at the K edge (Figure 1.10) [1]. This raises the question: why was this particular source chosen to measure Gd using XRF?

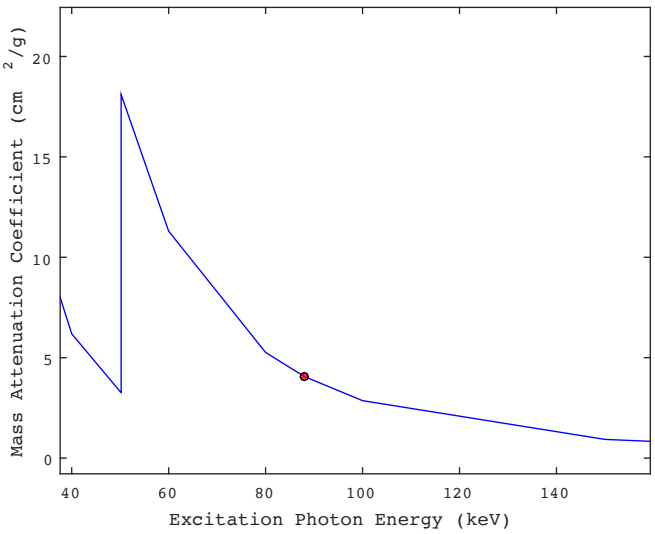

Figure 1.10: The photoelectric cross section of Gd for a range of excitation photon energies. The K-edge for Gd lies at 50.2 keV, with a high cross section of 18.1 cm^2/g. The Cd-109 excitation energy (represented by the red dot) lies at 88 keV, with a lower cross section of 4.061 cm^2/g [1].

The photoelectric cross section is not the only factor to be considered when choosing an excitation source for XRF measurements. The excitation energy will also affect the placement of other features on the collected spectrum, such as the Compton scatter peak, which can sometimes hide the peaks of interest. For the measurement geometry (to be addressed in Chapter 2) and excitation energy of 88 keV, the Compton peak is around 65.5 keV. This feature does not obstruct the Gd x-ray peaks of interest (42.3 and 43.0 keV). If we were to have a source with an excitation energy of around 51 keV, it would technically create the highest photoelectric cross section and therefore produce the most Gd x-rays. However, the Compton peak would be located at 42.5 keV, which would completely hide the Gd x-ray peaks. Another potential source would be Am-241 with an excitation energy of 59.5 keV, which is closer to the Gd K-edge compared to Cd-109. The Compton peak for this source would be located 48.3 keV, and the tail of the peak would still be overlapping with the Gd K x-rays. Through these simple calculations it is apparent that Cd-109 is not obviously worse than other sources, and it is difficult to come up with a better solution for an excitation source to measure Gd. Additionally, secondary fluence resulting from inter-

actions of the 88 keV excitation γ-rays in tissue and bone contribute to the excitation of Gd, making up for the low photoelectric cross section achieved with Cd-109 [94]. The contribution of secondary fluence to the excitation of Gd is discussed in greater detail in Paper III.

Chapter 2

Methods

The following chapter describes the experimental details for the development of the XRF system, the execution of Gd bone measurements, as well as subsequent data analysis. The manuscripts included in chapters 3-7 provide all methods for the presented results. However, this chapter will provide greater detail and supplementary information that was not included in these manuscripts due to journal length restrictions. In this chapter, the methods for preparing phantoms will be described, followed by the setup geometries for phantom, bone sample, and human measurements. Next, the two XRF detection systems used in this thesis work will be described, followed by the analysis of the measured Gd peaks.

2.1 Bone phantoms

At the beginning of this thesis work, bone phantoms with varying concentrations of Gd were constructed to assess the feasibility of using the XRF system for detecting Gd in bone. Initially, phantoms were constructed out of Plaster of Paris (PoP) to represent bone (Papers I, II & III). Later, hydroxyapetite (HPa) phantoms were constructed (Papers IV & V), since bone mineral is composed of HPa. Multiple sets of phantom measurements were conducted on bare bone phantoms, as well as bone phantoms with varying thicknesses of overlaying tissue equivalent material. The use of Gd bone phantoms in this thesis work was essential for developing the XRF system

that was eventually used for human measurements. A great deal of preparation went into the process of constructing these phantoms to ensure a set of phantoms with precise Gd concentrations was created. This section discusses the process for creating the bone phantoms.

2.1.1 Measurement location

The tibia was deemed as the most appropriate measurement location for *in vivo* measurements of Gd in bone for multiple reasons. From an experimental perspective, the tibia is located in the lower leg with a small amount of overlaying tissue, thus reducing attenuation of the entering 88 keV excitation γ-rays, and the exiting Gd Kα1 (43 keV) and Kα2 (42.3 keV) x-rays. From a radiation safety perspective, since the tibia is located in an extremity of the body, the effective dose received by the measured individual is reduced. For a 30-minute XRF measurement with a 5 GBq Cd-109 source, the local maximum equivalent dose to the tibia is 357 μSv and the effective dose is 0.13 μSv [95]. The Canadian Nuclear Safety Commission lists their maximum effective dose in a calendar year to be 1 mSv (1000 μSv), and a typical chest x-ray to be 100 μSv. The effective dose of a 30-minute measurement in this study is 0.13% of a chest x-ray, making the measurement a very low risk for volunteers. Lastly, from a volunteer comfort perspective, measuring the tibia allows the volunteer to sit in a chair with their lower leg placed against the Cd-109 excitation source for an extended period of time without movement.

The tibia is a long bone located in the lower leg and is the second largest bone in the body. The tibia consists of the two types of bone tissue: cortical and trabecular. Cortical bone tissue is hard and dense, and provides structural support for the body. Trabelcular bone tissue is porous, with a spongy appearance. It is less dense and serves as an internal tissue in bone structure. The tibia consists of a long shaft composed of cortical bone, with bone marrow contained in a central cavity called the Medullary cavity. Bone marrow is composed of blood forming cells, fat cells, and blood vessels [96]. It does not contain the same hydroxyapatite matrix structure as bone and is therefore not considered as a potential long-term storage site for Gd

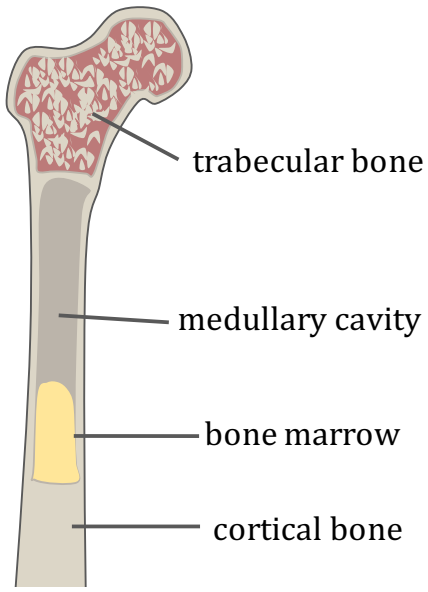

Figure 2.1: A cross section of the upper half of a tibia, displaying the internal bone structure composed of cortical and trabecular bone tissue with bone marrow in the central shaft.

in the body. Trabecular bone is found in upper and lower extremities of the tibia, contained by cortical bone (Figure 2.1) [97].

Since all human measurements were carried out on the mid-shaft of the tibia, only cortical bone was considered for photon attenuation. From Section 1.2.3, we know that the 88 keV excitation γ-rays emitted by the Cd-109 source are able to excite Gd, resulting in the release of Gd Kα x-rays from the measured material. However, in order for any present Gd to be excited, the 88 keV γ-rays must be able to penetrate into the cortical bone. Additionally the measured Gd Kα x-rays must be able to penetrate out of the bone without total attenuation. In a recent study measuring the cortical thickness of the tibia shaft, a group of healthy adult volunteers had an average cortical thickness of approximately 0.804 cm [98]. This thickness will be used as a reference for the following photon attenuation calculations to look at the attenuation of the 88 keV excitation γ-rays, as well as the Gd Kα1 (43 keV) and Kα2 (42.3 keV) x-rays in bone.

The half value layer (HVL) is defined as the distance at which the intensity of photons is attenuated by 50% in a medium, and is described by the relationship: $HVL = ln2/\mu$, where μ is the linear attenuation coefficient for a photon with an energy of 88 keV in cortical bone. For the 88 keV γ-rays in cortical bone, the HVL is 1.81 cm, which is greater than the average cortical thickness in a group of healthy adults (0.804 cm). Therefore, the Cd-109 excitation γ-rays are able to penetrate cortical bone well. To be conservative, let us assume Gd Kα x-rays are produced at the maximum depth of 0.804 cm in bone (i.e. cortical thickness). Approximately 40% of the Gd Kα x-rays will be attenuated when exiting cortical bone if produced at the maximum depth. Thus, detection of Gd in cortical bone using XRF is possible with the given energies.

2.1.2 Bone phantom production

For this thesis work, I wanted Gd concentrations in bone phantoms to be comparable to concentrations previously measured in bone. Prior to the commencement of phantom production, Gd had only been measured using the technique of inductively coupled plasma mass spectrometry (ICP-MS) in bone samples of patients undergoing hip replacement surgery. Gd concentrations of 0.42 - 6.02 μg Gd/g bone had been reported for multiple contrast agents including both macrocyclic and linear GBCAs [32, 33, 63]. I made 9 bone phantoms with desired concentrations of 0, 3, 6, 9, 12, 30, 60, 90, and 120 ppm Gd. A greater number of phantoms were produced in the lower concentration range (0 - 12 ppm) to stay true to previously measured Gd concentrations in bone, and higher concentration phantoms were created for calibration purposes. The concentration unit of "ppm" for phantoms is equivalent to μg Gd/g bone phantom. In Paper I, all concentrations were referred to as ppm, although the specific unit was μg Gd/g PoP. In Papers II, III, IV & V, I discontinued the use of ppm due to its vagueness, and described concentration in terms of μg Gd/g material.

To keep the phantoms anthropomorphic to a human tibia, the bone equivalent material was set in clear plastic cylindrical containers with lengths of 115.0 mm, diameters of 28.0 mm, and wall thicknesses of 1.0 mm. Each phantom had a total

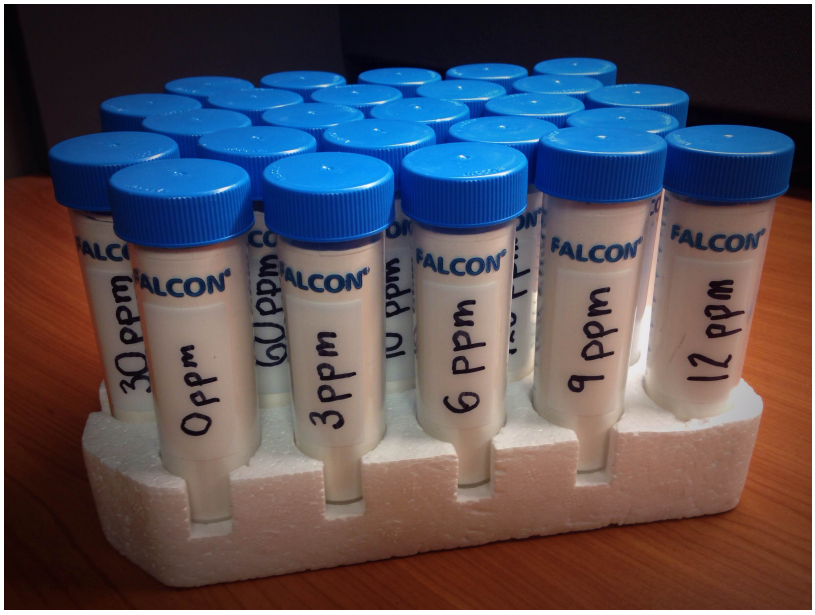

Figure 2.2: Plaster of Paris tibia bone phantoms created with various concentrations of Gd.

volume of approximately 50 mL in a 50 mL cylindrical container with a lid (Figure 2.2). The Gd stock solution (Sigma Aldrich, St. Louis, Missouri, United States) had a concentration of 980 ppm, and consisted of gadolinium oxide (Gd_2O_3) in nitric acid (HNO_3). This solution was further diluted in nitric acid to obtain the desired Gd concentrations before combining with PoP or HPa. Once the bone equivalent material was added to the cylindrical container, the mixture was shaken vigorously to ensure a homogeneous distribution of Gd throughout each phantom, then allowed to dry for 1 week before use.

PoP ($CaSO_4 \cdot 2H_2O$) was used to create bone equivalent material in a set of Gd bone phantoms for Papers I, II & III, which were constructed at McMaster University with the help of Michael Inskip. PoP has been the standard material used when creating calibration bone phantoms for measureing metals, such as lead and strontium, with an XRF detection system. However, PoP is not entirely bone equivalent, and requires a conversion factor to be applied when conducting *in vivo* trace element measurements in order to obtain an accurate concentration in bone. This conversion factor is referred to as the coherent Conversion Factor (CCF), and will

be discussed in Section 2.4.2. Concern has been raised with respect to the purity of PoP affecting the reliability of this conversion factor used to calculate bone metal concentration [99, 100]. The use of HPa ($Ca_5(PO_4)_3(OH)$) to create phantoms for the calibration of *in vivo* XRF systems was first explored by Dr. Eric Da Silva, in which he created a protocol for constructing HPa phantoms that have the same crystal structure as bone mineral [101]. A set of HPa phantoms was constructed using this protocol at Ryerson University with the help of Dr. Eric Da Silva. The HPa phantoms eliminated the need to use a conversion factor when measuring Gd in bone, thus reducing uncertainty in the measured Gd concentrations for Papers IV & V.

2.1.3 Overlaying tissue equivalent material

A tissue equivalent plastic called SolidWater® was used to simulate tissue over the tibia bone for phantom measurements. At the time of tibia bone phantom preparation, our lab group had multiple cylinders of SolidWater® material available from past work. I cut holes at various depths within one cylinder to create multiple thicknesses to overlay the bone phantoms. Pejović-Milić *et al.* measured the average tissue thickness over the tibia in healthy adult volunteers to be 4.8 ± 0.2 mm [102]. The tissue equivalent plastic was created with thicknesses of 3.3 ± 0.1, 4.0 ± 0.1, 5.5 ± 0.1, 7.5 ± 0.1, and 12.2 ± 0.1 mm (Figure 2.3). The varying thicknesses were created to account for the possible different body compositions being measured with the XRF system.

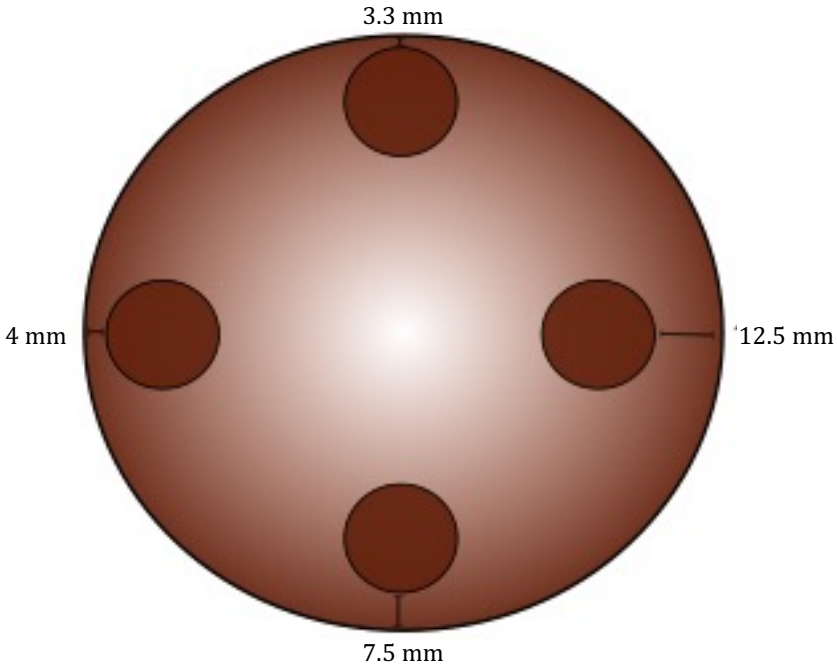

Figure 2.3: A cylinder of SolidWater® tissue equivalent plastic with holes placed at various depths to create different overlaying thicknesses for an inserted bone phantom. The 5.5 ± 0.1 mm thickness was created on a separate cylinder of SolidWater®.

Simple photon attenuation calculations were carried out to ensure little attenuation of the 88 keV excitation γ-rays and the exiting Gd Kα x-rays. For an overlaying tissue thickness of 5.0 mm, 9.4% of the 88 keV γ-rays are attenuated, and 12.9% of the Kα x-rays are attenuated.

2.2 Setup geometry

2.2.1 Phantom and bone sample measurements

Phantom and bone sample measurements were performed for Papers I, II & III. These measurements were essential for investigating the feasibility of the XRF system for detecting Gd in bone. Phantom measurements also served as a calibration for the XRF system when performing human measurements.

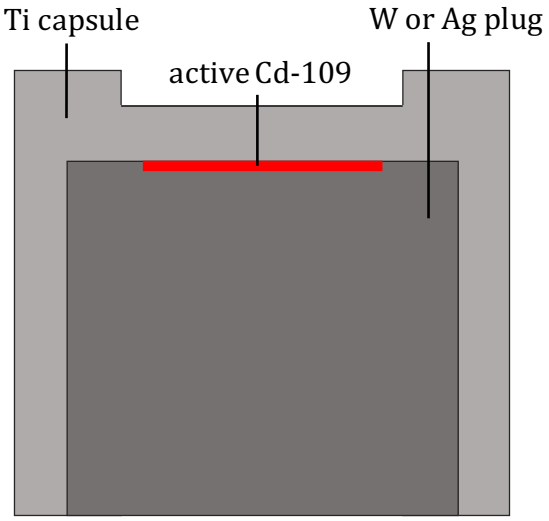

Figure 2.4: Cross section of the 3 mm × 3 mm Cd-109 source. A 1 mm active diameter is backed by a W or Ag plug and enclosed in a Ti capsule. The front of the source is the side that the active volume is closest to.

The Cd-109 point sources used for XRF measurements were small cylinders with dimensions of 3 mm length and 3 mm diameter, and were obtained with an initial activity of 5 GBq. The activity of the source for each phantom measurement varied since Cd-109 decays over time. The exact source activities for each set of phantom measurements are reported in the papers presented in chapters 3-7. The Cd-109 source consisted of a 1 mm active diameter of Cd-109, with a W or Ag plug, enclosed in a Ti capsule (Figure 2.4). Phantom measurements in Paper I used a Cd-109 source with a W plug, which was later replaced in Paper II by a Cd-109 source with a Ag plug.

The Cd-109 source was enclosed in a W or Pb collimator with a Cu face to filter out the Ag x-rays produced from the decay of Cd-109 (Section 1.2.2), while allowing the 88 keV γ-rays to pass through. The source was purposefully placed in the collimator to ensure that the front of the source faced the Cu filter. The W collimator was initially used in Paper I, but was switched to the Pb collimator to reduce background near the Gd peaks of interest, which is discussed in greater detail in Paper II. The W or Pb collimator containing the Cd-109 source was then placed in a plastic holder on the face of the detector. The measured phantom was placed directly in front of the Cu face of the collimator, creating a 180^o geometry. For 88 keV excitation γ-rays, the 180^o scattering geometry should theoretically result in a Compton peak located at 65.5 keV. However, in all experimental spectra, the Compton peak was located at 66.5 keV, resulting in a mean scattering angle of 151.6^o. The difference between the mean Compton scattering angle and the theoretical geometry of 180^o is a result of the detector having a size, and thus detecting a range of scattering angles. The phantoms were placed at a close distance of 1 mm from the Cu face of the collimator, as this distance was found to maximize the number of collected counts (i.e. radiation events detected) in the region of the Gd Kα x-rays (Figure 2.5).

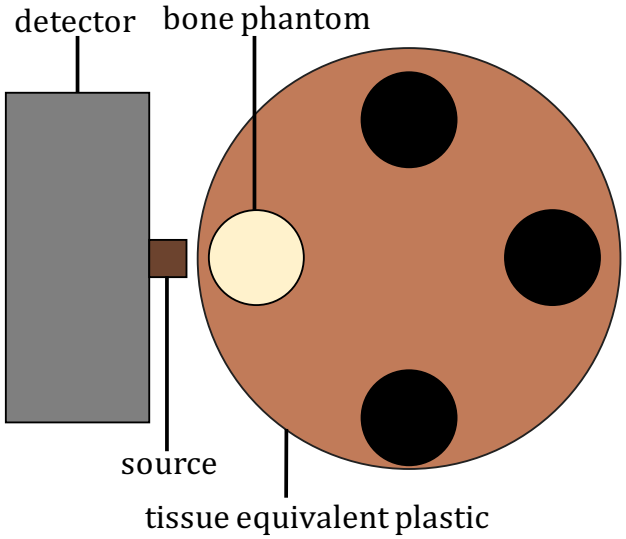

Figure 2.5: An aerial view of a tibial phantom measurement with an XRF detection system. The bone phantom was placed in one of the holes cut in the tissue equivalent SolidWater® to obtain a desired thickness over the bone phantom. The entire phantom was then placed approximately 1 mm from the Cu face of the collimator, which was mounted on the face of the detector.

2.2.2 *In vivo* human measurements

For consistency, a measurement geometry of 180^o was maintained for human measurements. The volunteer sat in a chair and placed their leg of choice in front of the detector face. The most comfortable and sustainable measurement position was attained when the individual leaned back in the seat rather than leaned forward. The volunteer was instructed to feel where their tibia is most prominent (i.e. least amount of skin and fat), and to place that area directly in front of the collimator face. The space between the leg and collimator was minimal - approximately 1 mm. The leg was then strapped in place to minimize movement throughout the measurement. The setup was visually inspected throughout the measurement to ensure the tibia bone was directly in front of the collimator face and that the leg had not shifted. The growth of the 88 keV coherent peak on each spectrum was monitored throughout the measurement, since most of the coherent scatter comes from high Z material such

as bone. If tissue and fat were being measured rather than bone, the coherent peak stopped growing as rapidly, which indicated that the position of the leg had changed and the tibia was no longer being measured.

Figure 2.6: The setup for a human tibial measurement of Gd in bone using an XRF detection system. Photo by: Paulina Kowalczyk.

2.3 X-ray fluorescence detection systems

2.3.1 Single HPGe Detector

The original HPGe detector and electronics used in Paper I are from Canberra Industries, Inc. (Meriden, Connecticut, 06450, USA). The detector consists of a single HPGe crystal located behind a thin 0.5 mm Be window, with a cross sectional area of 2000 mm^2 and thickness of 20 mm. Once a radiation event strikes the detector crystal and creates charge carriers as described in Section 1.2.2, the preamplifier (Canberra 2001 CP) creates a voltage output with a magnitude proportional to the energy deposited in the detector, which then travels to the digital pulse processing system (Canberra DSA 1000). Finally, Genie 2000 Gamma Analysis Software from Canberra sorts the pulses by binning the number of pulses into channels representing voltage magnitude, thus creating a spectrum of number of counts (i.e. radiation

events) versus energy. Each collected spectrum was saved and exported to MATLAB for peak fitting and further analysis.

2.3.2 Cloverleaf HPGe Detector

For phantom and bone measurements conducted in Paper II, a stronger Cd-109 source of 5 GBq was obtained in attempt to shorten the measurement time and improve the detection limits for human measurements of Gd in bone. However, the single HPGe detector electronics could not handle the large count rate produced by the high activity source. The output voltage pulse of each radiation event rides on the exponential decay of the previous event (Figure 2.7). As the count rate increases, the pile-up of voltage pulses builds and the preamplifier cannot return to the baseline voltage. Eventually, the preamplifier will "saturate" and no longer output any pulses.

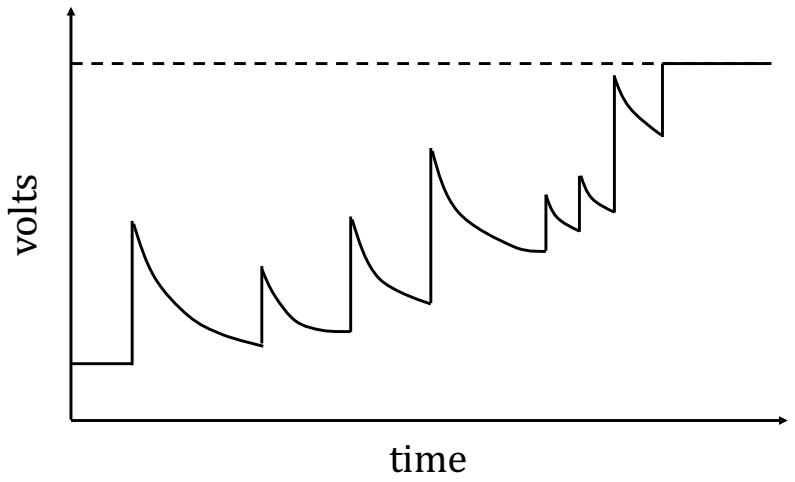

Figure 2.7: Output voltage pulses in a premaplifier riding on the exponential decay of their previous pulses. Eventually the preamplifier reaches saturation where it can no longer output voltage pulses.

A "cloverleaf" XRF detection system composed of 4 HPGe detector crystals and 4 sets of electronics was tested with the higher activity Cd-109 source, due to its ability to process higher count rates compared to the single detector. This detector was introduced for XRF measurements in Paper II, and consists of four HPGe

detectors in a "cloverleaf" formation, with cross sectional areas of approximately 200 mm^2, and thicknesses of 10 mm (Canberra GL0210R/S). Each detector crystal is connected to its own set of pulse processing electronics, including a preamplifier (Canberra 2002CP), and DSA 1000 pulse processing system. Genie 2000 Gamma Analysis Software recorded a spectrum for each detector per measurement. Therefore, a single phantom measurement resulted in 4 spectra, which were exported to MATLAB for further analysis.

2.4 Gadolinium peak analysis

Each collected spectrum from a phantom, bone sample, or human measurements had several prominent features, which are displayed in Figure 2.8. The largest feature on every spectrum was the Compton backscatter peak, produced from 88 keV excitation γ-rays undergoing inelastic scattering with free electrons at an angle of 180^o. As previously mentioned in Section 2.2, the size of the detector crystal caused the Compton backscatter peak to be slightly shifted from its theoretical location. The double Compton backscatter peak at 52.1 keV is a result of the Compton backscattered photons passing through the detector and being backscattered again. An important peak on the spectrum, which was used to normalize interpatient variability for human measurements (Paper III), is the coherent scatter peak at 88 keV. This peak appeared on the spectrum from the 88 keV excitation γ-rays undergoing elastic scattering within the phantoms. The 88 keV excitation γ-rays released by Cd-109 were able to excite W present in the source or collimator, causing the production of W Kα x-rays at 57.9 and 59.3 keV. These x-rays could then undergo Compton backscatter at an angle of 180^o, producing a W Compton backscatter peak at 48.1 keV. This peak provided the greatest source of background when analyzing the Gd Kα x-ray peaks, which is why a significant effort was put towards eliminating W from both the source and collimator in Paper II. Lastly, the two most important peaks on the spectrum are the Gd Kα x-ray peaks at 42.3 and 43.0 keV. These peaks were often unresolvable by the human eye for lower concentration phantoms (0-12 ppm), and relied on a peak fitting algorithm for extraction from each spectrum.

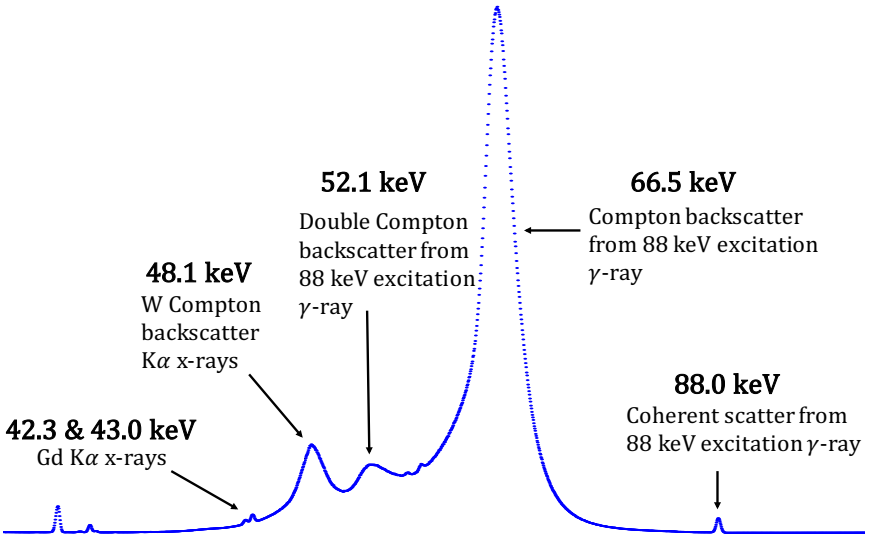

Figure 2.8: Spectrum features for a Gd bone phantom measurement. A bone phantom measurement was chosen as the example spectrum since it produced the clearest features.

A peak fitting algorithm was written in the form of a MATLAB (The MathWorks Inc., Natick, Massachusetts) script to fit the Gd peaks with a double Gaussian function and cubic polynomial background (Figure 2.9). The script used the built-in MATLAB function "fittype", which uses the method of Nonlinear Least Squares to fit a curve. The following equation was found to produce the best fit for the two Gd peaks and the background:

$$p_1x^3 + p_2x^2 + p_3x + p_4 + a_1e^{-\left(\frac{x-b_1}{c_1}\right)^2} + a_2e^{-\left(\frac{x-b_2}{c_2}\right)^2} \tag{2.1}$$

where, p_1, p_2, p_3, and p_4 are constants for the polynomial background fit, $a1$, $b1$, $c1$ are the height, center, and width of the Kα2 peak respectively, and $a2$, $b2$, $c2$ are the height, center, and width of the Kα1 peak respectively. The number of variables in the equation were reduced, with the intention of lowering the uncertainty of the fit, by fixing the widths of the Gaussian peaks ($c1$ and $c2$) obtained from a series of

measurements on high concentration phantoms, and fixing the distance between the Gd peak centres ($b1$ and $b2$). The peak height variables $a1$ and $a2$ were attempted to be fixed together in the early stages of developing the peak fitting algorithm. However, it was found that having too many variables tied together worsened the reduced chi-squared (χ^2) of the fit.

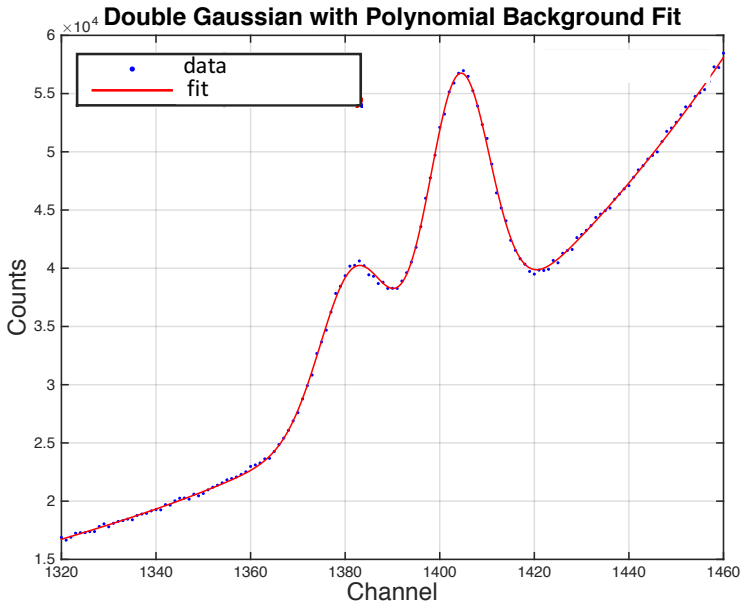

Figure 2.9: Gd Kα1 and Kα2 peaks fit with a double Gaussian and cubic polynomial function. Blue points represent the experimental data from a 120 μg Gd/g PoP bone phantom measurement, and the red line represents the fit.

The goodness of fit was measured by the reduced chi-squared statistic χ^2, which is the chi-squared value per degree of freedom:

$$\chi^2 = \sum_i \frac{\frac{(O_i - F_i)^2}{F_i}}{\nu} \tag{2.2}$$

where O is the observed data (counts), F is the fit data, and ν is the degree of freedom (number of observations minus the number of fitted parameters). Only fits that

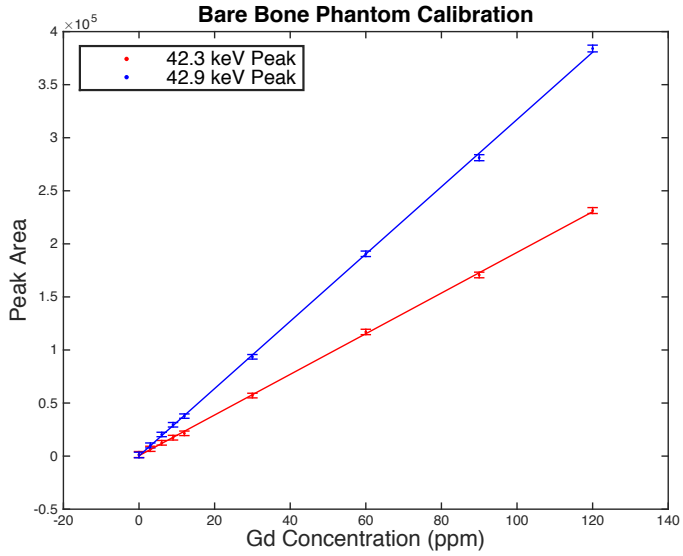

Figure 2.10: Phantom calibration lines created from plotting the area of each Gd peak as a function of known phantom concentration. The data points were fit using a linear regression, creating a calibration line for each Gd peak.

resulted in a χ^2 value of 1.0 $\pm$ 0.25 were accepted as appropriate for Gd peak area calculations. Accepted fitting parameters were then used to calculate the area under each Gd peak using the equation for the area of a Gaussian:

$$A = ac\sqrt{\pi} \tag{2.3}$$

where A is the area under one of the Gd peaks, a is the height of the peak, and c is the width of the peak. Since the peak fitting algorithm describes a Gaussian in the form: $ae^{-\left(\frac{x-b}{c}\right)^2}$, the peak width c is related to FWHM as follows: FWHM= 1.665c. The calculated areas of the Gd Kα x-ray peaks were plotted as a function of known phantom concentration and fit using a linear regression, creating two calibration lines for the Kα1 and Kα2 x-rays (Figure 2.10). Calibration lines were used to calculate the minimum detection limit of the XRF system (Section 2.4.1), as well as the Gd concentration in measured bone samples or human measurements (Section 2.4.2).

2.4.1 Minimum detection limit

The minimum detection limit (MDL) is defined as the minimum number of counts that can be sure of detection. My method for calculating the MDL consisted of using the relationship between peak area (A) and phantom concentration (x), to find the uncertainty in Gd concentration (σ_x).

The calibration lines shown in Figure 2.10 represent the relationship between the peak area of the Gd Kα1 (43 keV) and Kα2 (42.3 keV) peaks, and the Gd concentration in the phantoms. As the experiments were sequentially carried out with phantoms of higher Gd concentration, the area of both Kα peaks increased linearly.

The calibration lines from Figure 2.10 are in the form of:

$$A = Bx + C \tag{2.4}$$

where A is the peak area, B is the slope of the calibration line, x is the Gd concentration, and C is the intercept of the calibration line. To calculate the uncertainty in Gd concentration:

From Bevington (2003) [103],

if,

$$x = f(u, v, ...)$$

then,

$$\sigma_x{}^2 = \sigma_u{}^2 \left(\frac{\partial x}{\partial u}\right)^2 + \sigma_v{}^2 \left(\frac{\partial x}{\partial v}\right)^2 + ... + 2\sigma_{uv}{}^2 \left(\frac{\partial x}{\partial u}\right)\left(\frac{\partial x}{\partial v}\right)$$

Rearranging the calibration line equation for x gives:

$$x = \frac{A}{B} - \frac{C}{B} \tag{2.5}$$

So,

$$\begin{aligned}{\sigma_x}^2 = {\sigma_A}^2 \left(\frac{\partial x}{\partial A}\right)^2 + {\sigma_B}^2 \left(\frac{\partial x}{\partial B}\right)^2 + {\sigma_C}^2 \left(\frac{\partial x}{\partial C}\right)^2 \\ + 2{\sigma_{AB}}^2 \left(\frac{\partial x}{\partial A}\right)\left(\frac{\partial x}{\partial B}\right) + 2{\sigma_{BC}}^2 \left(\frac{\partial x}{\partial B}\right)\left(\frac{\partial x}{\partial C}\right) + 2{\sigma_{AC}}^2 \left(\frac{\partial x}{\partial A}\right)\left(\frac{\partial x}{\partial C}\right)\end{aligned} \tag{2.6}$$

where ${\sigma_{AB}}^2, {\sigma_{BC}}^2, {\sigma_{AC}}^2$ are covariances. However, since the area of the peaks (A) is independent of the slope and intercept of the calibration line, the covariances ${\sigma_{AB}}^2$ and ${\sigma_{AC}}^2$ are zero.

Taking the partial derivatives from equation 2.5 gives:

$$\begin{aligned}\left(\frac{\partial x}{\partial A}\right) &= \frac{1}{B} \\ \left(\frac{\partial x}{\partial B}\right) &= -\frac{A-C}{B^2} \\ \left(\frac{\partial x}{\partial C}\right) &= -\frac{1}{B}\end{aligned}$$

Plugging these partial derivatives into equation 2.6 results in:

$${\sigma_x}^2 = \frac{{\sigma_A}^2}{B^2} + \frac{{\sigma_B}^2(A-C)^2}{B^4} + \frac{{\sigma_C}^2}{B^2} + 2\frac{{\sigma_{BC}}^2(A-C)}{B^3} \tag{2.7}$$

The minimum detection limit was then calculated using the result from equation 2.7 in the following relationship: $MDL = 2\sigma_x$. The MDLs for the Kα1 and Kα2 were calculated separately, then combined using inverse variance weighting. However, since the MDL is an uncertainty in concentration, the variance of the inverse variance weighted average was used:

$$MDL^2 = \frac{1}{1/{MDL_1}^2 + 1/{MDL_2}^2}$$

For the cloverleaf system, since four spectra were obtained per measurement, four sets of Gd peaks were fit, and four MDLs were calculated. The MDLs were then combined through inverse variance weighting further.

2.4.2 Gd concentration calculation

In this thesis work, Gd concentrations were calculated for measurements performed on autopsy bone samples in Paper II, as well as for *in vivo* human measurements in Papers IV & V. For the work in Paper II, our research group received autopsy bone samples from the Wadsworth Center's Trace Elements lab. I performed XRF measurements with the cloverleaf XRF system and obtained four spectra for each measurement. The Gd peaks from each spectrum were fit appropriately and their areas were calculated, as described in Section 2.4. A MATLAB script was written to calculate Gd concentration (x) using the peak area (A) and calibration line coefficients (B, C) with equation 2.5. A Gd concentration was calculated for each of the four detectors (x_1, x_2, x_3, x_4) then combined using inverse variance weighting to obtain a final Gd concentration (x_{Total}) for the measured bone sample:

$$x_{Total} = \frac{x_1/{\sigma_{x_1}}^2}{1/{\sigma_{x_1}}^2} + \frac{x_2/{\sigma_{x_2}}^2}{1/{\sigma_{x_2}}^2} + \frac{x_3/{\sigma_{x_3}}^2}{1/{\sigma_{x_3}}^2} + \frac{x_4/{\sigma_{x_4}}^2}{1/{\sigma_{x_4}}^2}$$

The error in final concentration (σ_{xTotal}) was calculated using the standard deviation of the inverse variance weighted average:

$$\sigma_{xTotal} = \sqrt{\frac{1}{1/{\sigma_{x_1}}^2} + \frac{1}{1/{\sigma_{x_2}}^2} + \frac{1}{1/{\sigma_{x_3}}^2} + \frac{1}{1/{\sigma_{x_4}}^2}}$$

At the time of these bone sample measurements, the MDL of the system was 0.78 μg Gd/g PoP for a 30 minute measurement time and excitation source activity of 4.7 GBq. Therefore any calculated concentration below 0.78 μg Gd/g PoP was considered to be within statistical error and the sample was labelled as containing "zero Gd".

At the time of measurement for the work in Paper II, the cloverleaf XRF system had been calibrated with the set of PoP phantoms. Therefore, the units of concentration for all measured autopsy bone samples were μg Gd/g PoP. Although PoP is a material that is commonly used to simulate human cortical bone, the composition is not exactly the same, leading to different contributions of coherent scatter in each material. This causes Gd concentrations measured in bone not to be directly comparable to Gd concentrations in the POP phantoms. Since Gd incorporates into bone mineral, the desired units of measurement are μg Gd/g bone mineral. In order to convert concentration units of μg Gd/g PoP to μg Gd/g bone mineral, a coherent conversion factor (CCF) was calculated to find the ratio of the differential coherent scattering cross sections for PoP and bone mineral. The details of the CCF calculation are described in Paper II, and resulted in a conversion factor of 1.46 when converting from μg Gd/g PoP to μg Gd/g bone mineral.

For the *in vivo* human measurements carried out in Papers IV & V, the cloverleaf XRF system had been calibrated with the set of HPa phantoms. Therefore, the units of concentration calculated for all human measurements were in μg Gd/g HPa, which is equivalent to μg Gd/g bone mineral, since bone mineral is composed of HPa. Using HPa bone phantoms allowed for the additional step of using the CCF to be removed when calculating the concentration of Gd in bone, thus reducing the uncertainty in the calculated value.

Chapter 3

Paper I: A phantom-based feasibility study for detection of gadolinium in bone *in-vivo* using x-ray fluorescence

The following five chapters contain the five papers that comprise the work of this thesis. Each paper represents an important step in this thesis work, beginning with the development of the XRF detection system to detect Gd in bone, ending with human measurements in individuals who self-report themselves to be symptomatic of Gd toxicity. Each paper will be prefaced with a summary of the project, as well as my contribution to each project.

These papers focus on the development of an XRF-based detection system consisting of a Cd-109 excitation source and a four-element "cloverleaf" HPGe detector, which was then used to conduct the first non-invasive human measurements of Gd in bone in a small pilot study. Papers I and II are phantom-based studies that investigate the feasibility of using XRF-based detection systems to measure Gd in bone *in vivo*. Paper I used a set of 9 PoP bone phantoms with increasing Gd concentration and a single HPGe detection system to calculate the MDL of the system. From this study, it was concluded that an XRF detection system is feasible for carrying out

measurements of Gd in bone. However, significant improvements to the system were needed before human measurements could be performed. An updated Cd-109 source with a higher activity of 5 GBq was needed, along with an upgraded cloverleaf HPGe detector to allow for a higher count rate to be processed. Paper II tested the feasibility of this updated system for detecting Gd in bone, and calculated MDLs for this system using PoP bone phantoms. MDLs for this system were shown to be within previously measured concentrations of Gd in bone in published literature. This system was also cross validated by measuring autopsy bone samples that had also been measured using the sensitive technique of ICP-MS. Gd concentrations measured with XRF were comparable to ICP-MS measurements, validating the XRF detection system further for human measurements. Before human measurements could take place, the challenge of interpatient variability for XRF measurements, such as variation in tissue thickness overlaying the tibia, needed to be addressed. In Paper III, normalization of the Gd Kα x-rays with the coherently scattered excitation γ-ray was explored to correct for interpatient variability through phantom measurements, as well as Monte Carlo simulations. Experimental and simulation results deemed coherent normalization to be a valid approach, as the Gd peak area to coherent peak area ratio remained constant across a range of tissue thicknesses. Paper IV contains the first reported successful non-invasive measurement of Gd retention in human bone. In this small pilot study, the cloverleaf XRF detection system was used to measure a small population: 11 individuals who had previously received GBCAs, and 11 control individuals who had never received GBCAs. Gd concentration in bone was found to be significantly higher in the exposed group compared to the control group, and the XRF system was deemed successful in measuring Gd bone concentration in small populations. Upon publishing the study, I was contacted by numerous individuals with self-reported symptoms of Gd toxicity. Since all measurement subjects in Paper IV were healthy adult volunteers, I was eager to perform additional measurements on these individuals with symptoms of Gd toxicity. Paper V presents additional Gd bone measurements for this exposed group along with additional controls. Gd urine measurements were also carried out to compare Gd concentrations in excreted urine to measured Gd concentrations in bone. In Paper V, I analysed Gd concentration in bone and urine for 3 groups of participants: control, symptomatic exposed, and

non-symptomatic exposed. The results of this paper opened further questions as well as possible avenues for investigating the retention of Gd in the body, as I found a strong correlation between Gd concentration excreted in the urine and GBCA dose, yet no correlation between Gd urine concentration and Gd concentration in bone. This suggests that there are long-term storage sites of Gd in the body, other than bone.

A phantom-based feasibility study for detection of gadolinium in bone in-vivo using x-ray fluorescence

M.L. Lord, F.E. McNeill, J.L. Gräfe, M.D. Noseworthy and D.R. Chettle, Appl. Radiat. Isot., **112**, 103-109 (2016).

Paper I investigated the feasibility of using the technique of XRF with a single HPGe detection system for non-invasively measuring Gd in the tibia bone. This was a phantom-based study in which a set of 9 PoP phantoms with increasing Gd concentration were measured with varying thicknesses of overlaying tissue equivalent material (SolidWater®). Throughout the phantom measurements, the activity of the Cd-109 source was approximately 0.11 GBq, 45 times weaker than its initial activity of 5 GBq. Given the low excitation source activity, bare bone phantoms and bone phantoms with a tissue overlay of 5.5 mm were measured for 20-hour counting periods to ensure Gd peaks were present on the collected spectra. Following these experiments, I cut holes in a SolidWater® disk at varying depths to account for possible differences in body compositions. Creating this phantom allowed for measurements with tissue thicknesses of 3.3 ± 0.1, 4.0 ± 0.1, 7.5 ± 0.1, and 12.2 ± 0.1 mm overlaying the bone phantom, which produced 36 additional measurements. Therefore, due to time restrictions, the counting periods for these additional measurements were decreased from 20 hours to 7 hours. MDLs calculated from the 20-hour counting periods were scaled to 7-hour counting periods for comparison, using the relationship of MDL $\propto 1/\sqrt{t}$, where t is the measurement time.

For a 20-hour counting time, the MDL for this system was found to be 0.87 ppm for bare bone phantoms, and an increased value of 1.34 ppm for a tissue overlay of 5.5 mm, due to the increased photon attenuation decreasing the intensity of the Gd Kα x-rays. All MDLs were scaled to realistic counting times of 30 min (live time) for human measurements, from which it was clear that for a successful *in vivo* XRF measurement of Gd in tibia bone, the strength of the Cd-109 source would need to be greatly improved. Results from this study were scaled to predict MDLs for two upgraded XRF systems: (1) The current single HPGe detection system with a 1 GBq

source, and (2) the four element cloverleaf HPGe detection system with a 5 GBq source. The most significant improvement to the system was predicted to be a result of increasing the activity of the source to 5 GBq, and updating the single HPGe detection system to a cloverleaf HPGe detection system, which could handle a higher count rate. Using the source strength ratio of the new source (A) to the original source (A_0) through the relationship MDL $\propto 1/\sqrt{A/A_0}$, and the predicted dead time for the cloverleaf detector, the MDL for the cloverleaf system was predicted to be 0.98 ppm for a 30 min measurement.

The work in this paper demonstrated that it was feasible to use the XRF system for measuring Gd in bone, given that system improvements were made. The suggestion of a new high activity source and cloverleaf system were predicted to result in acceptable MDLs, a factor of 2.4 times lower than the system used in this paper, and that the improved system should be investigated further before human measurements take place.

This project was suggested by David Chettle and Fiona McNeill as the first step in designing a system to measure Gd in bone using XRF. The experimental design and setup, as well as phantom production and phantom measurements were completed by myself, under the supervision of David Chettle and Fiona McNeill. I wrote the algorithm for fitting Gd peaks, as well as the script for calculating the MDLs. James Gräfe and Mike Noseworthy provided additional expert guidance throughout the project. I wrote the first draft of the manuscript, which was then revised by the co-authors of this paper.

Applied Radiation and Isotopes 112 (2016) 103–109

Contents lists available at ScienceDirect

Applied Radiation and Isotopes

journal homepage: www.elsevier.com/locate/apradiso

A phantom-based feasibility study for detection of gadolinium in bone *in-vivo* using X-ray fluorescence

M.L. Lord [a,*], F.E. McNeill [a], J.L. Gräfe [b], M.D. Noseworthy [a,c,d,e,f], D.R. Chettle [a]

[a] Department of Medical Physics and Radiation Science, McMaster University, Main St. W., Hamilton, Canada L8S 4L8
[b] Department of Physics, Ryerson University, Victoria St., Toronto, Canada M5B 2K3
[c] McMaster School of Biomedical Engineering, McMaster University, Main St. W., Hamilton, Canada L8S 4L8
[d] Imaging Research, St. Joseph's Healthcare, Charlton Ave. E., Hamilton, Canada L8N 4A6
[e] Department of Radiology, McMaster University, Main St. W., Hamilton, Canada L8S 4L8
[f] Department of Electrical and Computer Engineering, McMaster University, Main St. W., Hamilton, Canada L8S 4L8

HIGHLIGHTS

- The feasibility of using X-ray fluorescence to detect gadolinium in bone *in vivo* is explored.
- Bone phantoms mimicking human tibia were doped with gadolinium concentrations ranging from 0 to 120 ppm.
- The current X-ray fluorescence system results in a minimum detection limit of 3.60–3.64 ppm.
- A stronger source and improved detector system predicts an improved minimum detection limit of 1.49–1.52 ppm.

ARTICLE INFO

Article history:
Received 6 January 2016
Received in revised form
18 March 2016
Accepted 19 March 2016
Available online 21 March 2016

Keywords:
X-ray fluorescence (XRF)
Gadolinium
MRI
Minimum detection limit

ABSTRACT

Gadolinium (Gd) based contrast agents have been commonly used over the past three decades to improve contrast in magnetic resonance imaging. These complexes, originally thought to be stable and clear from the body shortly after administration, have been shown to dissociate to a small extent and deposit in organs such as bone. A safe and non-invasive method for measuring Gd in bone is necessary for further exploring Gd retention in the body following the administration of a contrast agent. A feasibility study using a K x-ray fluorescence (K-XRF) system to measure Gd in human tibias was investigated. Bone phantoms mimicking human tibia were created with Gd concentrations ranging from 0 to 120 ppm. The minimum detection limit (MDL) was calculated from 20-hour and 7-hour phantom measurements with a source activity of 0.11 GBq. All MDL values were scaled to a more realistic measurement time of 30-minutes with a stronger source. Scaling arguments were based on activity ratio, measurement time, and system dead time. The MDL for a 1 GBq source was estimated to be 3.60–3.64 ppm, for an average range of tissue thicknesses overlaying a human tibia. For a stronger source of 5 GBq and a four detector cloverleaf system, the MDL was estimated to be 1.49–1.52 ppm. Determined and predicted MDLs are within the range of previous *in-vitro* Gd measurement data. The K-XRF system shows promising results for detecting Gd in bone and should be seriously considered for in-vivo measurements.

1. Introduction

Gd based contrast agents are used on a regular basis in hospitals world-wide to enhance the quality of magnetic resonance imaging. The 7 unpaired electrons in the Gd^{3+} ion are responsible for paramagnetic properties causing a proton relaxation effect. This distinct effect on relaxation times in magnetic resonance imaging was first investigated in the early 1980s to test the viability of using Gd ions and chelates as contrast agents (Weinmann et al., 1984; Carr et al., 1984). Gd chelates were originally thought to be completely stable, clearing from the body with a short half-life of less than 2 h. However, for patients with renal disease, the Gd chelates cannot be excreted at the same rate, remaining in the body for 30–120 h (Joffe et al., 1998). The longer the Gd complexes remain in the body, the higher the probability of the complex dechelating, producing free Gd ions (Grobner, 2006). In 2006, Grobner and Marckman linked Nephrogenic Systemic Fibrosis (NSF) to the use of Gd contrast agents in patients with renal disease, as all patients with NSF had received a Gd contrast agent

* Corresponding author.
E-mail addresses: lordml@mcmaster.ca (M.L. Lord), fmcneill@mcmaster.ca (F.E. McNeill), james.grafe@ryerson.ca (J.L. Gräfe), nosewor@mcmaster.ca (M.D. Noseworthy), chettle@mcmaster.ca (D.R. Chettle).

http://dx.doi.org/10.1016/j.apradiso.2016.03.021
0969-8043/

prior to developing symptoms (Grobner, 2006; Marckmann et al., 2006; Thomsen et al., 2006).

Since rare earth elements such as Gd are bone-seeking, free Gd ions have the possibility of depositing in bone, causing a long-term source of Gd in the body. This may explain the increasing severity of NSF over time (Abraham et al., 2008; Thakral et al., 2007). Separate studies lead by Darrah et al. and White et al. measured Gd concentration in the femoral head of patients who had undergone hip replacement surgery, as well as received previous contrast enhanced MRI scans. Both studies produced evidence of unusually high Gd concentrations in bone samples of patients who had previously received a contrast agent with a Gd chelate. The accumulation of Gd in bone indicates the instability of Gd chelates *in-vivo*, resulting in the release of Gd^{3+}. Combining data from both studies results in a range of 0.42–6.02 ppm for Gd concentrations measured in bone (Darrah et al., 2006; White et al., 2006).

As of late, multiple studies have produced evidence suggesting Gd retention can also occur in patients with normal renal function, due to the dechelation of Gd contrast agents in the body (Kanal and Tweedle, 2015). Through a series of MRI scans, T1 signal intensity was observed to increase linearly with respect to the number of past Gd contrast agents the patients had received (Errante et al., 2014; Kanda et al., 2013; McDonald et al., 2015). The increase in T1 signal intensity supports the hypothesis that Gd ions are dissociating from their chelate form and being retained in the body long term, regardless of the patients' renal function. Clincal implications of the dissociation of Gd^{3+} are currently unknown and warrant further investigation (Kanal and Tweedle, 2015).

Currently, measurements of Gd retained in bone have only been carried out *in-vitro* on femoral heads of patients who have received hip replacements (Darrah et al., 2006; White et al., 2006). A non-invasive *in-vivo* method for measuring Gd in bone of patients who previously received Gd based contrast agent would be both convenient and beneficial for further exploring the clinical implications of dissociated Gd complexes in the body. We have tested the feasibility of using a K-XRF system for non-invasively measuring the concentration of Gd in the tibia. A set of anthropomorphic bone phantoms were created with varying concentrations of Gd, as well as varying thicknesses of overlaying tissue equivalent material, to create a realistic *in-vivo* experimental setup and accurate estimations of detection limits for the K-XRF system.

2. Methods

2.1. Phantom preparation

In this study, the tibia was chosen as the location for Gd measurement in bone. The main reason being that the tibia has a relatively thin layer of overlying tissue, reducing X-ray and γ-ray attenuation. Since the tibia is located in an extremity of the body, the dose to the core of the body can be minimized, which also provides comfort for future volunteers being measured with this system. To keep the phantoms anthropomorphic, clear plastic cylindrical containers with a length of 115.0 mm, diameter of 28.0 mm, and wall thickness of 1.0 mm were used to contain the bone equivalent material of the tibia. A total of 9 cylindrical shaft phantoms were prepared using Plaster of Paris (PoP) to represent bone, containing varying concentrations of Gd for measurement purposes. To ensure a homogeneous distribution of Gd throughout the PoP, a Gd stock solution was diluted in nitric acid to obtain the various Gd concentrations prior to mixing with PoP. Phantoms of concentrations: 0, 3, 6, 9, 12, 30, 60, 90, and 120 ppm were prepared. More phantoms were prepared at low Gd concentration (in the 0–12 ppm range), since this is the range of Gd content that previous studies have found in bone samples. Higher concentration phantoms were included for calibration purposes.

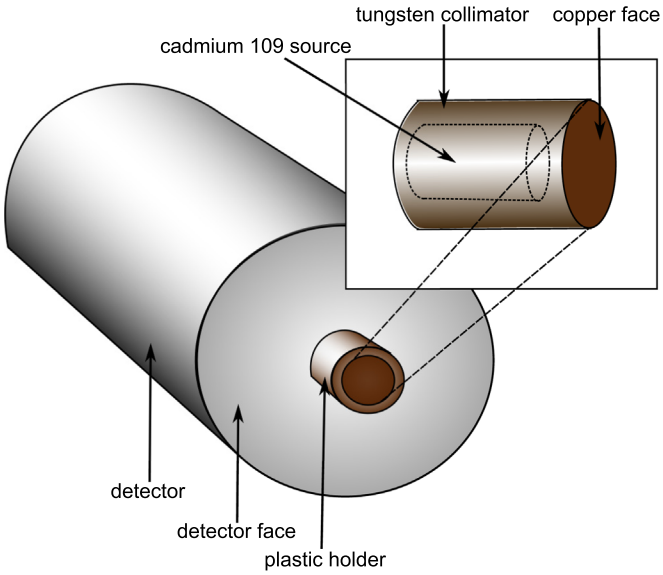

Fig. 1. Detector face with plastic holder containing the tungsten collimator and Cd-109 source.

2.2. Experimental setup

Measurements were taken on the K-XRF system using the Cd-109 excitation source, producing γ-rays of 88 keV and silver X-rays in the range of 22–24 keV. The Cd-109 source is encased in a tungsten collimator with a copper face to eliminate the silver X-rays, while allowing the 88 keV γ-rays to pass through. The tungsten collimator containing the source was placed in a plastic holder on the face of the detector with the copper face directed towards the phantom (Fig. 1). The activity of the Cd-109 source was 5 GBq when first obtained on April 21, 2008. Experiments for this study were carried out approximately 7 years later (approximately 5.5Cd-109 half lives), which puts the activity of the source at 0.11 GBq at the time of the experiments, 45 times weaker than the initial activity.

The K-XRF system used was composed of a high-purity germanium (HPGe) detector and pulse processing electronics from Canberra Industries, Inc. (Meriden, Connecticut, 06450, USA). The higher atomic number of germanium (Ge) allows for more attenuation within the detector crystal, and therefore hard x-rays such as the Gd x-rays of interest can be detected. Due to the small band gap energy of Ge, the Ge crystal is enclosed in a vacuum tight container within a liquid nitrogen cooled cryostat to avoid any leakage current. The detector used (Canberra GL 2020R) has a Ge crystal 20 mm thick and 2000 mm^2 in cross sectional area, and is located behind a thin 0.5 mm beryllium window. The detector output first travels through a preamplifier (Canberra 2001 CP), then to a digital pulse processing system (Canberra DSA 1000). The spectra are collected using Genie 2000 Gamma Analysis Software from Canberra, then transferred to MATLAB for further analysis.

2.3. Spectra collection

Counts were first collected from each of 9 tibia phantoms with no additional overlying material, essentially representing bare bone. A counting time of 20 h for each phantom was used; long enough to ensure the Gd peaks were present in the collected spectra given the low activity of the Cd-109 source used. The bone phantom was placed closely at 1 mm from the copper face of the tungsten collimator to maximize the counts collected. The

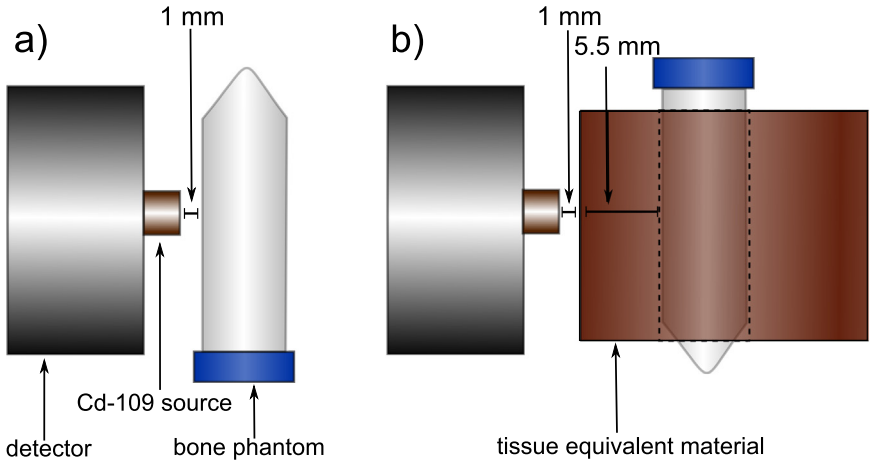

Fig. 2. Experimental setup for 20-hour count collection for (a) bone phantom with no overlying tissue equivalent material and (b) bone phantom with a tissue equivalent material overlay of 5.5 ± 0.1 mm.

measurements were repeated on the same set of phantoms but with an overlaying tissue equivalent material (Solid Water®) of 5.5 ± 0.1 mm. Refer to Fig. 2 for experimental setup diagrams for the 20-hour count times.

Experiments were repeated with varying overlaying tissue thickness in order to account for different body compositions of future volunteers. The set of 9 tibia phantoms was measured with overlaying tissue equivalent material (Solid Water®) of 3.3 ± 0.1, 4.0 ± 0.1, 7.5 ± 0.1, and 12.5 ± 0.1 mm. A counting time of 7 h for each phantom was used instead of 20 h due to time constraints. The source-to-phantom distance remained 1 mm, as it was in the 20-hour count experiments, for consistency.

2.4. Gadolinium peak fitting

Two Gd peaks were present on the collected spectra: Kα1 at 42.99 keV, and Kα2 at 42.31 keV. A sample of a collected 20 h spectrum is shown in Fig. 3. The Gd peaks were extracted from each spectrum and analyzed using a MATLAB script designed to find the peaks, fit them as two Gaussians with a polynomial background, and calculate the area of the peaks. A cubic polynomial was chosen to describe the background of the Gd peaks. Although exponentials and quadratic polynomials are more commonly used, we found the cubic polynomial gave the most accurate fit, as it resulted in the best χ^2 values. The method of Non-Linear Least Squares was used to attain a fit for the peaks with the following equation:

$$p_1x^3 + p_2x^2 + p_3x + p_4 + a_1e^{-\left(\frac{x-b_1}{c_1}\right)^2} + a_2e^{-\left(\frac{x-b_2}{c_2}\right)^2} \quad (1)$$

where, p_1, p_2, p_3, and p_4 are constants for the polynomial background fit, $a1$, $b1$, $c1$ are the height, center, and width of the Kα2 peak respectively, and $a2$, $b2$, $c2$ are the height, center, and width of the Kα1 peak respectively. The Gd peak widths $c1$ and $c2$ were obtained through a series of count periods on high concentration phantoms and included as fixed parameters in the fitting algorithm, along with the distance between the two peak centers $b2 - b1$.

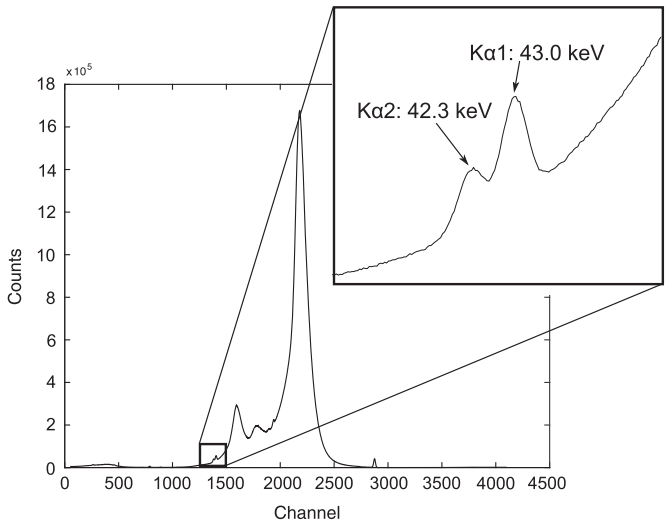

Fig. 3. Sample spectrum for 20-hour counting time of 120 ppm bare bone phantom. Gadolinium Kα2 and Kα1 are located at 42.3 keV and 43.0 keV respectively.

2.5. Minimum detection limit

The minimum detection limit (MDL) is defined as two times the uncertainty of Gd concentration, which theoretically should be the lowest Gd concentration that our system can detect. To find the MDL of the K-XRF system, the relationship between Gd peak area and the respective concentration of the phantoms is plotted and fit using a linear regression. The fit line is referred to as the calibration line and takes the form:

$$A = Bx + C \quad (2)$$

where A is the peak area, B is the slope of the calibration line, x is the Gd concentration, and C is the intercept of the calibration line. Using the approach described by Bevington, (Bevington and Robinson, 2003), the uncertainty for x can be expressed as:

$$\sigma_x^2 = \frac{\sigma_A^2}{B^2} + \frac{\sigma_B^2(A-C)^2}{B^4} + \frac{\sigma_C^2}{B^2} + 2\frac{\sigma_{BC}^2(A-C)}{B^3} \quad (3)$$

where σ_x is the uncertainty in Gd concentration, σ_A is the uncertainty of peak area, σ_B is the uncertainty of the calibration line slope, σ_C is the uncertainty of the calibration line intercept, and σ_{BC}^2 is the covariance between the calibration line slope and intercept. The MDL is defined as $MDL = 2\sigma_x$, and was calculated for each of the two Gd peaks, then combined through an inverse variance weighted mean to give an overall MDL for both Gd peaks (Chamberlain et al., 2012).

$$MDL = \left(\frac{1}{1/MDL_1^2 + 1/MDL_2^2}\right)^{1/2} \quad (4)$$

Experiments were run over three months, which means the Cd-109 source activity was decreasing over that time period. The

activity of the source at the start of each experiment was calculated and used to find the activity ratio A/A_0, which is the ratio of the current activity to the initial activity at the start of the first experiment (0.11 GBq). Since the MDL is proportional to the square root of the activity ratio, each MDL value was scaled to account for the decaying source.

3. Results

Spectra were collected for each of the 9 phantoms using 20-hour counts on both bare bone phantoms and bone phantoms with a tissue overlay of 5.5 ± 0.1 mm. Experiments were then repeated on the 9 phantoms for varying overlaying tissue thickness, this time for 7-hour counts due to time constraints. Both sets of experiments were analyzed using the methods previously described. The fit for the Gd peaks agreed well with the spectra, resulting in an average chi squared value of 1.01, ranging from 0.84 to 1.22, for the 20-hour count spectra. The fits for the 7-hour counts had similar results with an average chi squared value of 1.01, ranging from 0.82 to 1.25. An example fit for the Gd peaks is shown in Fig. 4 for a 20-hour count on the 120 ppm bare bone phantom.

3.1. 20-hour count data for bare bone and tissue overlay phantoms

All spectra collected from both the bare bone phantoms and tissue overlay phantoms were fit to determine the area of the Kα1 and Kα2 Gd peaks. The areas were then plotted as a function of the known Gd concentration for each phantom and, subsequently, fit using a linear regression to create a calibration line for each Gd peak. From the calibration lines, the MDL for each peak was calculated as well as a combined MDL.

The calibration lines for the bare bone and tissue overlay phantoms are displayed in Fig. 5. The decrease in slope going from the Kα1 to Kα2 peak represents the higher relative intensity of the Kα1 emission line. The decrease in slopes going from the bare bone calibration lines to the tissue overlay calibration lines represents an increase in the MDL. Having overlaying tissue causes more attenuation of both the incoming 88 keV γ-ray as well as the exiting Gd x-rays. Since fewer Gd x-rays are hitting the detector, the MDL will increase for a tissue overlay. The MDLs calculated are consistent with this, as the MDL for the bare bone phantoms is 0.87 ppm and increases to 1.34 ppm with the added 5.5 ± 0.1 mm of overlaying tissue. The calculated MDLs for each calibration line are summarized in Table 1.

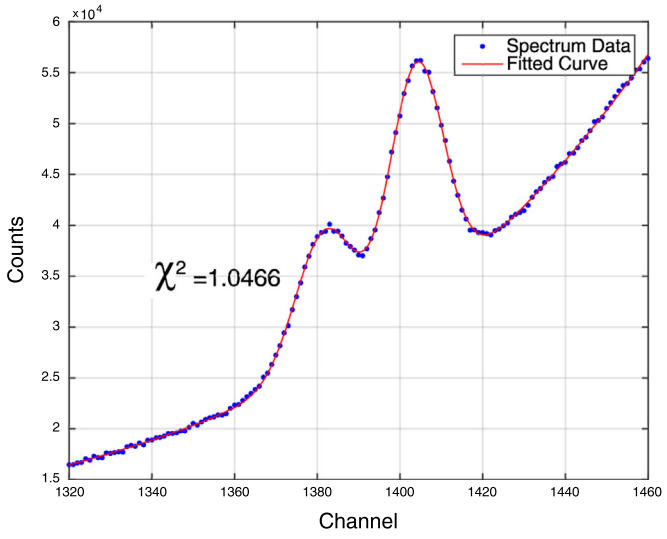

Fig. 4. Sample fit for Gd peaks from the 120 ppm bare bone phantom for a 20-hour counting time. Spectrum data are represented by the blue dots, and the fit is represented by the red curve. This fit agrees well with the data and results in a chi squared value of 1.05. (For interpretation of the references to color in this figure legend, the reader is referred to the web version of this article.).

3.2. 7-hour count data for varying tissue thickness phantoms

The experimental procedure used for the 20-hour counts was repeated for the same set of bone phantoms, but with varying overlaying tissue thicknesses. These experiments were carried out to investigate how varying tissue thickness over the tibia will affect the MDL for *in-vivo* measurements, since body composition varies from person to person. A shorter count time of 7-hours was used for four different thicknesses: 3.3 ± 0.1, 4.0 ± 0.1, 7.5 ± 0.1, and 12.5 ± 0.1 mm. Gd peak area was again plotted against the known phantom concentration, which was fit to create calibration lines. A total of 8 calibrations lines were generated: a Kα1 and Kα2 line for each of the four tissue thickness values.

Calculated MDLs are plotted as a function of tissue thickness in Fig. 6, and follow a non-linear decrease as the overlaying tissue becomes thinner. This is an anticipated result since one would expect less attenuation with less tissue. The MDLs appear to level off once the tissue thickness is 4 mm or less, as the MDL for the 3.3 ± 0.1 and 4.0 ± 0.1 mm tissue overlay are not statistically different. The MDL from the 20-hour count on the bone phantom with 5.5 ± 0.1 mm tissue overlay was scaled down to an MDL value for 7 h, using the relationship MDL $\propto 1/\sqrt{t}$. The data points scaled from the 20-hour count experiment are shown as triangles in Fig. 6 and are consistent with the other MDL values from the 7-hour counts.

4. Discussion

This study was conducted as an investigation of feasibility for *in-vivo* measurements. Since count times were 20 h and 7 h long, the MDLs should be scaled to give estimates for a more realistic count time of 30 min, for volunteers to be measured on the K-XRF system in our lab. For a shorter counting time to be successful in detecting Gd, the source activity would need to be improved by replacing the current source with a new source of higher activity. Improvements to the K-XRF system equipment is also a viable step to improve detection limits. One option is to switch to a cloverleaf detection system, which consists of four detectors and four sets of electronics, rather than one detector and one set of electronics. A further improvement to the current K-XRF system for *in-vivo* measurements would be to upgrade the equipment for pulse processing, using pulse pileup recognition and restoration. The last item to be addressed for the possibility of *in-vivo* measurements is the dose that volunteers would receive from having their leg exposed to the source for a 30 min measurement.

4.1. MDL for 30 min count time and 1 GBq source

The current Cd-109 source could be replaced by purchasing a new 5 GBq source. However, the current electronics used in the K-XRF system cannot process a count rate from a source with an activity greater than 1 GBq. Therefore, the phantom or volunteer's leg would have to be placed at a distance from the source where the activity is equivalent to 1 GBq. All MDL calculations for a stronger source will be carried out for an activity of 1 GBq for this reason. The MDL for a new 1 GBq source can be predicted by using the argument that the MDL is proportional to the square root of the source strength ratio: MDL $\propto \sqrt{A/A_0}$, where A is the activity of

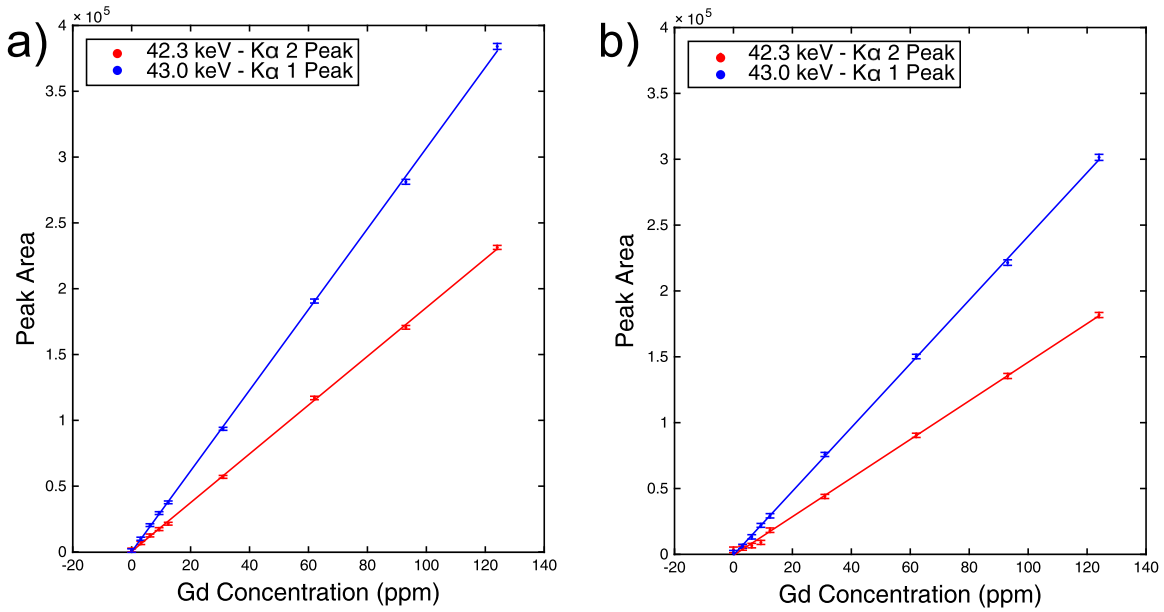

Fig. 5. Measured Gd peak area as a function of known Gd phantom concentration, creating calibration lines for (a) the bare bone phantoms and (b) phantoms with a tissue overlay of 5.5 ± 0.1 mm, both with a 20-hour count time. Peak areas for the Kα1 peak are plotted in blue and areas for the Kα2 peak are plotted in red, both with error bars. Calibration lines are overlaying each set of data with their respective colors. All four calibration lines have an R-squared value of 0.999. (For interpretation of the references to color in this figure legend, the reader is referred to the web version of this article.).

Table 1
Summary of MDL values calculated for 20-hour counting times.

	Bare bone phantom	Tissue overlay phantom
Kα1 MDL (ppm)	1.06	1.51
Kα2 MDL (ppm)	1.52	2.88
Combined MDL (ppm)	**0.87**	**1.34**

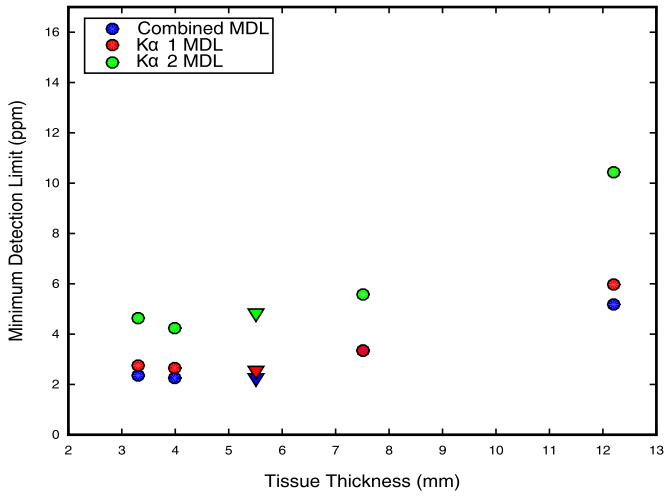

Fig. 6. MDL as a function of tissue thicknesses for a 7-hour count time. Green data points represent Kα2 values, red data points represent Kα1 values, and blue data points represent the combined MDL. Triangle data points are MDL values scaled from the 20-hour counts on the phantoms with 5.5 ± 0.1 mm tissue overlay. (For interpretation of the references to color in this figure legend, the reader is referred to the web version of this article.).

the new source and A_0 is the activity of the original source (0.11 GBq). In this case, the source strength ratio is 9.09. Dead time is negligible for the original source, and is estimated to be around 40% for a 1 GBq source, given the current detector equipment used. This means approximately 60% of events hitting the detector will be counted, decreasing the source strength ratio to 5.45. Taking the square root of the source strength ratio, as well as accounting for dead time, results in a factor of 2.33. Therefore, using a 1 GBq source will decrease the MDL by a factor of 2.33. To scale the new MDL values to a counting time of 30 minutes, the relationship of MDL $\propto 1/\sqrt{t}$, was used.

Using both the source and time scaling arguments, the MDL for bare bone phantoms was calculated to be 2.35 ppm. The MDLs for the bone phantoms with different tissue overlays are displayed in Fig. 7a. The combined MDL values range from 3.82 ppm for the thinnest overlay of 3.3 ± 0.1 mm, to 8.33 ppm for the thickest overlay of 12.5 ± 0.1 mm. The average value of tissue thickness over the tibia, measured by Pejović-Milić et al., was found to be 4.8 ± 0.2 mm and is shown by the yellow highlighted region in Fig. 7a, with the thicknesses above and below the average value highlighted as representative. The study conducted by Pejović-Milić et al. reported the average overlaying tissue thickness for 10 healthy volunteers, 5 male and 5 female, ranging from 20 to 67 years of age (Pejović-Milić et al., 2002). The MDL values for the 4.0 ± 0.1 and 5.5 ± 0.1 mm tissue thicknesses, which are 3.60 and 3.64 ppm respectively, will be used as a standard for analysing the feasibility of the current K-XRF system for *in-vivo* measurements, since they are the closest tissue thicknesses to the measured average value.

Concentrations of Gd previously found in bone range from 0.47 to 6.02 ppm (Darrah et al., 2006; White et al., 2006), which is the red highlighted region in Fig. 7a. It is clear that the MDLs for an average tibia thickness fall well within the range of recorded Gd concentrations in bone, making the K-XRF system feasible for detecting Gd in the tibia over a 30 min measurement. The data points for the 12.5 ± 0.1 mm tissue thickness fall outside the red highlighted region, limiting measurements to volunteers with less than approximately 10 mm of tissue overlay. It is important to note that Gd concentrations in bone are not always reported in the same units. The previous measurements in bone were reported in units of ppm ($\mu g\, Gd^{-1}\, g$) wet bone, where our phantom concentration units are ppm ($\mu g\, Gd^{-1}\, g$) dry phantom. Since there is no conversion factor between wet bone and dry phantom, mapping phantom based detection limits onto actual measurements is carried out with some uncertainty.

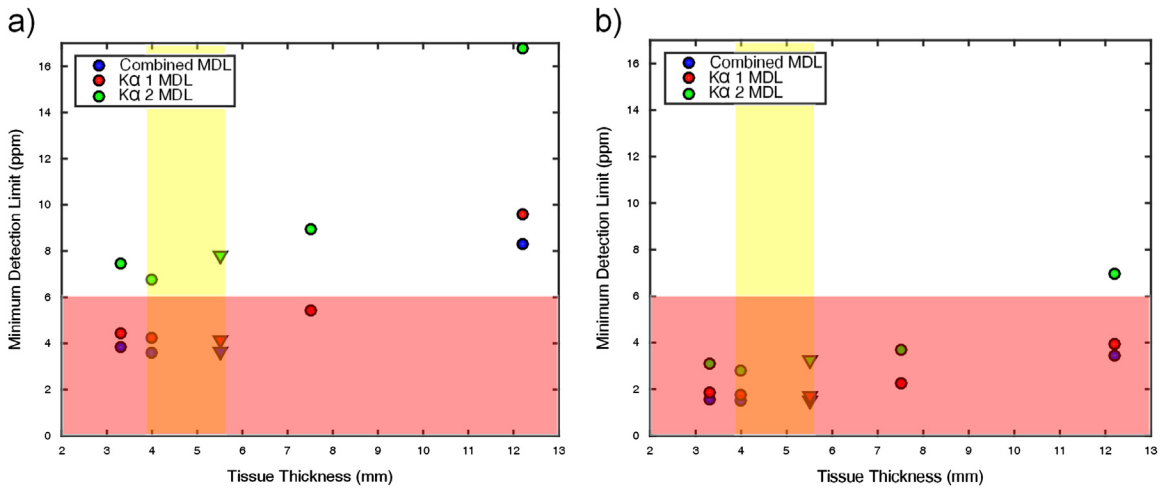

Fig. 7. MDL as a function of tissue thicknesses for a) a 1 GBq source and a count time of 30 minutes using the current one detector K-XRF system, and b) a 5 GBq source and a count time of 30 minutes using the four element cloverleaf K-XRF system. Green data points represent Kα2 values, red data points represent Kα1 values, and blue data points represent the combined MDL. Triangle data points are MDL values scaled from the 20-hour counts on the phantoms with 5.5 ± 0.1 mm tissue overlay, where circular data points are scaled from the 7-hour counts. The yellow highlighted region indicates the average measured tissue thickness over the tibia(4.8 ± 0.2 mm) with thicknesses above and below highlighted as representative, and the red highlighted region represents the concentrations of Gd previously found in human bone (0.47–6.21 ppm). (For interpretation of the references to color in this figure legend, the reader is referred to the web version of this article.).

4.2. MDL for 30 min count time and 5 GBq source using a four element detection system

A study comparing the MDL of lead in bone for a one detector K-XRF system to a four element cloverleaf K-XRF system was carried out in our lab by Nie et al., using a Cd-109 source and plaster of Paris leg phantoms with overlaying tissue equivalent material. The experimental and Monte Carlo simulation results found that the MDL was improved by a factor of 3.0 by using the cloverleaf system and a source of higher activity (Nie et al., 2004). The MDL of the cloverleaf system was also investigated in human measurements by Behinaein et al. and was found to improve by a factor of 3.1 for in vivo measurements of lead in bones of smelter workers (Behinaein et al., 2011). A source of 5 GBq is compatible with the cloverleaf system due to the ability of multiple detectors and electronics to process higher count rates. Simple scaling arguments can be made on the MDL data from our experiments to estimate new values for a 30 minute count time and a 5 GBq source using the cloverleaf system. Accounting for the source activity, measurement time, and dead time, the MDL values were scaled in the same manner as in Section 4.1.

The MDL for a 30 minute count time and 5 GBq source on the cloverleaf K-XRF system for bare bone phantoms was calculated to be 0.98 ppm, which is lower than the MDL calculated for a 1 GBq source on the current K-XRF system by a factor of 2.4. The MDLs for the bone phantoms with different tissue overlays are displayed in Fig. 7b. The combined MDL values range from 1.58 ppm for the thinnest overlay of 3.3 ± 0.1 mm, to 3.44 ppm for the thickest overlay of 12.5 ± 0.1 mm. The MDL values in the range of average tibia overlaying tissue thickness are 1.49 and 1.52 ppm. All MDL values estimated for the bone phantoms with tissue overlay on the cloverleaf system are lower than the the MDLs calculated for the current K-XRF system by a factor of 2.4. This factor is fairly close to the experimentally derived factors of 3.0 and 3.1 found in past studies (Nie et al., 2004; Behinaein et al., 2011).

Fig. 7 b shows how the MDLs for an average tissue thickness range, represented by the yellow highlighted region, are lower for the cloverleaf system and are well within the range of previously measured Gd concentrations in human bones, which is highlighted by the red region. MDLs for larger tissue thicknesses now fall within the regions of previously measured Gd, meaning the cloverleaf system will be more successful at detecting Gd within the bone of patients with a large tissue thickness overlaying the tibia.

4.3. Pulse restoration on current K-XRF system

The conventional technique for pulse processing involves fast digital filters and logic circuits to detect multiple radiation events arriving within the resolving time of the detector, then rejecting these events from appearing on the final spectrum. This method leads to dead time of the system and loss of information. New pulse processing algorithms allow data disrupted by pulse pileup to be recovered, rather than rejected. XIA has designed and implemented a new pulse processing algorithm into a digital pulse processor called FalconX, that can accurately process and recover most radiation events at high count rates with very little degredation to the energy resolution (Scoullar et al., 2011). The use of a FalconX digital pulse processor would allow a high count rate to be processed with a low dead time, and minimal loss of information from rejecting pulses. Both of these improvements would result in a lower MDL, since the MDL is inversely proportional to the square root of the count rate. Further investigations of the FalconX should be carried out on our current detection system to verify the effect of a high count rate on the dead time and energy resolution of the system.

4.4. Dose

A dosimetry study by Nie et al. was conducted on a K-XRF system in our lab, designed to measure lead in bone. The system is similar to the K-XRF system used in this study: a Cd-109 source was used, and the lower leg was the target for bone measurement. The dosimetry study resulted in negligibly small doses to all organs other than the targeted leg used for the measurements. The (total body) effective dose for adults was found to be 0.26 μSv, for a 1-hour measurement and a source activity of 5 GBq (Nie et al., 2007). For our K-XRF system, the volunteer would be exposed for a lower measurement time of 30 minutes and to a source with a lower activity of 1 GBq. Scaling by measurement time and source activity gives a total body effective dose of 0.026 μSv. A 30 minute measurement on the cloverleaf system with a 5 GBq source would result in a effective dose of 0.13 μSv. The Canadian Nuclear Safety Committee lists their maximum effective dose in a calendar year

to be 1 mSv for non-nuclear energy workers, and a typical chest x-ray to be 0.1 mSv. The effective dose of the current K-XRF system and the cloverleaf system is negligible in comparison, making the 30 min measurements a very low risk for volunteers.

5. Conclusions

A feasibility study for the measurement of Gd in human tibia was carried out using a K-XRF system consisting of a HpGe detector and Cd-109 source of activity 0.11 GBq. All MDL values were scaled for a 30 min count time and a stronger source of 1 GBq for more realistic *in-vivo* estimates. MDLs were also scaled for a 30 min count time and 5 GBq source to investigate the feasibility of using the four detector cloverleaf system. Both the current K-XRF and cloverleaf system show promising results with detecting Gd in a human tibia. The current K-XRF system was estimated to have a MDL of 3.60–3.64 ppm, and the cloverleaf system 1.49–1.52 ppm, for an average range of tissue thicknesses overlaying the human tibia. All MDL values are well within the range of previously measured Gd concentrations in human bone, 0.47–6.21 ppm, leading to the conclusion that both the current K-XRF system as well as the cloverleaf system are capable of detecting small concentrations of Gd in the human tibia within a reasonable measurement time. The cloverleaf results in MDLs approximately 2.4 times lower than the current K-XRF system, and would be the preferred system for *in-vivo* measurements if available.

Conflicts of interest

The authors affirm that none of them has any conflict of interest.

Acknowledgements

This study was funded by Natural Sciences and Engineering Research Discovery Grants to FEMcN (203611-2012) and Canada (RGPIN06399-15), and Ontario Graduate Scholarship to MLL.

References

Abraham, J., Thakral, C., Skov, L., Rossen, K., Marckmann, P., 2008. Dermal inorganic gadolinium concentrations: evidence for in vivo transmetallation and long-term persistence in nephrogenic systemic fibrosis. Br. J. Dermatol. 158 (2), 273–280.

Behinaein, S., Chettle, D.R., Atanackovic, J., Egden, L.M., Fleming, D.E., Nie, L.H., Richard, N., Stever, S., 2011. In vivo measurement of lead in the bones of smelter workers using the four-element'clover-leaf'geometry detector system. Phys. Med. Biol. 56 (3), 653.

Bevington, P., Robinson, D., 2003. Data Reduction and Error Analysis for the Physical Sciences. McGraw-Hill Higher Education, McGraw-Hill, New York, NY ⟨https://www.books.google.ca/books?id=0poQAQAAIAAJ⟩.

Carr, D., Brown, J., Bydder, G., Steiner, R., Weinmann, H., Speck, U., Hall, A., Young, I., 1984. Gadolinium-DTPA as a contrast agent in MRI: initial clinical experience in 20 patients. Am. J. Roentgenol. 143 (2), 215–224.

Chamberlain, M., Gräfe, J., Byun, S., Chettle, D., Egden, L., Orchard, G., Webber, C., McNeill, F., 2012. The feasibility of in vivo quantification of bone-fluorine in humans by delayed neutron activation analysis: a pilot study. Physiol. Meas. 33 (2), 243.

Darrah, T.H., Prutsman-Pfeiffer, J.J., Poreda, R.J., Campbell, M.E., Hauschka, P.V., Hannigan, R.E., 2009. Incorporation of excess gadolinium into human bone from medical contrast agents. Metallomics 1 (6), 479–488.

Errante, Y., Cirimele, V., Mallio, C.A., Di Lazzaro, V., Zobel, B.B., Quattrocchi, C.C., 2014. Progressive increase of T1 signal intensity of the dentate nucleus on unenhanced magnetic resonance images is associated with cumulative doses of intravenously administered gadodiamide in patients with normal renal function, suggesting dechelation. Investig. Radiol. 49 (10), 685–690.

Grobner, T., 2006. Gadolinium-a specific trigger for the development of nephrogenic fibrosing dermopathy and nephrogenic systemic fibrosis? Nephrol. Dial. Transplant. 21 (4), 1104–1108.

Joffe, P., Thomsen, H.S., Meusel, M., 1998. Pharmacokinetics of gadodiamide injection in patients with severe renal insufficiency and patients undergoing hemodialysis or continuous ambulatory peritoneal dialysis. Acad. Radiol. 5 (7), 491–502.

Kanal, E., Tweedle, M.F., 2015. Residual or retained gadolinium: practical implications for radiologists and our patients. Radiology 275 (3), 630–634.

Kanda, T., Ishii, K., Kawaguchi, H., Kitajima, K., Takenaka, D., 2013. High signal intensity in the dentate nucleus and globus pallidus on unenhanced T1-weighted MR images: relationship with increasing cumulative dose of a gadolinium-based contrast material. Radiology 270 (3), 834–841.

Marckmann, P., Skov, L., Rossen, K., Dupont, A., Damholt, M.B., Heaf, J.G., Thomsen, H.S., 2006. Nephrogenic systemic fibrosis: suspected causative role of gadodiamide used for contrast-enhanced magnetic resonance imaging. J. Am. Soc. Nephrol. 17 (9), 2359–2362.

McDonald, R.J., McDonald, J.S., Kallmes, D.F., Jentoft, M.E., Murray, D.L., Thielen, K.R., Williamson, E.E., Eckel, L.J., 2015. Intracranial gadolinium deposition after contrast-enhanced mr imaging. Radiology 275 (3), 772–782.

Nie, H., Chettle, D., Luo, L., O'Meara, J., 2007. Dosimetry study for a new in vivo x-ray fluorescence (xrf) bone lead measurement system. Nucl. Instrum. Methods Phys. Res. Section B: Beam Interact. Mater. At. 263 (1), 225–230.

Nie, H., Chettle, D., Stronach, I., Arnold, M., Huang, S., McNeill, F., O'Meara, J., 2004. A study of MDL improvement for the in vivo measurement of lead in bone. Nucl. Instrum. Methods Phys. Res. Section B: Beam Interact. Mater. At. 213, 579–583.

Pejović-Milić, A., Brito, J., Gyorffy, J., Chettle, D., 2002. Ultrasound measurements of overlying soft tissue thickness at four skeletal sites suitable for in vivo x-ray fluorescence. Med. Phys. 29 (11), 2687–2691.

Scoullar, P.A., McLean, C.C., Evans, R.J., Hamm, M.E., Hamm, R.W., 2011. Real time pulse pile-up recovery in a high throughput digital pulse processor, in: Proceedings of the AIP Conference – American Institute of Physics, Vol. 1412, p. 270.

Thakral, C., Alhariri, J., Abraham, J.L., 2007. Long-term retention of gadolinium in tissues from nephrogenic systemic fibrosis patient after multiple gadolinium-enhanced mri scans: case report and implications. Contrast Media Mol. Imaging 2 (4), 199–205.

Thomsen, H., Morcos, S., Dawson, P., 2006. Is there a causal relation between the administration of gadolinium based contrast media and the development of nephrogenic systemic fibrosis (NSF)? Clin. Radiol. 61 (11), 905–906.

Weinmann, H., Brasch, R., Press, W., Wesbey, G., 1984. Characteristics of gadolinium-DTPA complex – a potential NMR contrast agent. Am. J. Roentgenol. 142 (3), 619–624.

White, G.W., Gibby, W.A., Tweedle, M.F., 2006. Comparison of gd (DTPA-BMA) (omniscan) versus Gd (HP-DO3A)(prohance) relative to gadolinium retention in human bone tissue by inductively coupled plasma mass spectroscopy. Investig. Radiol. 41 (3), 272–278.

Chapter 4

Paper II: Confirming improved detection of gadolinium in bone using *in vivo* XRF

M.L. Lord, F.E. McNeill, J.L. Gräfe, A.L. Galusha, P.J. Parsons, M.D. Noseworthy, L. Howard, and D.R. Chettle, Appl. Radiat. Isot., **120**, 111-118 (2017).

This paper was a continuation of the work completed in Paper I, as it investigated the feasibility of using the updated XRF system suggested in Paper I for *in vivo* detection of Gd in bone. This paper presents the experimental methods and results of the updated XRF system in preparation for human measurements. In addition, a cross-validation study was performed to validate the XRF system further by comparing my measured values with ICP-MS measurements performed at the Wadsworth centre in Albany, NY.

The experimental system in this study was changed significantly from Paper I: the single HPGe detector was updated to the four-detector cloverleaf system, the Cd-109 source was upgraded from 0.11 GBq to 5 GBq, the W collimator was replaced with a Pb collimator, and lastly the new Cd-109 source was ordered with a Ag plug, rather

than W. However, I questioned whether the source was actually W free, as I was not able to eliminate it from the acquired spectra completely. Realistic measurement times of 30 min were used on the bone phantoms and bone samples to reflect an actual human measurement. From Paper I, the MDLs for the updated XRF system were predicted to be 1.49 - 1.52 μg Gd/g PoP for an average overlaying tissue thickness. The experimental MDLs for an average overlaying tissue thickness were found to be 1.64 - 1.72 μg Gd/g PoP, which were slightly higher than the predicted values due to the unexpected increase in system dead time with the addition of the tissue equivalent material over the bone phantom. The calculated MDLs for the updated XRF system were within the previously measured levels of Gd in bone presented in published literature, and the XRF system was deemed feasible for carrying out *in vivo* human measurements of Gd in bone.

The cross validation study completed in this paper was in collaboration with the Laboratory of Inorganic and Nuclear Chemistry at the Wadsworth Centre in Albany, New York. While conducting her thesis work, Aubrey Galusha discovered extremely high concentrations of rare earth elements in bone from individuals who had received long term parenteral nutrition, with one of these elements being Gd. Our research group received a set of 7 bone samples from unidentified patients who were either on long term parenteral nutrition, or control patients. The bone samples varied in size and structure. The Wadsworth Centre performed the ICP-MS on these samples prior to sending them to us, and did not release their data until I had performed my XRF measurements. Out of the 7 samples sent to us, 2 had observable amounts of Gd by XRF, with one sample being as high as 32.4 μg Gd/g bone mineral. Gd concentrations measured by XRF were found to be comparable with reported ICP-MS values within the given measurement uncertainties.

This project was a natural extension of the work in Paper I. The system design and XRF measurements were carried out by myself, under the supervision of David Chettle and Fiona McNeill. I altered the scripts for fitting Gd peaks and calculating the MDLs specifically for the cloverleaf system, and carried out the calculations for the coherent conversion factor. James Gräfe and Mike Noseworthy were consulted

throughout the project. The ICP-MS measurements of Gd in the bone samples were completed by Aubrey Galusha under the supervision of Patrick Parsons and Lyn Howard. Patrick Parsons was consulted for converting XRF units of μg Gd/g bone mineral to μg Gd/g dry weight bone, which are the units in which ICP-MS values are reported. I wrote the first draft of this manuscript, which was subsequently edited by all authors of this paper.

Applied Radiation and Isotopes 120 (2017) 111–118

Contents lists available at ScienceDirect

Applied Radiation and Isotopes

journal homepage: www.elsevier.com/locate/apradiso

Confirming improved detection of gadolinium in bone using *in vivo* XRF

M.L. Lord[a,*], F.E. McNeill[b], J.L. Gräfe[c], A.L. Galusha[d,e], P.J. Parsons[d,e], M.D. Noseworthy[f,g,h,i], L. Howard[j], D.R. Chettle[b]

[a] Radiation Sciences Graduate Program, McMaster University, Hamilton, Canada L8S 4L8
[b] Department of Physics and Astronomy, McMaster University, Hamilton, Canada L8S 4L8
[c] Department of Physics, Ryerson University, Toronto, Canada M5B 2K3
[d] Department of Environmental Health Sciences, School of Public Health, The University at Albany, State University of New York, Albany, New York 12222 United States
[e] Laboratory of Inorganic and Nuclear Chemistry, Wadsworth Center, New York State Department of Health, Albany, New York 12201 United States
[f] McMaster School of Biomedical Engineering, McMaster University, Hamilton, Canada L8S 4L8
[g] Imaging Research, St. Joseph's Healthcare, Hamilton, Canada L8N 4A6
[h] Department of Radiology, McMaster University, Hamilton, Canada L8S 4L8
[i] Department of Electrical and Computer Engineering, McMaster University, Hamilton, Canada L8S 4L8
[j] Department of Medicine, Division of Gastroenterology and Nutrition, Albany Medical College, Albany, New York 12208 United States

ARTICLE INFO

Keywords:
X-ray fluorescence
ICP-MS
Gadolinium retention
Gadolinium in bone
MRI

ABSTRACT

The safety of using Gd in MRI contrast agents has recently been questioned, due to recent evidence of the retention of Gd in individuals with healthy renal function. Bone has proven to be a storage site for Gd, as unusually high concentrations have been measured in femoral heads of patients undergoing hip replacement surgery, as well as in autopsy samples. All previous measurements of Gd in bone have been invasive and required the bone to be removed from the body. X-ray fluorescence (XRF) offers a non-invasive and non-destructive method for carrying out *in vivo* measurements of Gd in humans. An updated XRF system provides improved detection limits in a short measurement time of 30-min. A new four-detector system and higher activity Cd-109 excitation source of 5 GBq results in minimum detection limits (MDLs) of 1.64–1.72 μg Gd/g plaster for an average overlaying tissue thickness of the tibia. These levels are well within the range of previous *in vitro* Gd measurements. Additional validation through comparison with ICP-MS measurements has confirmed the ability of the XRF system for detecting Gd further, proving it is a feasible system to carry out human measurements.

1. Introduction

Gadolinium (Gd) is used in MRI contrast agents, which are commonly administered prior to receiving MRI scans to improve contrast in certain tissues. When Gd-based contrast agents (GBCAs) were first introduced in the early 80's, they were thought to be completely stable and excreted from the body within a matter of hours (Weinmann et al., 2005; Carr et al., 1984). However, in 2006 GBCAs were linked to nephrogenic systemic fibrosis (NSF) in patients with renal disease, suggesting they are accumulating in the body, rather than being excreted (Grobner, 2006; Marckmann et al., 2006; Thomsen et al., 2006). NSF is a painful condition involving hardening of the skin, due to the formation of papules and plaques, for which there is no clear cure (Cowper et al., 2001). Since the association of GBCAs with NSF, extra precautions are being taken to prevent individuals with renal disease from receiving GBCAs prior to an MRI scan. However, Gd accumulation does not only occur in individuals with renal disease, as it has recently been found in patients with normal renal function (McDonald et al., 2015; Quattrocchi et al., 2015; Errante et al., 2014; Kanda et al., 2013, 2015; Murata et al., 2016), which is why the safety of GBCAs is currently such an important topic in the MRI community.

One of the main sites of interest for Gd accumulation in the body is the brain, specifically the dentate nucleus and the pons. Multiple research groups have carried out image analysis studies, showing an increase in T1 signal intensity with increasing doses of Gd-based contrast agents, which suggests Gd accumulation in the brain (McDonald et al., 2015; Quattrocchi et al., 2015; Errante et al., 2014; Kanda et al., 2013). Inductively coupled plasma mass spectrometry (ICP-MS) was used on autopsy samples by Kanda et al. and demonstrated a correlation between Gd accumulation in the brain and GBCA dose (Kanda et al., 2015). All studies regarding Gd accumulation in the brain were performed on patients with healthy renal function.

* Corresponding author.
E-mail addresses: lordml@mcmaster.ca (M.L. Lord), fmcneill@mcmaster.ca (F.E. McNeill), james.grafe@ryerson.ca (J.L. Gräfe), aubrey.galusha@health.ny.gov (A.L. Galusha), patrick.parsons@health.ny.gov (P.J. Parsons), nosewor@mcmaster.ca (M.D. Noseworthy), howardL@mail.amc.edu (L. Howard), chettle@mcmaster.ca (D.R. Chettle).

http://dx.doi.org/10.1016/j.apradiso.2016.12.011
Received 3 August 2016; Received in revised form 22 November 2016; Accepted 8 December 2016
Available online 11 December 2016

Another site of interest for Gd accumulation in the body is bone. Rare earth elements such as Gd are known to be bone seeking, with Gd^{3+} having a similar radial size to Ca^{2+} and higher ionic charge, thus leading to competitive inhibition for processes involving Ca^{2+}. It is assumed that Gd incorporates into human bone mineral, as it is the storage site for the majority of Ca in the body (Sherry et al., 2009; Thakral et al., 2007; Darrah et al., 2009; Rogosnitzky and Branch, 2016). Darrah et al. and White et al. found unusually high concentrations of Gd, ranging from 0.42 to 6.02 μg Gd/g bone, in the femoral heads of patients undergoing hip replacement surgery who had previously received GBCA (Darrah et al., 2009; White et al., 2006). Murata et. al measured Gd in brain and bone autopsy samples from patients who had received GBCA, all with healthy renal function. Gd levels measured in bone, ranging from 0.1 to 5.3 μg Gd/g bone, were 23 times higher than levels in brain and showed a significant correlation between concentrations in the bone and brain (Murata et al., 2016). Overall, bone proves to be a main storage site for Gd and would serve as a convenient measurement location to investigate Gd accumulation in the body.

All studies previously discussed used *in vitro* methods, where the bone sample is removed from the body to be measured by ICP-MS, which is a destructive technique. X-ray fluorescence (XRF) is a non-invasive and non-destructive technique, that allows for *in vivo* measurements of Gd, through Gd excitation and measurement of produced fluorescent x-rays. A previous study by Lord et al. in our research group investigated the feasibility of using an XRF system to measure Gd by using bone phantoms anthropomorphic to a human tibia. For a single high-purity germanium (HPGe) detector, and a 0.11 GBq Cd-109 excitation source, the minimum detection limit (MDL) was calculated to be 0.87 μg Gd/g plaster for a bare bone phantom, and 1.34 μg Gd/g plaster for a bone phantom with an overlaying tissue thickness of 5.5 mm. Due to the weak activity of the Cd-109 source used, measurement times had to be extended to 20-h to detect the Gd properly (Lord et al., 2016). A 20-h measurement is unrealistic for human *in vivo* measurements, and MDLs for this system increase to 5.5 μg Gd/g plaster for bare bone and 8.47 μg Gd/g plaster for an overlaying tissue thickness of 5.5 mm for a realistic measurement time of 30-min. It is clear that these values are too large to detect trace amounts of Gd in bone properly, considering previous measurements of Gd in bone range from 0.1 to 6.02 μg Gd/g bone. Therefore it is necessary to update to a stronger source and a new detection system for human measurements.

MDL values in Lord et al. were scaled to create estimated MDLs for a 30-min measurement time with an updated four-detector cloverleaf system and a stronger source of 5 GBq. These values proved to be very promising for *in vivo* measurements, ranging from 1.49 to 1.52 μg Gd/g plaster for an average overlaying tissue thickness, with an effective dose of approximately 0.13 μSv (Lord et al., 2016). This report presents the experimental methods and data for Gd measurements, including MDLs for a range of tissue overlay thicknesses, for an updated (cloverleaf design) XRF system in preparation for human measurements. In addition, we present data from a cross validation study, performed on a set of autopsy bone samples, and compare our XRF measurements to ICP-MS measurements performed at the Wadsworth Center in Albany, New York.

2. Methods

2.1. Measurement location

A measurement location of the tibia was chosen due to the relatively thin layer of overlaying tissue on the tibia, thus reducing attenuation of Gd x-rays exiting the bone. A lower (total body) effective dose is received by the individual being measured since the tibia is located in an extremity of the body and there is no active red bone marrow in the adult tibia. In addition, measuring the leg provides comfort for individuals during a measurement, in terms of physical comfort and in knowing that a high dose is not being delivered to the core of the body. To begin a feasibility study for the updated XRF system detecting Gd, nine tibia mimicking phantoms were constructed from Plaster of Paris ($CaSO_4{\cdot}2H_2O$) ranging in Gd (Gd_2O_3) concentrations of 0–120 μg Gd/g plaster, as described by Lord et al. (2016). These phantoms were used for calibrating the XRF system for further measurements, as well as calculating the MDL of the XRF system.

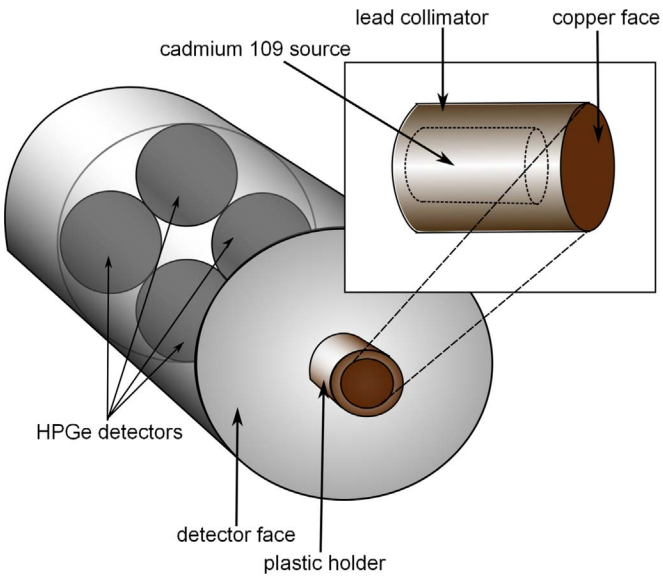

Fig. 1. Cloverleaf XRF system consisting of four HPGe detectors (each being 16 mm in diameter and 10 mm thick) in a cloverleaf formation, and a Cd-109 source enclosed in a lead collimator with a copper face, situated on the face of the detector.

2.2. Cloverleaf XRF system

This XRF system consists of a four-element “cloverleaf” detection system (Canberra GL0210R/S), previously used by our group for *in vivo* bone lead measurements Nie et al., 2006, and a Cd-109 excitation source used for all measurements on tibia phantoms and autopsy bone samples. The detection system is composed of four HPGe detectors, each being 16 mm in diameter and 10 mm thick, in a cloverleaf formation as shown in Fig. 1, and four sets of pulse processing electronics from Canberra Industries, Inc. (Meridan, Connecticut, 06450, USA). Each detector output passes through its own preamplifier (Canberra 2002CP), digital pulse processing system (Canberra DSA 1000), and is collected as a spectrum on Genie 2000 Gamma Analysis Software from Canberra. Four spectra are collected for each measurement, one spectrum per detector, and exported to MATLAB for peak fitting and further analysis.

A new 5 GBq Cd-109 excitation source was obtained for this set of experiments, which has a significantly improved activity compared with the 0.11 GBq Cd-109 source previously used by our group. In addition to an improved activity, the new Cd-109 excitation source was constructed with a silver plug, rather than the tungsten plug present in the old excitation source. The tungsten plug was replaced with silver due to the backscattered tungsten Kα x-rays causing extra background in the region of the Gd Kα peaks. Although the silver plug eliminated a large amount of the background caused from tungsten plug, the background could not completely be eliminated due to a small amount of tungsten still present in the Cd-109 source. The excitation source was manufactured on February 9, 2016, and had an initial measured activity of 5.59 GBq. All measurements were taken between June 2–7, 2016, which is 114–119 days after the initial activity measurement. The half life of Cd-109 is 464 days, which means the activity at the time of measurement was between 4.68–4.71 GBq. The difference in activity throughout the measurement period is negligible, and is therefore not

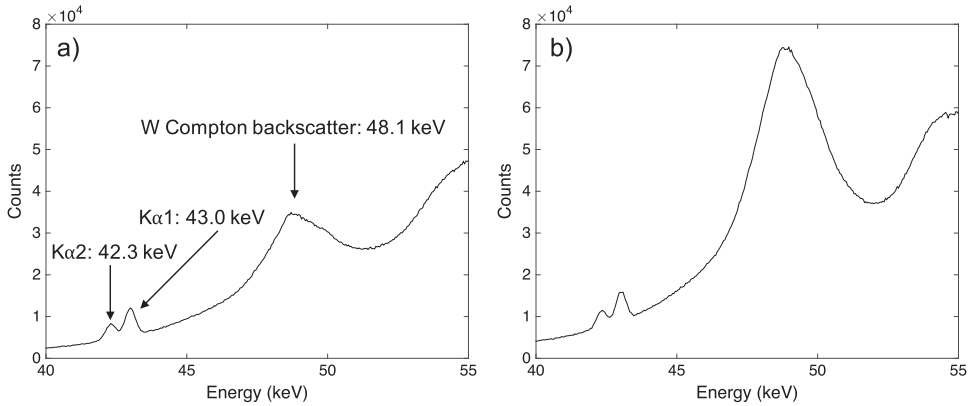

Fig. 2. Spectra in the energy range of 40–50 keV, displaying the Gd Kα peaks and backscattered W Kα peak for a) the Pb collimator and b) the W collimator.

taken into account when calculating the MDL values.

The Cd-109 source emits 88 keV gamma rays, and silver x-rays in the energy range of 22–24 keV. The collimator used for these measurements was changed from tungsten to lead collimator to investigate the effect on background. The tungsten collimator used by Lord et al. effectively collimated the Cd-109 source; however, the extra backscattered tungsten Kα x-rays produced by the collimator caused extraneous background in the region of the Gd Kα peaks of interest, much like the tungsten plug on the old excitation source. Eliminating tungsten from the collimator by switching to lead allowed the Gd peaks to be a more prominent feature on the spectra (Fig. 2). The lead collimator was therefore used for all measurements in this study to investigate the improvement of the reduced background on the detection limits of the system.

2.3. Data collection and analysis

A 180° backscatter geometry was used while conducting measurements, where the tibia phantoms and bone samples were placed at a close distance of 1 mm from the copper filter of the collimator. Counts were collected from each of the 9 tibia bone phantoms using a 30-min measurement real time. Measurements of the same length were then repeated on the tibia bone phantoms with overlaying tissue equivalent material (Solid Water®) with thicknesses of 3.3 ± 0.1 mm, 4.0 ± 0.1 mm, 7.5 ± 0.1 mm, and 12.2 ± 0.1 mm in order to account for possible different body compositions being measured on the XRF system. It should be noted that as overlaying tissue was added to the bone phantom, the distance from the source to the entire phantom was kept consistent at 1 mm, causing the distance from the source to bone phantom to increase. Each of the bone samples was measured for 30 min, and placed on a plastic stand as most samples were significantly smaller than the phantoms (Fig. 3).

The collected spectra have several prominent features: a coherent peak at 88 keV, a Compton backscatter peak at 66.5 keV, and the Gd Kα peaks of interest at 42.3 and 43.0 keV. A script written in MATLAB was designed to extract the Gd Kα peaks from the spectra, and fit them using the method of Non-Linear Least Squares with a double Gaussian and polynomial background function:

$$p_1x^3 + p_2x^2 + p_3x + p_4 + a_1e^{-\left(\frac{x-b_1}{c_1}\right)^2} + a_2e^{-\left(\frac{x-b_2}{c_2}\right)^2} \quad (1)$$

The widths of the Gaussian peaks ($c1$ and $c2$) were fixed parameters obtained from a series of measurements on high concentration phantoms, and the peak centres ($b1$ and $b2$) were fixed to one another, reducing the number of variables and leading to a smaller uncertainty. Out of the multiple functions tested, a cubic function resulted in the best χ^2 value while fitting the Gd peaks, and was therefore chosen over the commonly used exponential or quadratic background. The coherent peaks were fit with a simple Gaussian function for coherent normalization purposes. Once the Gd peaks had been properly fit with an acceptable χ^2 value of 1.0 ± 0.20, the areas under the peaks were calculated and plotted as a function of known phantom Gd concentration.

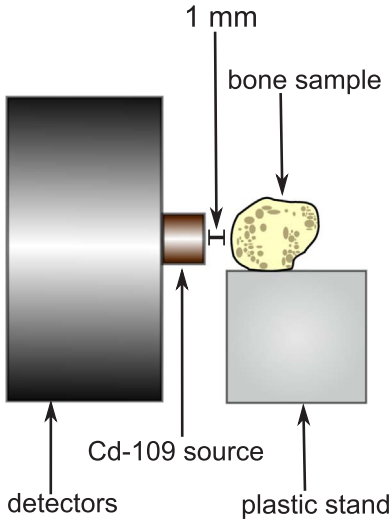

Fig. 3. Measurement setup consisting of a 180° geometry, with the phantoms and bone samples placed closely in front of the Cd-109 source, at a distance of 1 mm.

The MDL should theoretically be the lowest Gd concentration that the system can detect, and is defined as two times the uncertainty of Gd concentration ($2\sigma_x$), which can be calculated from the calibration lines, as described in detail by Lord et al. (2016). Since the cloverleaf XRF system consists of four detectors and sets of electronics, four sets of Gd peaks are fit for each phantom or bone sample being measured. Therefore, a MDL is calculated for each set of peaks, then combined through an inverse variance weighted mean to give an overall MDL for the system (Chamberlain et al., 2012).

$$MDL = \left(\frac{1}{1/MDL_1^2 + 1/MDL_2^2 + 1/MDL_3^2 + 1/MDL_4^2}\right)^{1/2} \quad (2)$$

2.4. Autopsy bone samples

To test the feasibility of the system for measuring Gd in bone further, we obtained a set of autopsy bone samples from Laboratory of Inorganic and Nuclear Chemistry at the Wadsworth Center in Albany, New York. Out of the seven patients of whom the bone samples belonged to, an unknown number at the time of the XRF measurement had been previously exposed to a GBCA. The analysis of human bone samples was considered exempt by the New York State Department of

Health Institutional Review Board under category 4 of the pertinent federal regulations.

2.4.1. Preparation

The bones were prepared for ICP-MS by soaking in 30 % hydrogen peroxide solution overnight to remove trapped blood, followed by diethyl ether to dissolve fat deposits, and rinsed with double deionized water for trace element analysis. All samples were subsequently freeze dried in a five-segment drying process (Kruger et al., 2014). Two sections of the bone were digested and analysed by ICP-MS and, where possible, a third section was sent to our group at McMaster University for XRF measurements. The analysis for Gd by ICP-MS/MS is detailed below in Section 2.4.4.

2.4.2. Concentration calculation

The lead collimator used in bone sample measurements had slightly thinner walls than desired (2 mm), leading to a breakthrough of the 88 keV excitation photons through the back of the collimator. To account for the breakthrough radiation when carrying out concentration calculations, the coherent peak area for a blank measurement (no phantom present) was subtracted from the coherent peak area for each bone sample measurement, resulting in a corrected coherent peak. Each sample measured produced four spectra, which were fit using the same algorithm used for phantom peak fitting. For the spectra that had Gd peaks present, the area under the peaks was calculated, normalized with the corrected coherent peak, then used with the bare bone phantom calibration line relationship to determine the concentration of Gd in the bone sample. It should be noted that the calibration lines for bare bone phantoms were also normalized to their respective corrected coherent peaks for consistency:

$$A = Bx + C \tag{3}$$

where A is the area under the Gd peak normalized to the corrected coherent peak, B is the slope of the calibration line, x is the Gd concentration, and C is the intercept of the calibration line. Four Gd concentrations were calculated for each bone sample since each measurement produces four spectra. These concentrations are combined through an inverse variance weighted mean to give the overall concentration in the bone sample.

2.4.3. Plaster to bone mineral conversion factor

The units of measurement when calculating Gd concentration are ppm, as in μg Gd/g plaster, due to the calibration lines being based upon plaster phantom measurements. Since Gd incorporates into bone mineral, the desired units of measurement are μg Gd/g bone mineral. Previous studies using XRF to measure lead in the tibia with a Cd-109 excitation source have investigated the relationship between lead concentrations in plaster phantoms and bone mineral. Since gadolinium is assumed to deposit in bone mineral, replacing calcium, the same conversion factor used for these lead studies can be used when converting *in vivo* Gd measurements from μg Gd/g plaster, to μg Gd/g bone mineral.

The coherent conversion factor (CCF) is the ratio of the differential coherent scattering cross sections for plaster and bone mineral, which is given by:

$$CCF = \frac{\frac{1}{2} r_e^2 (1 + \cos^2\theta) F(q, Z)^2_{bone\ mineral} d\Omega}{\frac{1}{2} r_e^2 (1 + \cos^2\theta) F(q, Z)^2_{plaster} d\Omega} \tag{4}$$

$$CCF = \frac{F(q, Z)^2_{bone\ mineral}}{F(q, Z)^2_{plaster}} \tag{5}$$

where r_e is the classical electron radius, θ is the scattering angle in degrees, $F(q, Z)$ is the relativistic atomic form factor, and $d\Omega$ is an element of solid angle. All terms that are independent of material composition cancel, leaving the CCF described as the ratio of the square of the form factors. All form factor values are dependent on atomic number (Z) of the material and the momentum transfer variable q, which itself is dependent on scattering angle (θ) and photon energy (E):

$$q = \frac{E(\sin(\theta/2))}{hc} \tag{6}$$

where h is Plank's constant, and c is the speed of light.

Todd (2000) investigated the CCF for measuring lead in bone by comparing values from three previous studies that used the same method (Todd, 2000). The CCF values for the three previous studies were compared to each other, all of which were found to be 1.46 for mean scattering angles ranging from 153.25 to 167.7° (Todd et al., 1992; Gordon et al., 1994; Somervaille et al., 1985). A CCF value of 1.45 was reported for a mean scattering angle of 140° by Chettle et al. (1991). However, this value does not take into account the additional Gd content in plaster phantoms and the bone. Since Gd has a lower Z value than Pb, Gd in bone will not contribute as much to coherent scatter, and it is there fore not expected for the CCF to change from the value of 1.46 used for bone lead studies.

A complete revaluation of the CCF was completed for Gd at the mean scattering angle for our system of 151.6°. Taking the ratio of the form factors for plaster and bone mineral without Gd results in a CCF of 1.458 (Table 1), which perfectly agrees with values from previous studies. The addition of 120 ppm Gd results in a CCF value of 1.456 (Table 1), which is an 0.11 % difference from the CCF without Gd, and also agrees with CCF values from previous studies.

Since it has been shown that any additional Gd incorporated into the plaster phantom or cortical bone in the tibia does not significantly change the value of the CCF, it is safe to continue to use the well established value of 1.46 when converting *in vivo* Gd measurements from μg Gd/g plaster to μg Gd/g bone mineral.

2.4.4. Measurements by ICP-MS/MS

Reference measurements for Gd in bone were performed by the Wadsworth Center's Trace Elements lab using a method based on inorganic mass spectrometry following acid digestion. Briefly, the method requires that the bone samples are dried and defatted prior to being digested under pressure in concentrated nitric acid using a microwave assisted heating system (MARS 5, CEM, Matthews, NC) (Kruger et al., 2014). Digested bone samples are diluted with an Ir internal standard for analysis using an Agilent 8800 ICP-MS/MS (Agilent Technologies, New Castle, DE).

The Agilent 8800 ICP-MS/MS is a “tandem” instrument equipped with an octopole reaction system (ORS) situated between two mass analysing quadrupoles. This instrumental configuration is ideal for measuring rare earth elements such as Gd, which tend to form stable oxides, making the analysis a challenge using standard ICP-MS instrumentation. The final, optimized MS/MS method for Gd in bone, based on monitoring ^{157}Gd with H_2 as the ORS gas, was validated against seven biological Certified Reference Materials (CRM) for which some had certified values for Gd while for others, the Gd data were information and/or obtained from the literature. The CRMs included two SRMs from NIST: NIST SRM 1400 Bone Ash; and NIST SRM 1486 Bone Meal, for which non-certified data were available. The use of ICP-MS/MS, calibrated with NIST-traceable standards, coupled with multiple CRM data, provide a degree of confidence in the traceability of Gd

Table 1
Form factors and coherent conversion factors calculated for plaster and cortical bone, including an added Gd concentration of 120 ppm.

Material	Form factor	Form factor with 120 ppm Gd	% Difference
plaster	1.200×10^{-3}	1.204×10^{-3}	0.33
Cortical bone	1.750×10^{-3}	1.754×10^{-3}	0.24
CCF:	**1.45778**	**1.45617**	**0.11**

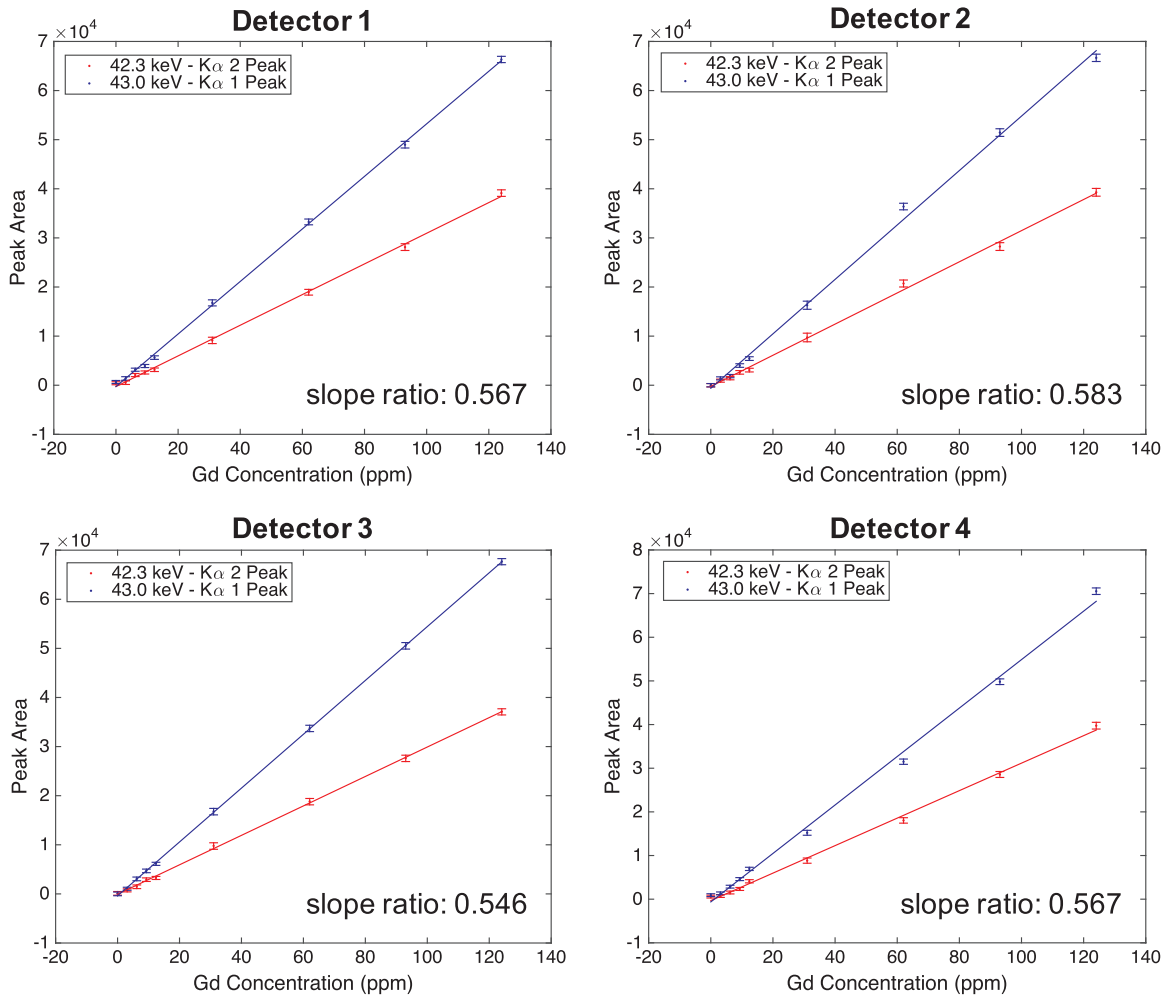

Fig. 4. Kα2 and Kα1 calibration lines for each detector for the bare bone phantom, plotted in red and blue respectively, with error bars representing the standard deviation on the peak area. All calibration lines have an R-squared value of 0.99 and a Kα2 to Kα1 ratio ranging from 0.55 to 0.58. (For interpretation of the references to color in this figure legend, the reader is referred to the web version of this article.)

measurements to SI units (Galusha, 2015).

3. Results

3.1. Peak fitting

Measurements for all samples were carried out in 30-min real time counting intervals. Since the XRF system consists of four HPGe detectors, four spectra were acquired for each sample measured, and four sets of Gd peaks were fit as described in the previous section. All sets of peaks were fit well, resulting in an average χ^2 value of 1.04, ranging from 0.88–1.20, for all the samples measured.

Once the Gd peaks were properly fit for phantom measurements, the areas under the peaks were calculated and plotted against the known Gd phantom concentration to create four sets of calibration lines. An example set of calibration lines for the bare bone phantoms is shown in Fig. 4. The expected slope ratio of the Kα2 to Kα1 calibration lines is 0.56, since this is the ratio of emission probability for the Kα2 and Kα1 emission lines. Slope ratios were calculated for each set of calibration lines to validate that the Gd peaks had been properly fit further. Slope ratios had an average value of 0.59, ranging from 0.53–0.65 for all bare bone and tissue overlay phantoms.

A MDL was calculated for each detector, then combined using Eq. (2) to achieve an overall MDL for the XRF system.

3.2. Tibia bone phantom measurements

Bare bone phantom measurements were performed with a system dead time of approximately 40 %, which is a standard dead time to run at for previous measurements executed on the cloverleaf system in our lab. The MDL was calculated using the calibration lines in Fig. 4, and was found to be 0.78 μg Gd/g plaster. When overlaying tissue was added to the tibia bone phantoms, the system dead time increased to around 55 %, which was slightly higher than expected. The effect of the higher dead time for the tissue overlay phantoms will be further addressed in the *discussion* section. MDLs calculated for the tissue overlay phantoms range from 1.64–4.87 μg Gd/g plaster, and are plotted as a function of tissue thickness in Fig. 5.

3.3. Autopsy bone sample measurements

The autopsy bone samples obtained from the Wadsworth Center were measured on the XRF system for 30 min with the same Cd-109 source used for the tibia bone phantoms. We were told that some of the samples were from patients who had previously received GBCAs, but were initially blinded to how many and which ones. Out of the seven patients that the bones belonged to, two of the patients had observable levels of Gd by XRF. All others were below the detection limit of the system. The calculated concentrations of detectable Gd in the bone samples are displayed in Table 2.

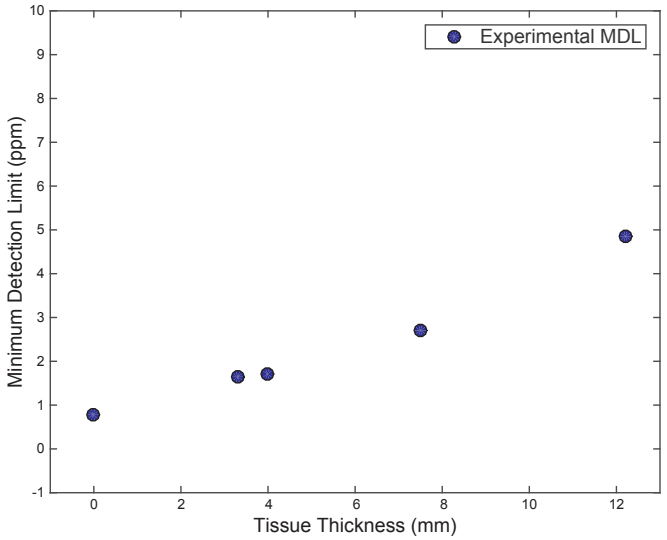

Fig. 5. MDLs as a function of overlaying tissue thickness, including the bare bone phantom MDL. Values range from 0.78–4.87 μg Gd/g plaster, and increase monotonically as the tissue thickness increases.

Table 2
Gd concentrations of bone samples with observable Gd, measured on the XRF system.

Patient 1	Patient 2
32.4 ± 0.4 μg Gd/g bone mineral	7.7 ± 1.0 μg Gd/g bone mineral

4. Discussion

4.1. Estimated MDLs from a single detector system

In our previous Gd study, a single HPGe detector was used with a 0.11 GBq Cd-109 source (Lord et al., 2016). Due to the weak activity of the excitation source, the measurement times had to be approximately 20 h to achieve reasonable MDLs. Therefore MDL values from this study were scaled to give estimated MDL values for a 30-min measurement on the cloverleaf system with a much stronger 5 GBq source. The relationship of MDL $\propto 1/\sqrt{t}$ was used to scale the time from a 20–30 min measurement. The increase in activity was accounted for through the source strength ratio relationship of MDL $\propto \sqrt{A/A_0}$, where A is the 5 GBq source and A_0 is the 0.11 GBq source. Lastly, the dead time for the cloverleaf system was assumed to be 40 %, since this is a standard dead time that has been previously observed for the system. Through these scaling arguments, the MDL estimates for the current cloverleaf system were calculated, which are displayed in Fig. 6 with experimental values for comparison.

As shown in Fig. 6, the experimental MDL for the bare bone phantom was slightly better than what was predicted. This is most likely due to the fact that the collimator was switched from tungsten to lead, reducing background and making the Gd peaks more prominent. The change in collimator material was not accounted for in the estimated values, as we had not originally planned to make that change.

For the tissue overlay phantoms, the experimental MDLs become slightly worse compared to the predicted values as more tissue is added to the phantom. This is simply an effect of increasing dead time. As more overlaying tissue is added to the phantom, the size becomes larger and there are more interactions occurring, thus increasing the system dead time. Moving the phantom further away from the source improves the deadtime value; however, this decreases the signal-to-noise ratio, which worsens the MDL. For this reason, the phantoms were kept at a close distance of 1 mm from the source, despite the higher deadtime values. The large deadtime value only becomes a problem for the

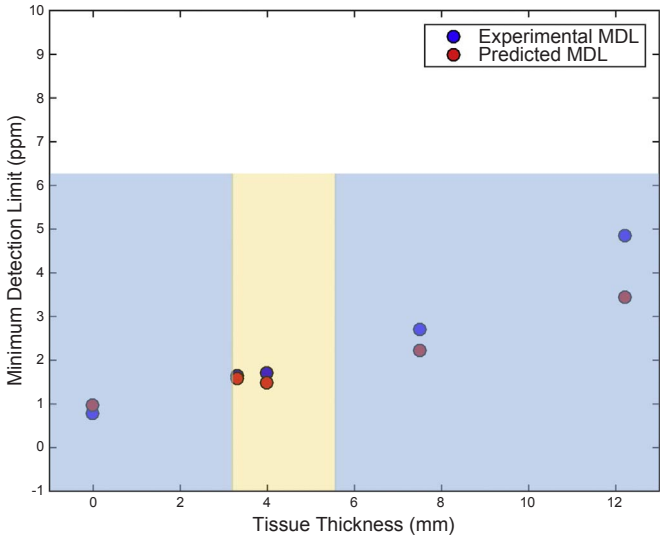

Fig. 6. Predicted MDLs based on scaling arguments from previous measurements on another XRF system, and experimental MDLs as a function of overlaying tissue thickness. The addition of tissue equivalent material over the tibia bone phantom increases system dead time, causing experimental values to be slightly worse than predicted values. The average dead times are 40.3 %, 55.0 %, 55.3 %, 55.8 %, and 56.2 % for 0 mm, 3.3 mm, 4.0 mm, 7.5 mm, and 12.2 mm, respectively. The blue region represents previous concentrations of Gd measured in bone from other studies, and the yellow region represents the average tissue thickness overlaying an adult tibia. (For interpretation of the references to color in this figure legend, the reader is referred to the web version of this article.)

12 mm tissue overlay phantom, where the experimental value is significantly worse than the predicted. As previously mentioned, a considerable amount of excitation photons are escaping out the back of our lead collimator as the walls are slightly too thin. This causes a higher dead time when using the lead collimator compared to the tungsten collimator. A possible solution would be to increase the wall thickness of the lead collimator by 0.5 mm to significantly attenuate the 88 keV excitation photons, and therefore decrease the dead time.

The blue region of Fig. 6 represents the Gd concentrations previously measured in bone by other studies, which range from 0.1–6.02 μg Gd/g bone, and the yellow region represents an average tissue thickness over an adult tibia (Pejović-Milić et al., 2002). The MDL values for the XRF system lie well within the previously measured concentrations. The MDLs within the region representing the average overlaying tissue thickness are 1.64 and 1.72 μg Gd/g plaster, which are similar to the estimated values of 1.49 and 1.52 μg Gd/g plaster.

4.2. Comparison to recent XRF measurements of Gd in bone

A recent abstract submitted by Mostafaei and Nie (2016), to be presented at the 58th annual meeting for the American Association of Physicists in Medicine in August 2016, shows comparable MDLs for a similar XRF system. From the information provided in the abstract, Mostafaei & Nie used a 5 GBq Cd-109 excitation source, and a set of bone equivalent phantoms doped with Gd to determine the MDLs for bare bone phantoms, as well as bone phantoms with varying overlaying tissue thicknesses. A MDL of 0.8 ppm was reported for bare bone measurements, which is essentially the same as our value of 0.78 ppm (μg Gd/g plaster). However, we are unsure if phantoms constructed by Mostafaei & Nie are plaster. For tissue thicknesses ranging from 0.61–6.13 mm, Mostafaei & Nie report MDLs of 1.8–3.5 ppm (Mostafaei and Nie, 2016). These values are comparable to our MDL values for tissue thicknesses of 3.3–7.5 mm, which are 1.68–2.70 ppm (μg Gd/g plaster). The comparability of our MDL values to the values reported in the abstract by Mostafaei & Nie is promising, as it demonstrates the reproducibility of XRF for detecting Gd in bone. However, limited

information provided in the abstract leads to a few caveats when comparing MDL values. We are not sure of the exact measurement geometry used by Mostafaei & Nie, as well as the similarity between the plastic sheets used for tissue equivalent material and our Solid Water® material. The measurement time was also not included in the abstract, but is most likely around 30-min since the XRF system used is intended for future human measurements.

4.3. Cross validation with ICP-MS

To test the feasibility of the XRF system to detect Gd in bone further, we performed a cross validation study by measuring a set of autopsy bone samples acquired from the Wadsworth Center, and comparing XRF values to ICP-MS values. When we received the samples, they had already been measured using ICP-MS, and findings were not released to us until our measurements were complete. We found two patients with observable Gd levels using XRF, which were the same two patients in which the ICP-MS measurements had also reported elevated Gd levels. Medical records indicate that both patients had received GBCAs (Omniscan™). Patient 1 exhibited impaired renal function and developed NSF following an MRI scan; the patient passed away 7 years later. Patient 2 had a relatively healthy kidney function, received two MRI scans and passed away 4 weeks later with no clear symptoms of NSF (Galusha, 2015). Our XRF values and the ICP-MS values are displayed in Table 3 for comparison. A conversion factor of 0.676, which is the observed ash fraction in tibiae, has proven to be successful by the Wadsworth Laboratory for bone matrix conversions of XRF data from units of μg Gd/g bone mineral to μg Gd/g dry weight bone, which are the units in which ICP-MS values are reported Bellis et al., 2012.

With the given measurement uncertainties, the XRF values are compatible with the reported ICP-MS values. A quantitative comparison for the two techniques is challenging because we only have the in-measurement uncertainties, which are minimal estimates of uncertainties for the concentration values. A critical factor to note when comparing XRF values to ICP-MS values is the fact that the samples measured by XRF and ICP-MS were not the exact same samples, because ICP-MS is a destructive technique. The samples came from the same patient, but were from different parts of the bone. The assumption that two samples of bone have the same Gd concentration assumes that Gd is homogeneously distributed throughout all bone types and locations. The potential variability of Gd accumulation in the bone depending on location is a factor that needs to be considered when comparing XRF values to ICP-MS, and might account for the slight discrepancy in values. Additional complications with XRF measurements arise due to voids in bone structure, since all bone samples are trabecular bone, as well as the small size of the bone samples, which could effect the measurement geometry.

For the two samples that had observable Gd, an additional investigation was carried out to try and assess the uniformity of Gd deposited in bone mineral in the samples. Each bone sample was measured on the XRF system at ten different locations to compare Gd concentrations calculated from each measurement site. A z-score for each measurement site was calculated, resulting in values ranging from −1 to 1 for both samples. This indicates Gd concentrations from all measurement sites are within one standard deviation of the mean Gd concentration, and thus not statistically different from each other. Therefore, the z-scores indicate a uniform distribution of Gd only throughout each of the two small bone samples measured and do not necessarily indicate uniform Gd distribution across the skeleton as a whole.

Although a comparison with seven samples is not sufficient for a complete cross-validation study, the fact that the observed pattern across the seven samples is the same for both XRF and ICP-MS measurements places confidence in the ability of the XRF system to detect gadolinium. XRF found five samples had Gd levels below the detection limit, and ICP-MS data were consistent with values below the MDL of the current XRF method. Two bone samples were found to have detectable Gd levels by the XRF system, both with XRF and ICP-MS values in agreement. While a full validation with a large number of samples, each sample measured by both techniques, is ideal, these data provide confirmation that the XRF system is capable of detecting Gd in bone.

Finally, the bone sample data may also hint at a potential clinical role for this XRF system. Our system development has recently been focused on a system which can determine whether Gd is retained in the bones of healthy adults. Such a system is envisaged as being used in population studies to study the evidence for, or against, sub-clinical population health effects. We note, however, that we observed elevated Gd levels in patient 2, who did not exhibit signs of renal impairment. GBCAs, are, of course, no longer given to patients with renal impairment. However, the observation of Gd in this patient, at bone Gd levels that are at the high end for 'normal' volunteers, leads to the question of whether this patient may have been at risk for developing NSF (based on bone Gd levels) if he had survived longer. Investigation of whether elevated Gd levels in bone are an early indicator of subsequent clinical effects may be worth pursuing.

5. Conclusions

An improved XRF system for the detection of Gd in bone proved to have promising detection limits of 1.64–1.72 *μg* Gd/g plaster for overlying tissue thickness in the normal adult range. These experimentally determined detection limits were close to estimated values of 1.49–1.52 *μg* Gd/g plaster. These low MDL values suggest that the XRF system is capable of detecting the trace amounts of Gd that may remain in patient's bones after an MR imaging scan, since the published literature suggests retained levels of Gd in bone range from 0.1–6.01 μg Gd/g bone.

In addition to improved detection limits, autopsy bone samples measured by the XRF system gave comparable results to ICP-MS measurements performed at the Wadsworth Center. For both XRF and ICP-MS measurements, five patients had Gd levels below the MDL, while two of the patients had observable Gd levels with similar values between the two measurement techniques. The ability of the XRF system to measure such similar Gd concentrations to ICP-MS is promising and provides confidence in the XRF system's ability to identify Gd in bone in living subjects for human measurements of Gd. The XRF system has been deemed a feasible measurement system to detect Gd in bone, and has been commissioned to begin *in vivo* human measurements for a small population study, with the aim of observing Gd in an individual or within the population.

Conflicts of interest

The authors affirm that none of them has any conflict of interest.

Table 3
Gd concentration of bone samples with observable Gd, comparing XRF measurements with ICP-MS measurements.

Measurement technique	Patient 1	Patient 2
XRF	21.9 ± 0.3 μg Gd/g dry weight bone	5.2 ± 0.7 μg Gd/g dry weight bone
ICP-MS	17.0 ± 0.6 μg Gd/g dry weight bone	7.5 ± 0.5 μg Gd/g dry weight bone

Acknowledgements

This study was funded by Natural Sciences and Engineering Research Council of Canada Discovery Grants to FEMcN (203611-2012) and DRC (RGPIN06399-15).

References

Bellis, D.J., Todd, A.C., Parsons, P.J., 2012. An interlaboratory comparison of bone lead measurements via K-shell X-ray fluorescence spectrometry: validation against inductively coupled plasma mass: spectrometry. J. Anal. At. Spectrom. 27 (4), 595–603.

Carr, D., Brown, J., Bydder, G., Steiner, R., Weinmann, H., Speck, U., Hall, A., Young, I., 1984. Gadolinium-DTPA as a contrast agent in MRI: initial clinical experience in 20 patients. Am. J. Roentgenol. 143 (2), 215–224.

Chamberlain, M., Gräfe, J., Byun, S., Chettle, D., Egden, L., Orchard, G., Webber, C., McNeill, F., 2012. Aslam, The feasibility of in vivo quantification of bone-fluorine in humans by delayed neutron activation analysis: a pilot study. Physiol. Meas. 33 (2), 243–257.

Chettle, D., Scott, M., Somervaille, L., 1991. Lead in bone: sampling and quantitation using KX-rays excited by 109 Cd. Environ. Health Perspect. 91, 49–55.

Cowper, S.E., Su, L.D., Bhawan, J., Robin, H.S., LeBoit, P.E., 2001. Nephrogenic fibrosing dermopathy. Am. J. Dermatopathol. 23 (5), 383–393.

Darrah, T.H., Prutsman-Pfeiffer, J.J., Poreda, R.J., Campbell, M.E., Hauschka, P.V., Hannigan, R.E., 2009. Incorporation of excess gadolinium into human bone from medical contrast agents. Metallomics 1 (6), 479–488.

Errante, Y., Cirimele, V., Mallio, C.A., Di Lazzaro, V., Zobel, B.B., Quattrocchi, C.C., 2014. Progressive increase of T1 signal intensity of the dentate nucleus on unenhanced magnetic resonance images is associated with cumulative doses of intravenously administered gadodiamide in patients with normal renal function, suggesting dechelation. Invest. Radiol. 49 (10), 685–690.

Galusha, A.L., 2015. An Investigation of Alkaline Earth and Rare Earth Elements in Human Bone Following Long-term Parenteral Nutrition. State University of New York at Albany.

Gordon, C.L., Webber, C.E., Chettle, D.R., 1994. The reproducibility of 109Cd-based X-ray fluorescence measurements of bone lead. Environ. Health Perspect. 102 (8), 690–694.

Grobner, T., 2006. Gadolinium-a specific trigger for the development of nephrogenic fibrosing dermopathy and nephrogenic systemic fibrosis? Nephrol. Dial. Transplant. 21 (4), 1104–1108.

Kanda, T., Ishii, K., Kawaguchi, H., Kitajima, K., Takenaka, D., 2013. High signal intensity in the dentate nucleus and globus pallidus on unenhanced T1-weighted MR images: relationship with increasing cumulative dose of a gadolinium-based contrast material. Radiology 270 (3), 834–841.

Kanda, T., Fukusato, T., Matsuda, M., Toyoda, K., Oba, H., Kotoku, J., Haruyama, T., Kitajima, K., Furui, S., 2015. Gadolinium-based contrast agent accumulates in the brain even in subjects without severe renal dysfunction: evaluation of autopsy brain specimens with inductively coupled plasma mass spectroscopy. Radiology 276 (1), 228–232.

Kruger, P.C., Parsons, P.J., Galusha, A.L., Morrissette, M., Recker, R.R., Howard, L.J., 2014. Excessive aluminum accumulation in the bones of patients on long-term parenteral nutrition postmortem analysis by electrothermal atomic absorption spectrometry. J. Parenter. Enter. Nutr. 38 (6), 728–735.

Lord, M., McNeill, F., Gräfe, J., Noseworthy, M., Chettle, D., 2016. A phantom-based feasibility study for detection of gadolinium in bone in-vivo using x-ray fluorescence. Appl. Radiat. Isot. 112, 103–109.

Marckmann, P., Skov, L., Rossen, K., Dupont, A., Damholt, M.B., Heaf, J.G., Thomsen, H.S., 2006. Nephrogenic systemic fibrosis: suspected causative role of gadodiamide used for contrast-enhanced magnetic resonance imaging. J. Am. Soc. Nephrol. 17 (9), 2359–2362.

McDonald, R.J., McDonald, J.S., Kallmes, D.F., Jentoft, M.E., Murray, D.L., Thielen, K.R., Williamson, E.E., Eckel, L.J., 2015. Intracranial gadolinium deposition after contrast-enhanced MR imaging. Radiology 275 (3), 772–782.

Mostafaei, F., Nie, L., 2016. TH-AB-209-02: gadolinium measurements in human bone using in vivo KX-ray fluorescence (KXRF) technique. Med. Phys. 43 (6), 3863.

Murata, N., Gonzalez-Cuyar, L.F., Murata, K., Fligner, C., Dills, R., Hippe, D., Maravilla, K.R., 2016. Macrocyclic and other non-group 1 gadolinium contrast agents deposit low levels of gadolinium in brain and bone tissue: preliminary results from 9 patients with normal renal function. Invest. Radiol. 51 (7), 447–453.

Nie, H., Chettle, D., Luo, L., O'Meara, J., 2006. In vivo investigation of a new 109Cd γ-ray induced K-XRFbone lead measurement system. Phys. Med. Biol. 51 (2), 351–360.

Pejović-Milić, A., Brito, J., Gyorffy, J., Chettle, D., 2002. Ultrasound measurements of overlying soft tissue thickness at four skeletal sites suitable for in vivo x-ray fluorescence. Med. Phys. 29 (11), 2687–2691.

Quattrocchi, C.C., Mallio, C.A., Errante, Y., Cirimele, V., Carideo, L., Ax, A., Zobel, B.B., 2015. Gadodiamide and dentate nucleus T1 hyperintensity in patients with meningioma evaluated by multiple follow-up contrast-enhanced magnetic resonance examinations with no systemic interval therapy. Invest. Radiol. 50 (7), 470–472.

Rogosnitzky, M., Branch, S., 2016. Gadolinium-based contrast agent toxicity: a review of known and proposed mechanisms. BioMetals, 1–12.

Sherry, A.D., Caravan, P., Lenkinski, R.E., 2009. Primer on gadolinium chemistry. J. Magn. Reson. Imaging 30 (6), 1240–1248.

Somervaille, L.J., Chettle, D.R., Scott, M.C., 1985. In vivo measurement of lead in bone using x-ray fluorescence. Phys. Med. Biol. 30 (9), 929–943.

Thakral, C., Alhariri, J., Abraham, J.L., 2007. Long-term retention of gadolinium in tissues from nephrogenic systemic fibrosis patient after multiple gadolinium-enhanced MRI scans: case report and implications. Contrast Media Mol. Imaging 2 (4), 199–205.

Thomsen, H., Morcos, S., Dawson, P., 2006. Is there a causal relation between the administration of gadolinium based contrast media and the development of nephrogenic systemic fibrosis (NSF)? Clin. Radiol. 61 (11), 905–906.

Todd, A., 2000. Coherent scattering and matrix correction in bone-lead measurements. Phys. Med. Biol. 45 (7), 1953–1963.

Todd, A.C., McNeill, F.E., Fowler, B.A., 1992. In vivo X-ray fluorescence of lead in bone. Environ. Res. 59 (2), 326–335.

Weinmann, H.-J., Brasch, R., Press, W., Wesbey, G., 2005. Characteristics of gadolinium-DTPA complex: a potential NMR contrast agent. Class. Pap. Mod. Diagn. Radiol., 416–424.

White, G.W., Gibby, W.A., Tweedle, M.F., 2006. Comparison of Gd (DTPA-BMA) (Omniscan) versus Gd(HP-DO3A)(ProHance) relative to gadolinium retention in human bone tissue by inductively coupled plasma mass spectroscopy. Invest. Radiol. 41 (3), 272–278.

Chapter 5

Paper III: Coherent normalization for *in vivo* measurements of gadolinium in bone

Z. Keldani, M.L. Lord, F.E. McNeill, D.R. Chettle, and J.L. Gräfe Physiol. Meas., **38**, 1848-1858 (2017).

Following the work completed in Paper II, a developed XRF system was commissioned to perform *in vivo* measurements of Gd in bone. However, the challenge of interpatient variability for XRF measurements, such as variation in tissue thickness overlaying the tibia, still needed to be addressed before human measurements were able to take place. Coherent normalization involves normalizing the Gd Kα x-ray peaks to the 88 keV coherent peak on the spectra, and had been used to correct interpatient variability in previous trace element analysis studies in our research group. The feasibility of coherent normalization for Gd XRF measurements was initially questioned due to the large energy difference between the Gd Kα x-rays and excitation γ-ray not satisfying the four criteria for coherent normalization. However, we predicted that divergences from the four criteria would result in counteracting factors, such as secondary fluence, that deemed coherent normalization valid for the

Gd XRF system.

This study consisted of two parts: (1) experimental work at McMaster University, and (2) simulations at Ryerson University. A series of 24-hour phantom measurements was performed with the cloverleaf XRF detection system on the highest concentration phantom (120 μg Gd/g PoP) with overlaying tissue thicknesses of 0, 3.3 $\pm$ 0.1, 4.0 $\pm$ 0.1, 7.5 $\pm$ 0.1, and 12.2 $\pm$ 0.1 mm. Monte Carlo simulations were carried out using MCNP6 to model the cloverleaf HPGe detection system and simulate the experimental phantom measurements. For the experiment and simulation, the Gd peak areas were normalized with their respective coherent peaks and plotted as a function of tissue thickness. Coherent normalization was deemed valid for both experimental and MCNP simulations, as the Gd peak area to coherent peak area ratio remained constant across a range of tissue thicknesses (0 - 12.2 mm). In addition, the experimental and simulated average coherent normalization ratios over a range of tissue thicknesses were not significantly different (p=0.43)

To understand countering influences contributing to the validity of coherent normalization, MCNP6 was used to simulate the components of Gd Kα x-ray production from primary and secondary fluence, and subsequent attenuation. Simulation results showed that secondary fluence was the dominant contributing factor to the excitation of Gd in the bone phantoms, and provided a theoretical explanation of the experimental work demonstrating the effectiveness of the coherent normalization.

This project was suggested by David Chettle, Fiona McNeill, and James Gräfe, as a means to ensure coherent normalization would be appropriate to use for human measurements. All experimental measurements and calculations were carried out by myself at McMaster University under the supervision of David Chettle and Fiona McNeill. All Monte Carlo simulations were carried out by Zaid Keldani at Ryerson University under the supervision of James Gräfe. The writing of this manuscript was a joint effort, as Zaid Keldani and I share first-authorship. For the first draft of the manuscript, I wrote the introduction, experimental methods, experimental results, and conclusion. Zaid Keldani wrote the the simulation methods, and simulation

results. The discussion section was a collaborative effort between myself and Zaid Keldani. All authors of this paper were involved in editing the manuscript.

IOP Publishing | Institute of Physics and Engineering in Medicine Physiological Measurement

Physiol. Meas. **38** (2017) 1848–1858 https://doi.org/10.1088/1361-6579/aa87f0

Coherent normalization for *in vivo* measurements of gadolinium in bone

Z Keldani[1,4], M L Lord[2,4], F E McNeill[3], D R Chettle[3] and J L Gräfe[1]

[1] Department of Physics, Ryerson University, Toronto, M5B 2K3, Canada
[2] Radiation Sciences Graduate Program, McMaster University, Hamilton, L8S 4L8, Canada
[3] Department of Physics and Astronomy, McMaster University, Hamilton, L8S 4L8, Canada

E-mail: lordml@mcmaster.ca

Received 7 April 2017, revised 6 August 2017
Accepted for publication 23 August 2017
Published 21 September 2017

Abstract

Objective: Recent evidence of gadolinium (Gd) deposition in bones of healthy individuals who have previously received Gd-based contrast agents (GBCAs) for MRI has led to a demand for *in vivo* measurement techniques. The technique of x-ray fluorescence provides a low risk and painless method to assess Gd deposition in bone, and has the potential to be a useful clinical tool. However, interpatient variability creates a challenge while performing *in vivo* measurements. *Approach*: We explored the use of coherent normalization, which involves normalizing the Gd K x-rays to the coherent scattered γ-ray from the excitation source, for bone Gd measurements through a series of phantom-based experiments and Monte Carlo simulations. *Main results*: We found coherent normalization is able to correct for variation in overlying tissue thickness over a wide range (0–12.2 mm). The Gd signal to coherent signal ratio is independent of tissue thickness for both experiments and Monte Carlo simulations. *Significance*: Coherent normalization has been demonstrated to be used in practice with normal healthy adults to improve *in vivo* bone Gd measurements.

Keywords: x-ray fluorescence, coherent normalization, gadolinium deposition, gadolinium in bone, MRI

(Some figures may appear in colour only in the online journal)

[4] Authors contributed equally to this work.

1. Introduction

The routine use of gadolinium-based contrast agents (GBCAs) for MRI in hospitals worldwide is currently being questioned due to recent evidence of gadolinium (Gd) deposition in tissues of healthy individuals (Kanda *et al* 2013, Errante *et al* 2014, McDonald *et al* 2015, Quattrocchi *et al* 2015, Kanda *et al* 2015). Not only has Gd been identified in tissues, such as brain and bone, symptoms associated with Gd toxicity are now being recognized in some individuals who have previously received GBCAs (Ramalho *et al* 2016, Semelka *et al* 2016). For this reason, the safety of GBCAs is currently a major concern in the MRI community.

Bone tissue has been shown to serve as a major storage site for Gd in the body (Gibby *et al* 2004, White *et al* 2006, Darrah *et al* 2009, Murata *et al* 2016). The free Gd^{3+} ion is one of the largest competitive inhibitors for the Ca^{2+} ion, and is therefore believed to replace calcium in bone mineral (Sherry *et al* 2009). Currently Gd levels in bone can only be measured through invasive techniques, which are inconvenient and painful, and, in fact, much of the literature's data of Gd in bone stem only from autopsy samples. X-ray fluorescence (XRF) is a non-invasive, painless technique that can be used to detect Gd in bone through an *in vivo* measurement. The XRF system developed in our lab has been shown to be successful in measuring Gd in bone phantoms and autopsy bone samples, and is capable of carrying out 30 min tibial measurements on volunteers, involving a low dose of 0.13 μSv per measurement (Lord *et al* 2017). The measurement involves the subject placing their leg in front of a Cd-109 excitation source that is mounted on the face of a high purity germanium detector, which is described in further detail by Lord *et al* (2017).

Conducting human tibial measurements using the XRF system involves interpatient variability, with respect to the excitation source to measurement site distance, the size of the bone, and the depth of overlying tissue. Coherent normalization involves normalizing the measured K x-ray peak areas to the coherent peak area of the excitation source, and has been successfully used with previous XRF systems to correct for this interpatient variability.

Somervaille *et al* investigated the use of coherent normalization for a similar XRF system consisting of a Cd-109 excitation source to measure lead (Pb) in human tibia (Somervaille *et al* 1985). For coherent normalization to be valid, the system must satisfy four criteria:

(1) the Pb K x-rays and coherent scatter signals must be produced from the same fluence,
(2) both signals must be created from the same location in the sample,
(3) both signals must have the same angular distribution,
(4) both signals must be attenuated similarly on their way back to the detector.

The system described by Somervaille *et al* for bone-Pb measurements satisfies most criteria for coherent normalization. Firstly, since the Cd-109 γ-ray energy is close to the K-edge of Pb, the Pb K x-rays are mostly produced from the primary excitation γ-ray, and not from secondary fluence such as Compton scattered photons. Secondly, the coherent scattering cross section for the Cd-109 88 keV excitation energy in cortical bone is approximately 28 times larger than the cross section for soft tissue, meaning both the K x-rays and coherent γ-rays are produced in bone. Thirdly, the K x-rays are produced isotropically while the coherent scattering is not isotropic. However, the differential coherent scattering cross section is relatively constant over the angles encountered in the backscatter geometry at an energy of 88 keV. Lastly, the difference in attenuation between the Pb K x-ray (72.8 keV) and the coherent γ-ray (88 keV) through bone and tissue results in only a small difference in measured signals due to the similar energies (Somervaille *et al* 1985).

When comparing the XRF system used by Somervaille *et al* to our XRF system, there is one major difference: we are detecting Gd instead of Pb. The excitation source energy of

88 keV and 180° geometry remains the same, causing criteria (2) and (3) to be satisfied for the Gd XRF system. It is the large difference in energies of the Gd K x-rays (43 keV) and coherent γ-rays (88 keV) that leads to questioning the feasibility of coherent normalization for human measurements. For criterion (1), the 88 keV excitation energy is 37.7 keV above the Gd K-edge (50.24 keV). If the excitation γ-ray undergoes Compton backscatter, resulting in the maximum energy loss for a single Compton event, the scattered x-ray will still be 15.2 keV above the Gd K-edge. For this reason, it is very likely that Gd K x-rays are being produced by secondary fluence from Compton scatter. Therefore, coherent γ-rays are produced by the primary fluence of the excitation γ-rays, where Gd K x-rays are produced by both primary and secondary fluence. The difference in energy between the Gd K x-rays and coherent γ-rays lead to a differential attenuation through bone and tissue, causing criterion (4) to be left unsatisfied.

Although criteria (1) and (4) are not satisfied due to the lower Gd K x-ray energy, certain counteracting factors have deemed coherent normalization feasible in XRF systems where not all four criteria are met. An XRF system by O'Meara *et al* using a Co-57 excitation source to measure uranium (U) in bone did not meet criteria (1) and (4) due to the excitation energy of 122 keV being 6.5 keV above the U K-edge. Coherent normalization was not expected to work for this system, yet a Monte Carlo simulation showed that the ratio of U K x-rays to coherent γ-rays remains constant over a large range of overlying tissue, indicating the normalization is valid. As the overlying tissue thickness increases, the primary fluence from the excitation γ-ray decreases, thus decreasing both the XRF signal and coherently scattered signal. However, the secondary fluence from Compton events increases, which counters the decrease in primary fluence contributing to the XRF signal and may compensate for the differential attenuation of the excitation γ-ray and lower energy XRF signal. This effective cancellation could be the reason for coherent normalization functioning for this system, and could be a contributing factor in the Gd XRF system as well (O'Meara *et al* 1997). Sufficient countering influences were also present in an XRF system using a Co-57 source to measure lead in bone. The change in K x-ray signal to coherent signal ratio with overlaying tissue was investigated by experiment and Monte Carlo simulation and indicated that the normalization procedure is acceptable for this system (O'Meara *et al* 2001).

Given the examples of valid normalization on past XRF systems, it is possible that divergences from the four criteria will result in counteracting factors that deem normalization a valid procedure for Gd measurements conducted on our XRF system. In this paper, we investigate the use of coherent normalization through experiment and Monte Carlo simulation. We use the Monte Carlo code MCNP6 (Goorley 2014) to simulate the components of Gd K x-ray production and subsequent attenuation to understand countering influences contributing to the validity of coherent normalization.

2. Methods

2.1. Experimental measurement

A set of tibia bone phantoms was constructed using Plaster of Paris ($CaSO_4 \cdot 2H_2O$) to represent bone, for previous experiments that explored the feasibility of using our XRF-system to detect Gd in bone (Lord *et al* 2016, 2017). The bone phantoms are anthropomorphic to a human tibia, in the shape of a cylindrical shaft with a diameter of 28.0 mm and length of 115.0 mm. Gadolinium solution, prepared from gadolinium oxide (Gd_2O_3) dissolved in dilute nitric acid, was added to the plaster mixture to create phantoms of varying Gd concentrations. The bone phantom with a concentration of 120 μg Gd g^{-1} plaster was used for the

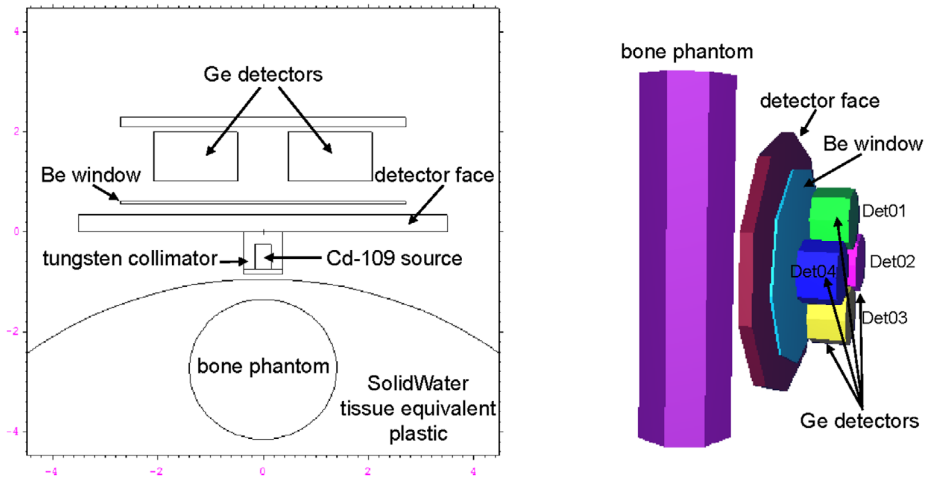

Figure 1. MCNP model of the XRF system. (a) Top view. (b) Isometric view (3D view).

experiments presented in this article, since this is the highest concentration and will therefore produce the strongest Gd signal in measurements.

The XRF system used is a 'cloverleaf' high purity germanium detector (HPGe) from Canberra Industries (GL0210R/S), consisting of four smaller detectors in a cloverleaf formation (figure 1). Each HPGe detector is 16 mm in diameter and 10 mm thick, and attached to its own set of pulse processing electronics, including a preamplifier (Canberra 2002CP) and digital pulse processing system (Canberra DSA 1000). Data are collected on four separate spectra using Genie 2000 Gamma Analysis Software from Canberra. The four spectra are then exported for further analysis of the Gd and Coherent signals using MATLAB.

A Cd-109 excitation source, with an activity ranging from 4.11–4.04 GBq at the time of these experiments, was mounted to the face of the detector. The Cd-109 source emits excitation γ-rays of 88 keV and silver x-rays in the range of 22–25 keV. The source was enclosed in a tungsten collimator with a copper face to filter out the silver x-rays (Lord *et al* 2016). The phantom was placed at a close distance of 1 mm directly in front of the source to create a 180-degree geometry. Measurements were conducted on the bone phantom for 24 h live-time, with tissue equivalent material (solid water®) of thicknesses of 3.3 ± 0.1 mm, 4.0 ± 0.1 mm, 7.5 ± 0.1 mm, and 12.2 ± 0.1 mm, to investigate how the Gd signal to coherent signal ratio changes with tissue thickness. A longer measurement time was chosen over a realistic *in vivo* measurement of 30 minutes, to lower measurement uncertainties.

For a measurement, each spectrum was analyzed by fitting the two Gd Kα peaks at 42.3 and 43 keV, as well as the coherent peak at 88 keV. The method of non-linear least squares was used in MATLAB to fit the Gd peaks with a double Gaussian function and a polynomial background, since the peaks were located on the side of another feature on the spectra. The coherent peak was fit using a single Gaussian and linear background, as this peak did not interfere with any other features on the spectra. All peak fits resulted in χ^2 values of 1.0 ± 0.20. Peak areas were then calculated from the Gaussian constants obtained from the fit, and the ratio of Gd signal to coherent signal was calculated and plotted as a function of overlying tissue equivalent material.

2.2. Monte Carlo simulations

The latest release of the general purpose Monte Carlo *N*-Particle (MCNP) radiation transport code, MCNP6, was used in this work. MCNP6 was first introduced by Los Alamos National Laboratories in 2012, and is the merger of capabilities of MCNP5 and MCNPX (Goorley *et al* 2012). Besides incorporating capabilities of earlier MCNP versions, MCNP6 offers several newly added features. Those of significance to this work are enhanced photon form factors and complete atomic relaxation processes (Hughes (2014b)). The enhanced code's performance is based on the introduction of the extended Evaluated Nuclear Data File (ENDF/B VI.8) as well as the improved transport methods (Hughes (2014b)). ENDF/B VI.8 contains extended form factor functions that cover a larger energy and angular range compared to previous releases. Previous versions could not adequately model coherent scattering for photon energies above 74 keV (Hughes (2014a)). Additionally, a correct logarithmic method replaced the older linear interpolation of form factors. These updates lead to a comprehensive representation of coherent and incoherent scatter events, which is significant for modelling backscattering experiments. The updated data can be requested using the .12p photon transport table in the material card of the input file (Hughes (2014b)). MCNP6 is able to model complete atomic relaxation processes including fluorescent photons and Auger electrons down to the energy cut-off of each. Previous MCNP versions considered only K-shell transitions as well as weighted L-shell transitions. The extended library includes data in energy ranges as low as 1 eV allowing for more comprehensive calculations to be done.

2.3. Monte Carlo model of the Gd K-XRF system

A realistic model of the Cd-109 based XRF system including the clover-leaf HPGe detection system, collimator, phantom and solid water® was created in MCNP6 (Lord *et al* 2017). This is shown in figure 1. The detector dimensions were extracted from the manufacturer's drawings and all other dimensions were chosen to reproduce the experimental set-up. The Cd-109 source was modelled as a simple point source inside the custom tungsten collimator. We modelled the experiment exactly, except we did not include the 1 mm thick overlying plastic of the bone phantoms. The Plaster of Paris (PoP) phantom and solid water® were modelled as non-concentric cylinders. In order to improve the statistical results in the Gd peak regions of interest, we modelled the bone phantom to contain a Gd concentration of 1200 μg Gd g^{-1} plaster. The Monte Carlo results were then scaled down to 120 μg Gd g^{-1} plaster, to match the experimental results. One concern with this approach would be the small contribution of the extra Gd to the coherent scattering within the phantom. We investigated this by turning off coherent scattering in Gd only, which is accomplished by not calling on the new .12p photon interaction tables for Gd in the material card, and found no significant effect on the coherent scattering from the phantom.

The pulse height tally, F8, was used to simulate the detector response in order to determine the Gd K x-ray peak intensities as well as the backscattered coherent peak intensity. Only data from one of the four cloverleaf detectors was tallied in the simulations. Although there is limited detector-to-detector variation, we compared the same detector (Det02) in both the simulation and experimental results. As mentioned earlier, photons emitted by Cd-109 are approximately 37.7 keV higher than the K-edge energy of Gd. That means, scattered photons of energies higher than the K-edge energy of Gd can still undergo a photoelectric effect and produce characteristic x-rays. Hence, the production of Gd x-rays is caused by two fluence components; the primary fluence, consisting of non-scattered photons, and a secondary fluence which includes Compton scattered photons. The code was used to determine the relative

contribution of the primary and secondary components to the Gd K x-ray fluorescence. The FM4 tally multiplier card was used to tally the photoelectric reaction rate per unit volume for the primary and secondary fluence components respectively:

$$R_{\text{primary}}(E) = n \int_{87.999}^{88.034\ keV} \Phi(E)\sigma(E)\mathrm{d}E \tag{1}$$

$$R_{\text{secondary}}(E) = n \int_{50.2}^{87.999\ keV} \Phi(E)\sigma(E)\mathrm{d}E \tag{2}$$

where n is the number of Gd atoms per unit volume. Equation (1) is written as an integral, but it essentially represents the reaction rate for the mono-energetic 88.034 keV primary photons with Gd. Equation (2), represents the integration of the photon fluence spectrum, $\Phi(E)$, over the energy dependent cross section $\sigma(E)$. The integration limits span energies above the K-edge of Gd to an energy of 87.999 keV (an energy we arbitrarily used to represent the cut-off between scattered and primary photons in the simulation). As in the experiments, the simulations were run for varying solid water® thicknesses ranging between 0 to 12.2 mm while keeping the distance between the measurement site and the collimator constant at 1 mm.

3. Results and discussion

The relative contribution of the primary and secondary components of the photon fluence to Gd K x-ray fluorescence interactions in the bone phantoms as a function of tissue thickness, modelled by Monte Carlo simulations, is shown in figure 2. The secondary fluence contributes a significant amount to the fluorescence of Gd. In fact, it is the dominant contribution. The Monte Carlo code cannot distinguish between interactions resulting in K-shell fluorescence and higher shells. Since photons with energy above the K-edge, by default possess enough energy to fluoresce the higher shells, these will be included in the integration results of equations (1) and (2). If the photon energy exceeds the K-edge, the relative amount of fluorescence events contributing to K-shell events compared to higher shell events is a fixed probability, and the ratio is typically about 4:1 (Podgoršak 2006), favouring the K-shell. Since both integrations in equations (1) and (2) only include photons with energies above the K-edge of Gd, by taking relative interaction rates, the K-shell to L-shell and higher shell fluorescence emission probability ratio will factor out.

The proportion of x-rays produced by the secondary fluence increases with tissue thickness, with the opposite being true for the primary fluence component. However, both components share the same degree of change (magnitude of slope) i.e. the rate of change of each component's contribution as a function of tissue thickness. The scattered fluence increases with thickness, while the primary fluence decreases with thickness, as expected.

For the 1200 μg Gd g^{-1} phantom Monte Carlo simulations, the coherent normalization of Gd K x-ray signal to coherently scattered signal as a function of tissue thickness results in a line with a slope of -0.0053 ± 0.0040 (one standard deviation). The slope is within 1.3 uncertainties of zero and is therefore not significant at the 95% confidence level. This suggests the signal ratio is independent of tissue thickness, and that the normalization method is acceptable for tissue thicknesses in the range of 0–12.2 mm. This relationship is shown in figure 3, and illustrates the relationship between Gd x-ray-to-coherent ratio and tissue thickness. The average ratio is 0.717 ± 0.025, suggesting the normalized signal varies by 3.5% within one standard deviation. This is acceptable considering other uncertainties involved in the *in vivo* measurement procedure. For tissue thicknesses ranging from 3.3–7.5 mm, the 1200 μg Gd g^{-1}

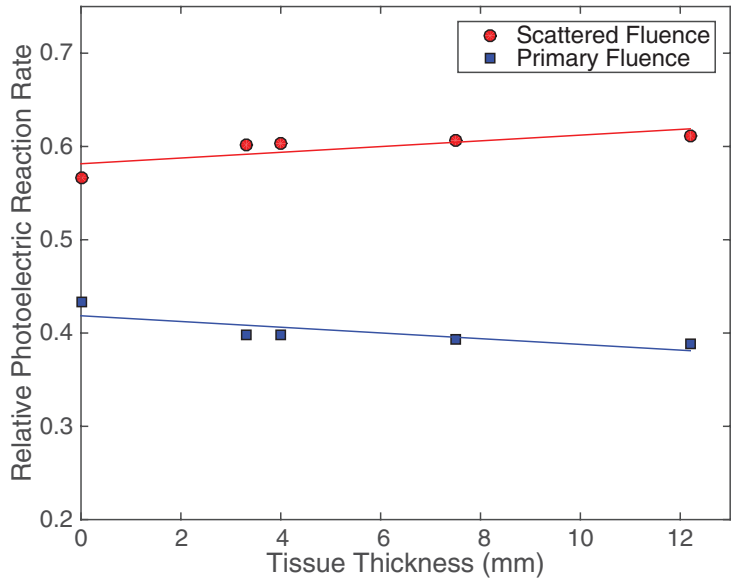

Figure 2. Relative contribution of the primary and secondary photon fluence to the Gd K x-ray fluorescence, both with a slope of magnitude 0.0031 ± 0.0017, with the scattered fluence having a positive slope, and primary fluence having a negative slope. The statistical uncertainties in these simulation results were less than 1%.

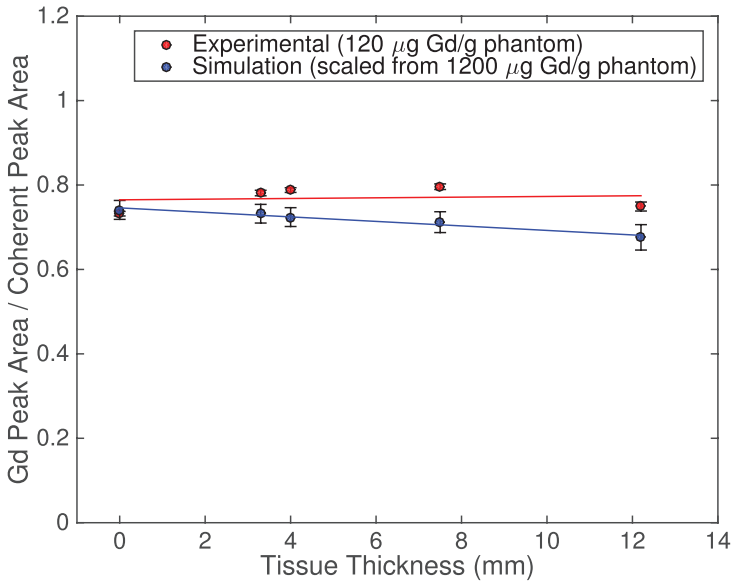

Figure 3. Gd K x-ray counts normalized to the Cd-109 88 keV coherently scattered gamma-rays for experimental values for the 120 μg Gd g^{-1} plaster phantom, and simulation values scaled from the 1200 μg Gd g^{-1} plaster phantom.

phantom simulation data results in an insignificant slope of -0.0043 ± 0.014. Since the average tissue thickness over an adult tibia is approximately 4–5 mm (Pejović-Milić *et al* 2002), the insignificant slope between 3.3–7.5 mm suggests coherent normalization is especially useful for the average healthy individual.

Experimental data are displayed in figure 3, which result in a line with a slope of zero within statistical uncertainties (0.0021 ± 0.0059), and an average ratio of 0.749 ± 0.019, suggesting the normalized signal varies by 2.5% within one standard deviation. As previously mentioned, all data illustrated in figure 3 are from one of four cloverleaf detectors (Det02), as data from each of the cloverleaf detectors are statistically the same. Experimental measurements resulted in an insignificant slope for tissue thicknesses ranging from 0–y12.2 mm, suggesting coherent normalization is valid over the entire range. Coherent normalization was also deemed valid over this tissue thickness range for the 1200 μg Gd g^{-1} phantom simulations, since the slope was insignificant at the 95% confidence level. There is a slight tendency towards a negative slope for the Monte Carlo simulations of the coherent normalization. This will be discussed below in comparison to the simulation, which separates each interaction into components. It should also be noted that we have made every attempt to model the detector positioning, components, and materials as exact to the experiment as possible, however, we have not made an attempt to benchmark the detection efficiency. Despite these limitations, we argue that it is remarkable to have the average coherent normalization ratio agree with the experiment ratio, as these numbers are not significantly different ($p = 0.43$).

As the overlying tissue thickness is increased there is an increase of secondary Compton scattered photons. As photons lose energy due to these scattering events they become closer in energy to the K-edge energy of Gd, meaning that they have a higher probability (larger cross section) of inducing a photoelectric effect. Both Gd x-rays and coherently scattered photons are attenuated by the tissue. Gd x-rays of approximately 43 keV, experience a higher attenuation compared to 88 keV coherently scattered photons. However, this differential attenuation is effectively counteracted by the increase in secondary fluence, which we will refer to as the secondary fluence fluorescence factor (SFFF). The SFFF is the ratio of the total photoelectric effect reaction rate (sum of equations (1) and (2)) to the primary reaction rate (equation (1)) in the bone phantoms, and represents the proportion of fluorescence emission induced by the secondary photon fluence. SFFF does not rely on the angular distribution contained in the cross section tables for any specific element. The normalized secondary fluence fluorescence factor (normalized to zero overlying tissue thickness to demonstrate the impact of tissue scattering) is plotted in figure 4. In addition, the ratio of the differential exponential attenuation of the approximately 43 keV Gd x-rays to the 88 keV as a function of solid water® thickness was also plotted. The product of these two components counteract each other, producing a relatively flat line with no significant slope. This method does not rely on the differential coherent scattering cross sections as a function of scattering angle (i.e. the angular dependence) as would the simulation of the detector measured spectrum from which the results of figure 3 are obtained. As coherent scattering with all elements over all energies is a new addition to the MCNP6 code, there may be some discrepancies inherent in the code, and this is an area of future research we intend to conduct. Furthermore, any deviations in the solid water® composition used in the experiment and Monte Carlo work could result in different coherent scattering within the solid water®, which may influence the coherent scattering ratio.

We have shown through experiment and Monte Carlo simulation that the coherent normalization procedure, originally designed for the bone-Pb system (Somervaille *et al* 1985), works reasonably well for the Gd system. The coherent normalization is valid for varying body types and overlying tissue thicknesses up to 12.2 mm for the bone-Gd system. The Monte Carlo

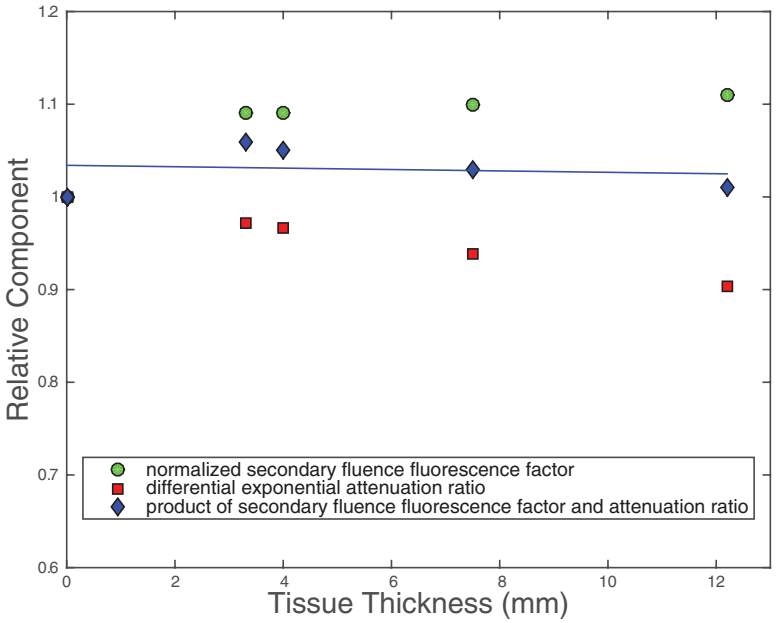

Figure 4. A plot demonstrating how the increase of secondary fluence (SFFF) compensates for the differential attenuation of Gd K x-rays and the coherently scattered gamma rays. The product of the secondary fluence fluorescence factor and exponential attenuation ratio results in an insignificant slope of $-0.000\,75 \pm 0.010\,00$.

simulation of the full experiment demonstrates a slight trend to a negative slope compared to experimental work, however over the typical range of overlying tissue thickness for healthy adults there is no trend in the coherent normalization. The simulation involving the components contributing to the coherent normalization removes any inherent unknown factors in the data tables utilized in the code, and provides a theoretical explanation of the experimental work demonstrating the effectiveness of the coherent normalization. Some limitations of our study are the use of solid water® as a tissue equivalent substitute at these energy ranges. It is difficult to match soft tissue composition, overlying fat or skin, at the energy range of interest for our work and this is obviously an area of future research. We have not investigated the coherent normalization as function of distance from the source, however, the design of our measurement system minimizes any potential participant movement.

4. Conclusions

The Monte Carlo simulations validate the experimental results and demonstrate that the coherent normalization procedure for the Cd-109 bone Gd x-ray fluorescence system is effective to better than 5% (3.5% for simulations, 2.5% for experimental) over a large range of tissue thicknesses (0–12.2 mm) for *in vivo* measurements. The variation in the experimentally measured Gd signal to coherent signal is 0.749 ± 0.019, and 0.717 ± 0.025 for the Monte Carlo simulation for a 120 μg Gd g^{-1} plaster phantom. The normalization is able to correct for variation in overlying tissue thickness within the investigated range typical of an adult population, and will be helpful for *in vivo* Gd measurements to correct for interpatient variability.

Acknowledgments

The Natural Sciences and Engineering Research Council of Canada (FEM DRC), and the Ontario Graduate Scholarship (MLL) is acknowledged for financial support of this study. JLG would like to acknowledge the support of Ryerson University in the form of internal start-up grants.

Conflicts of interest

The authors affirm that none of them has any conflict of interest.

ORCID iDs

J L Gräfe https://orcid.org/0000-0001-8309-0088

References

Darrah T H, Prutsman-Pfeiffer J J, Poreda R J, Campbell M E, Hauschka P V and Hannigan R E 2009 Incorporation of excess gadolinium into human bone from medical contrast agents *Metallomics* **1** 479–88

Errante Y, Cirimele V, Mallio C A, Di Lazzaro V, Zobel B B and Quattrocchi C C 2014 Progressive increase of T1 signal intensity of the dentate nucleus on unenhanced magnetic resonance images is associated with cumulative doses of intravenously administered gadodiamide in patients with normal renal function, suggesting dechelation *Investigative Radiol.* **49** 685–90

Gibby W A, Gibby K A and Gibby W A 2004 Comparison of Gd DTPA-BMA (Omniscan) versus Gd HP-DO3A (ProHance) retention in human bone tissue by inductively coupled plasma atomic emission spectroscopy *Investigative Radiol.* **39** 138–42

Goorley T 2014 Mcnp6 1.1-beta release notes *Los Alamos National Laboratory Technical Report*

Goorley T *et al* 2012 Initial MCNP6 release overview *Nucl. Technol.* **180** 298–315

Hughes H G 2014a Enhanced electron-photon transport in MCNP6 *Joint Int. Conf. on Supercomputing in Nuclear Applications + Monte Carlo' EDP Sciences* p 03105

Hughes H G 2014b Recent developments in low-energy electron/photon transport for MCNP6 *Prog. Nucl. Sci. Technol.* **4** 454–8

Kanda T, Fukusato T, Matsuda M, Toyoda K, Oba H, Kotoku J, Haruyama T, Kitajima K and Furui S 2015 Gadolinium-based contrast agent accumulates in the brain even in subjects without severe renal dysfunction: evaluation of autopsy brain specimens with inductively coupled plasma mass spectroscopy *Radiology* **276** 228–32

Kanda T, Ishii K, Kawaguchi H, Kitajima K and Takenaka D 2013 High signal intensity in the dentate nucleus and globus pallidus on unenhanced T1-weighted MR images: relationship with increasing cumulative dose of a gadolinium-based contrast material *Radiology* **270** 834–41

Lord M, McNeill F, Gräfe J, Galusha A, Parsons P, Noseworthy M, Howard L and Chettle D 2017 Confirming improved detection of gadolinium in bone using *in vivo* XRF *Appl. Radiat. Isot.* **120** 111–8

Lord M, McNeill F, Gräfe J, Noseworthy M and Chettle D 2016 A phantom-based feasibility study for detection of gadolinium in bone *in vivo* using x-ray fluorescence *Appl. Radiat. Isot.* **112** 103–9

McDonald R J, McDonald J S, Kallmes D F, Jentoft M E, Murray D L, Thielen K R, Williamson E E and Eckel L J 2015 Intracranial gadolinium deposition after contrast-enhanced MR imaging *Radiology* **275** 772–82

Murata N, Gonzalez-Cuyar L F, Murata K, Fligner C, Dills R, Hippe D and Maravilla K R 2016 Macrocyclic and other non-group 1 gadolinium contrast agents deposit low levels of gadolinium in brain and bone tissue: preliminary results from 9 patients with normal renal function *Investigative Radiol.* **51** 447–53

O'Meara J, Chettle D, McNeill F and Webber C 1997 The feasibility of measuring bone uranium concentrations *in vivo* using source excited K x-ray fluorescence *Phys. Med. Biol.* **42** 1109–20

O'Meara J M, Börjesson J, Chettle D R and Mattsson S 2001 Normalisation with coherent scatter signal: improvements in the calibration procedure of the 57Co-based *in vivo* XRF bone-Pb measurement *Appl. Radiat. Isot.* **54** 319–25

Pejović-Milić A, Brito J, Gyorffy J and Chettle D 2002 Ultrasound measurements of overlying soft tissue thickness at four skeletal sites suitable for *in vivo* x-ray fluorescence *Med. Phys.* **29** 2687–91

Podgoršak E B 2006 *Radiation Physics for Medical Physicists* (Berlin: Springer)

Quattrocchi C C, Mallio C A, Errante Y, Cirimele V, Carideo L, Ax A and Zobel B B 2015 Gadodiamide and dentate nucleus T1 hyperintensity in patients with meningioma evaluated by multiple follow-up contrast-enhanced magnetic resonance examinations with no systemic interval therapy *Investigative Radiol.* **50** 470–2

Ramalho J, Ramalho M and Semelka R C 2016 Gadolinium deposition and toxicity: a global concern *Curr. Radiol. Rep.* **4** 59

Semelka R C, Ramalho M, AlObaidy M and Ramalho J 2016 Gadolinium in humans: a family of disorders *Am. J. Roentgenol.* pp W1–5

Sherry A D, Caravan P and Lenkinski R E 2009 Primer on gadolinium chemistry *J. Magn. Reson. Imaging* **30** 1240–8

Somervaille L J, Chettle D R and Scott M C 1985 *In vivo* measurement of lead in bone using x-ray fluorescence *Phys. Med. Biol.* **30** 929–43

White G W, Gibby W A and Tweedle M F 2006 Comparison of Gd (DTPA-BMA)(Omniscan) versus Gd (HP-DO3A)(ProHance) relative to gadolinium retention in human bone tissue by inductively coupled plasma mass spectroscopy *Investigative Radiol.* **41** 272–8

Chapter 6

Paper IV: Observed deposition of gadolinium in bone using a new noninvasive *in vivo* biomedical device: results of a small pilot feasibility study

M. L. Lord, D. R. Chettle, J. L. Gräfe, M. D. Noseworthy and F. E. McNeill, Radiology, **287**, 96-103 (2017).

In this paper, we reported for the first time, successful non-invasive measurement of Gd retention in human bone. The cloverleaf XRF detection system established in Paper II was used to measure a small population: 11 individuals who had previously received GBCAs, and 11 control individuals who had never received GBCAs. The purpose of the work conducted in this paper was to perform a preliminary evaluation of the XRF system to detect Gd *in vivo*, and to investigate the possible relationship between Gd retention in bone and GBCA dose.

The study population for this pilot study was based on a previous study conducted by our research group in 2011, in which individuals were administered a dose of GBCA (Gadovist) to test the method of prompt γ neutron activation analysis to measure Gd retention in muscle tissue. I recruited 6 of the original 10 volunteers of this study, who had been "exposed" to GBCA. The additional 5 exposed volunteers were found when recruiting a control population, as certain individuals self-reported themselves as having previously received GBCAs. The 11 exposed participants were age and sex matched with 11 control participants. Each tibia measurement with the XRF system was 30 minutes long (live time), and consisted of the participants sitting in a chair with their leg placed in front of the Cd-109 source, as described in Section 2.2.2. Coherent normalization was applied to the measured Gd Kα peaks, as it was proven in Paper III to be successful for correcting interpatient variability in Gd XRF measurements. One-tailed t tests were performed to test if Gd bone concentrations in the exposed group were significantly different from the control group. The relationship between Gd concentration in bone and the GBCA dose was analysed with a linear regression.

Gd concentration in bone was found to be significantly higher in the exposed group compared to the control group ($p = 0.01$). The regression analysis of Gd concentration and GBCA dose showed a significant positive correlation ($p = 0.003$), suggesting that the amount of Gd retained in bone increases linearly with GBCA dose. Additionally, Gd was detected in individuals 5 years after a single injection of GBCA. It was difficult to draw any clinical conclusions from this paper, since the study was a small pilot study, and a larger population study would be required to do this. However, this paper proved that the XRF system was able to detect Gd within populations, and has the potential to be used to assess Gd retention in studies investigating the potential health effects of retained Gd in the body.

This project was the next step after establishing an XRF system feasible for performing *in vivo* measurements of Gd in bone. Since this was a human study, there was a laborious process to obtain approval from the Hamilton Integrated Research Ethics Board to recruit and measure participants. I wrote and submitted multiple rounds of

ethics reports with the help of David Chettle and Fiona McNeill. Once ethics approval was obtained, human measurements commenced at McMaster university. I performed all of 22 measurements, going over consent forms with each participant prior to their measurement. David Chettle or Fiona McNeill assisted with these measurements, and James Gräfe and Michael Noseworthy provided support and guidance throughout the human measurements. I wrote the first draft of this manuscript, which was then edited by all authors of this paper.

Radiology

Observed Deposition of Gadolinium in Bone Using a New Noninvasive in Vivo Biomedical Device: Results of a Small Pilot Feasibility Study[1]

Michelle L. Lord, BS
David R. Chettle, PhD
James L. Gräfe, PhD
Michael D. Noseworthy, PhD
Fiona E. McNeill, PhD

Purpose: To perform a preliminary evaluation of a noninvasive measurement system to assess gadolinium deposition in bone and to investigate the relationship between the administration of gadolinium-based contrast agents (GBCAs) and gadolinium retention in bone.

Materials and Methods: In vivo measurement of gadolinium retention in tibia bones was performed in 11 exposed subjects who previously received GBCAs (six exposed subjects were from a study performed 5 years previously involving injection of GBCAs in healthy volunteers; five exposed subjects had self-reported GBCA exposure), and 11 sex- and age-matched control subjects without a history of GBCA exposure. Each subject underwent one measurement of gadolinium retention in the tibia with x-ray fluorescence in a laboratory at McMaster University. A one-tailed *t* test was performed to compare gadolinium concentration in the exposed group with that in the control group. The relationship between the dose of GBCA administered and the gadolinium concentration measured in bone was analyzed with linear regression.

Results: Gadolinium concentration in bone was significantly higher in exposed subjects (mean, 1.19 μg Gd/g bone mineral ± 0.73 [standard deviation]) than in control subjects (mean, −1.06 μg Gd/g bone mineral ± 0.71) (P = .01). There was also a positive correlation between the dose of GBCA administered and the gadolinium concentration measured in bone (R^2 = 0.41); gadolinium concentration in bone increased by 0.39 μg Gd/g bone mineral ± 0.14 per 1 mL of GBCA administered. Gadolinium was detected in bone up to 5 years after one GBCA administration.

Conclusion: This x-ray fluorescence system is capable of measuring gadolinium deposition in bone noninvasively in vivo. Gadolinium can be retained in bone after one dose of GBCA in healthy subjects.

Online supplemental material is available for this article.

[1] From the Interdisciplinary Graduate Program in Radiation Sciences (M.L.L.), Department of Physics and Astronomy (D.R.C., F.E.M.), McMaster School of Biomedical Engineering (M.D.N.), and Department of Electrical and Computer Engineering (M.D.N.), McMaster University, 1280 Main St W, Hamilton, ON, Canada L8S 4L8; and Department of Physics, Ryerson University, Toronto, Ontario, Canada (J.L.G.). Received May 23, 2017; revision requested July 10; revision received August 17; accepted September 29; final version accepted October 12. **Address correspondence to** M.L.L. (e-mail: *lordml@mcmaster.ca*).

Supported by Ontario Graduate Scholarship and the Natural Sciences and Engineering Research Council of Canada (203611-2012, RGPIN06399-15).

The Canadian Institute of Health Information has stated that 49 of 1000 Canadians (1.7 million people) were examined with magnetic resonance (MR) imaging in 2012, the latest year for which data are available. MR imaging rates in other countries, such as the United States (98 per 1000 people annually) and Germany (95 per 1000 people annually), were approximately double this number (1). A large proportion of those people examined, perhaps up to one-third, received a gadolinium-based contrast agent (GBCA). These data suggest that millions of people are being injected with GBCAs around the world every year.

GBCAs have obvious utility: they are used, for example, in tumor detection and diagnosis. It is their effectiveness that has driven their widespread use. GBCAs were first introduced to the medical community in 1984 as potential agents for MR imaging because of the paramagnetic properties of ionic gadolinium (Gd^{3+}) (2). Free gadolinium is toxic; however, when it forms a chelate with a low-molecular-weight molecule, the resultant water-soluble complex was previously presumed to be entirely excreted from the body within a few hours after administration, thus rendering the contrast agent low risk (3,4). These GBCAs are so useful that, to date, there are nine varieties approved for clinical use, with over 200 million doses administered worldwide since the initial clinical use (5). Although there was some early evidence of gadolinium deposition in humans (6–8), the safety of GBCAs became of substantial concern in the MR imaging community when the first occurrence of nephrogenic systemic fibrosis appeared in individuals with chronic renal disease, suggesting these complexes were not being excreted as expected, but rather, were being deposited in the body (9–11). The use of GBCAs to image individuals with renal failure is now rare, due to the extra precautions taken to prevent nephrogenic systemic fibrosis (eg, immediate dialysis in patients with kidney problems). To our knowledge, no case of nephrogenic systemic fibrosis has been reported since 2009 (12), resulting in a generally restored confidence in the safety of GBCAs.

New concerns regarding the potential safety of GBCAs have arisen. Deposition of gadolinium in brain tissue of individuals with normal renal function has been reported (13–17). In addition, high concentrations of gadolinium have been found in femoral heads of patients who had previously received GBCAs (18–20), and gadolinium levels in bone have been found to be 23 times higher than gadolinium levels in the brain at autopsy (21); these findings suggest a large proportion of gadolinium retained in the body is located in the skeleton. Bone mineral is a likely site for long-term gadolinium deposition, as gadolinium naturally seeks bone and is one of the greatest competitive inhibitors for ionic calcium (Ca^{2+}) (22,23). Clinical implications for this deposition in brain and bone are currently unknown, as the discovery of gadolinium deposition in individuals with normal renal function is fairly recent. In 2016, symptoms of potential gadolinium toxicity were recognized in certain individuals hours to weeks after administration of GBCAs (24–28), sparking a demand for technology capable of measuring gadolinium deposition in vivo. Since bone has been shown to be a major storage site for gadolinium and since the brain is difficult to assess with noninvasive methods because it is covered by the skull, a noninvasive technique to measure gadolinium level in bone would be a useful tool to monitor gadolinium deposition while investigating the clinical implications of gadolinium deposition. Our laboratory has developed a device that has been proved to be successful in measuring low levels of gadolinium in both bone phantoms and autopsy samples and has been deemed feasible for 30-minute in vivo measurements in humans (29,30). Our purpose was to perform a preliminary evaluation of a noninvasive measurement system to assess gadolinium deposition in bone and to investigate the relationship between the administration of GBCAs and gadolinium retention in bone.

Implication for Patient Care

- A noninvasive technique to measure gadolinium level in bone could be useful to monitor gadolinium deposition in bone while investigating clinical implications of gadolinium deposition.

Materials and Methods

X-ray Fluorescence System

X-ray fluorescence (XRF) involves the use of high-energy photons, such as γ rays, to excite an element of interest and to produce x-rays characteristic of that element. In this study, we were looking for gadolinium, which has a K-shell energy of 50.2 keV. We used a cadmium 109 (^{109}Cd) excitation source with a γ ray energy of 88 keV and activity of approximately 4 GBq, which is able to excite any present gadolinium and initiate the production of characteristic x-rays at energies of 42.3 and 43.0 keV (gadolinium Kα1 and Kα2 emission lines) via the photoelectric effect.

The detector itself is composed of four separate high-purity germanium elements in a cloverleaf formation, displayed in Figure 1 (GL0210R/S; Canberra Industries, Concord, Ontario, Canada). Each detector is attached to its own set of pulse-processing electronics. Multichannel analyzer software (Genie 2000

https://doi.org/10.1148/radiol.2017171161

Content code: NM

Radiology 2018; 000:1–8

Abbreviations:
GBCA = gadolinium-based contrast agent
ICP = inductively coupled plasma
MS = mass spectrometry
XRF = x-ray fluorescence

Author contributions:
Guarantors of integrity of entire study, M.L.L., D.R.C., J.L.G., F.E.M.; study concepts/study design or data acquisition or data analysis/interpretation, all authors; manuscript drafting or manuscript revision for important intellectual content, all authors; approval of final version of submitted manuscript, all authors; agrees to ensure any questions related to the work are appropriately resolved, all authors; literature research, M.L.L., J.L.G.; clinical studies, M.L.L.; experimental studies, M.L.L., D.R.C., M.D.N.; statistical analysis, all authors; and manuscript editing, all authors

Conflicts of interest are listed at the end of this article.

Gamma Analysis Software; Canberra) displayed the multiple detected x-ray energies on a spectrum. The gadolinium x-rays appeared as two Gaussian-shaped peaks at 42.3 and 43.0 keV. The gadolinium peak data were then transferred to Matlab software (MathWorks, Natick, Mass) for further analysis.

Study Population

This study took place from August through October 2016. The selection of our study population was based on a previous study conducted by our research group in 2011 (31). This study involved administering one dose of 1.0 mmol/mL gadobutrol (Gadovist 1.0; Bayer, Mississauga, Canada) to 10 healthy adult volunteers to test the method of prompt γ neutron activation analysis to measure gadolinium deposition in muscle tissue. The known specifics of GBCA dose, date of administration, and other factors yielded an ideal exposed population to measure 5 years after administration to investigate the deposition of gadolinium in bone and to test the method of XRF for in vivo measurements.

We were granted approval by the Hamilton Integrated Research Ethics Board on May 3, 2016, to reopen the files from this study so that we could contact the volunteers and ask them to return for one 30-minute XRF measurement of their tibia. Data collection and analysis were planned and approved by the Hamilton Integrated Research Ethics Board before subjects were recruited for this study. Of the 10 original volunteers, six were able to come to our facilities to be measured. When recruiting control or nonexposed subjects, a number of individuals identified themselves as having received a GBCA for MR imaging. Of these five self-reporting subjects, four provided information with respect to dose and type of contrast agent used, and all were recruited into the exposed cohort. Overall, our exposed group consisted of six volunteers from the previous gadolinium study, none of whom had received any GBCA in the intervening 5-year period, and five individuals with self-reported gadolinium exposure, which resulted in a small exposed population having received varying doses and types of GBCAs. Each exposed subject was matched to a control subject of the same sex and age (±5 years) who self-identified as never having received any GBCAs for MR imaging. All exposed subjects were considered to be healthy adults. Participant demographics, GBCA dose and type, and date of administration are provided in Tables E1 and E2 (online).

Figure 1

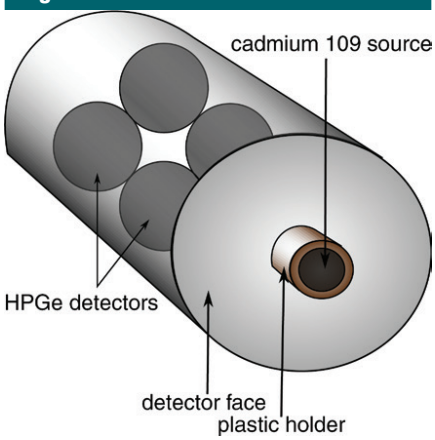

Figure 1: The XRF detector system used for tibial measurements consists of four high-purity germanium detectors in a cloverleaf formation and a ^{109}Cd source contained in a tungsten collimator and mounted on the face of the detector.

Figure 2

Figure 2: Tibial gadolinium measurement was performed with a 180° set-up geometry, in which the subject's leg was placed directly in front of the ^{109}Cd source.

XRF Measurement

The tibia was chosen as the measurement location since it is located in an extremity and has a relatively thin layer of overlying tissue. These two factors limit the effective dose received by the subject and reduce the attenuation of gadolinium signals from the bone, respectively. Each subject was asked to sit in a chair with his or her leg held against the collimated ^{109}Cd source, which was mounted on the face of the detector, for 30 minutes (Fig 2). To ensure the tibia was measured, the leg was positioned by the individual obtaining the measurement, and the subject was asked to remain still throughout the 30-minute measurement period. The placement of the leg was checked periodically throughout the measurement.

The risk of a 30-minute tibial XRF measurement involves a small radiation dose delivered to the subject. For a measurement, the local maximum equivalent dose to the tibia is 357 μSv, and the (total body) effective dose is approximately 0.13 μSv (32).

Data Analysis

Data from the collected spectra (Fig 3) were analyzed by using the aforementioned Matlab software, which involved fitting the two gadolinium Kα peaks as well as the 88-keV coherent scatter peak, described in detail by Lord et al (29,30). The areas under all peaks were determined from the individual fits and were used to calculate the ratio of gadolinium signal to coherent signal, known as coherent normalization. The process of coherent normalization has proved useful in correcting interpatient variability, such as shape and size of the subject, while conducting in vivo measurements of trace elements, such as lead, and has recently been shown to work well for gadolinium (33).

Statistical Analyses

In this study, we wished to answer the question, "Is bone gadolinium content in the exposed group higher than that in the control group?" For this reason, a one-tailed Student *t* test was performed to test gadolinium concentration in the exposed group against gadolinium concentration in the control group. We used the Anderson-Darling method to test for the absence of normality using Minitab 17 software *(https://minitab.com)*. Neither control (P = .26) nor exposed (P = .53) groups were found to deviate significantly from a normal distribution, so we used normal statistics to test for differences between the groups. In addition, we tested differences by using inverse variance weighted means. Our rationale for inverse variance weighting the data are that the measurement uncertainties vary on the individual measurements and by weighting by one divided by uncertainty squared, the mean is weighted toward more precise individual measurements (34). The variation in uncertainty in human measurements arises because each subject is different in terms of leg shape, size, mass, and thickness of tissue overlying the bone.

Since extremely low-level gadolinium signals are expected, the statistical variation in the background can result in some reporting of negative gadolinium concentrations. This is obviously not physically the case, but it arises because of the inherent Poisson statistics in radiation detection and measurement. We extracted the x-ray signal from a large x-ray scatter background. Both the gadolinium x-ray signal and the background under the x-ray peak were subject to statistical fluctuation, and the background under the x-ray peak was estimated from points on either side of the peak. Occasionally, the estimated background was higher than the measured background, resulting in a negative estimate when the background was subtracted. A zero-concentration phantom will be estimated as a small negative number 50% of the time and as a small positive number 50% of the time. On average, however, it will be determined to have zero x-ray signal. Full gadolinium concentration data are detailed in Tables E1 and E2 (online).

Figure 3

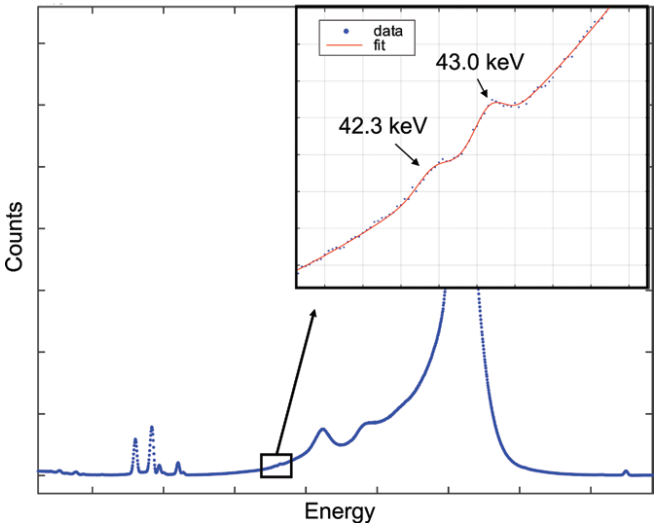

Figure 3: A sample spectrum for a 30-minute measurement of a hydroxyapatite phantom with a concentration of 60 μg Gd/g bone mineral. Gadolinium peaks of interest are located at 42.3 and 43.0 keV. A measurement output from a phantom with a higher concentration is displayed to exaggerate gadolinium peaks, as gadolinium peaks in humans are much smaller.

To investigate the relationship between gadolinium concentration in bone and the GBCA dose previously administered, the measured gadolinium concentration in bone was plotted as a function of known GBCA dose and was analyzed by using linear least-squares regression with Microsoft Excel 2016 spreadsheet software (Microsoft, Redmond, Wash). Correlation was assessed with R^2 values, and P values were used for significance. Mathematical models other than linear were tested, including piecewise linear, exponential, and power functions. These models were tested against a linear fit by using Akaike information criterion and were found to fit the data as well as but not better than a linear model ($P \geq .19$ in all cases). The GBCA dose data for an initial regression analysis were drawn from the study notes and protocols for the six individuals in our previous study who received 1.0 mmol/mL gadobutrol and from one self-reported individual (exposed subject 5) who provided us with dose data and who reported receiving gadobutrol. The 11 control subjects were all assumed to have doses of 0 mL based on their negative answer to the question "Have you ever had an MR imaging scan with contrast agent?" A self-reported individual (exposed subject 2) who reported receiving gadobutrol was excluded from this regression analysis because of the subject's self-report of undergoing dialysis shortly after administration of the GBCA. We were uncertain whether this would have altered redistribution of gadolinium into bone. An additional two subjects with self-reported exposure could not provide GBCA dose data; therefore, they could not be included in the linear regression analysis. We tested whether the self-reported data point altered the result and found that removing this point had little effect on the overall results of the regression. The slope was the same to within uncertainty with or without this data point. We also tested whether the increase in bone gadolinium level was correlated with gadolinium dose per unit of body mass via linear regression with the aforementioned spreadsheet software, as previously described. In addition, one subject self-reported having received two separate doses of 0.5

mmol/mL gadodiamide (Omniscan; GE Healthcare, Chicago, Ill) at two different times over the 2 years prior to being measured in our study. We reperformed the regressions, including this individual's data point (for their most recent dose only), with the gadobutrol data (Figs 4, 5).

Reproducibility measurements were performed in anthropomorphic hydroxyapatite phantoms replicating a tibia bone, with a 5-mm layer of tissue-equivalent plastic over the tibia phantom. A total of five phantom measurements were performed over a period of 2 months. The *z* scores were calculated for the gadolinium concentrations by using the mean of the five values and the individually derived measurement uncertainties. Reproducibility was also examined for an autopsy sample from an individual who had received GBCAs. The autopsy sample was measured 10 times over 1 month, and *z* scores were calculated.

Results

Comparing Gadolinium Concentration in the Exposed and Control Groups

Gadolinium concentration in bone is visibly higher in the exposed group than in the control group (Fig 6). Gadolinium concentration in the exposed group was 2.6 μg Gd/g bone mineral ± 1.6 higher than that in the control group (−1.23 μg Gd/g bone mineral ± 0.94) (P = .05). A one-tailed t test was performed on the variance-weighted means and determined that the exposed group had a 2.2 μg Gd/g bone mineral ± 1.0 higher concentration than did the control group (−1.06 μg Gd/g bone mineral ± 0.71) (P = .01).

Linear Regression for Gadolinium Concentration in Bone and GBCA Dose

The slope of regression for subjects who received gadobutrol was positive and estimated that the gadolinium concentration in bone increased by 0.39 μg Gd/g bone mineral ± 0.14 per 1 mL of administered gadobutrol (P = .01, R^2 = 0.42) (Fig 4). The result of the regression analysis of GBCA dose per mass of the subject produced a significant positive slope; bone gadolinium concentration increases by a mean of 28.2 μg Gd/g bone mineral ± 11.7 per 1 mL of gadobutrol per kilogram of body weight (P = .03, R^2 = 0.37) (Fig 5). The addition of the gadodiamide data point did not change the slopes of the regressions to within uncertainties, and it increased the significance of regression (P = .003 for gadolinium concentration vs dose, P = .005 for gadolinium concentration vs dose per unit mass).

Reproducibility

The *z* scores for gadolinium concentration from five hydroxyapatite phantom measurements ranged from −0.5 to 0.8. For 10 autopsy sample measurements, the gadolinium concentration values resulted in *z* scores ranging from −1.0 to 1.0.

Figure 4

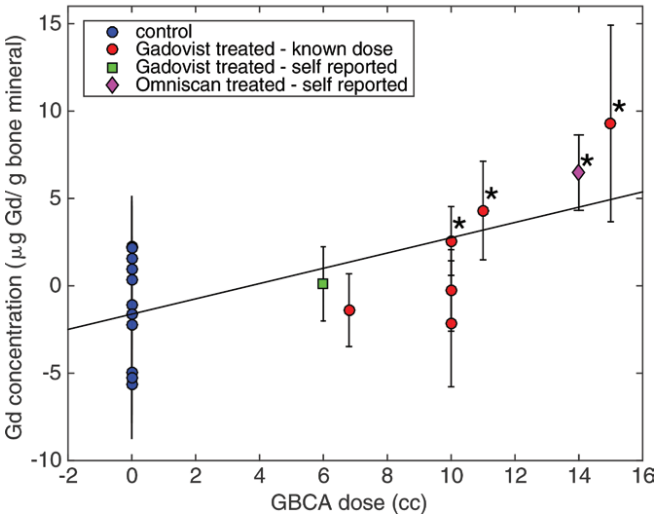

Figure 4: Regression analysis was performed to investigate the relationship between GBCA dose and gadolinium concentration in bone. A significant positive slope of 0.39 ± 0.14 (P = .014) describes the increase in gadolinium bone concentration in micrograms of gadolinium per gram of bone mineral per milliliter of injected GBCA (gadobutrol). The value of the slope does not change, and the significance of this slope increases (P = .003) with the addition of a data point from a subject who received two doses of gadodiamide. The coefficient of determination for this relationship is R^2 = 0.41. Error bars were determined from the algorithm used to fit the gadolinium peaks and calculate gadolinium concentration, and they represent the standard deviation of the reported gadolinium concentration. * = Gadolinium concentration is significantly higher than the control group mean ($P < .05$).

Discussion

Our data show a significant difference between the population means of the gadolinium-exposed and control groups, as well as a significant correlation between gadolinium in bone and GBCA dose per unit of body weight. In addition, of the 11 exposed subjects measured in this study, four subjects were each determined to have, on an individual basis, a significantly higher gadolinium concentration than the control group mean at the 95% confidence level ($P < .05$). One of these subjects had self-reported GBCA exposure: this person received two 14-mL doses of gadodiamide within the 2 years prior to this study. The three other subjects all received one dose of gadobutrol in 2011 as part of our previous study (all doses were ≥10 mL). Our ability to detect gadolinium in an individual 5 years after one injection

Figure 5

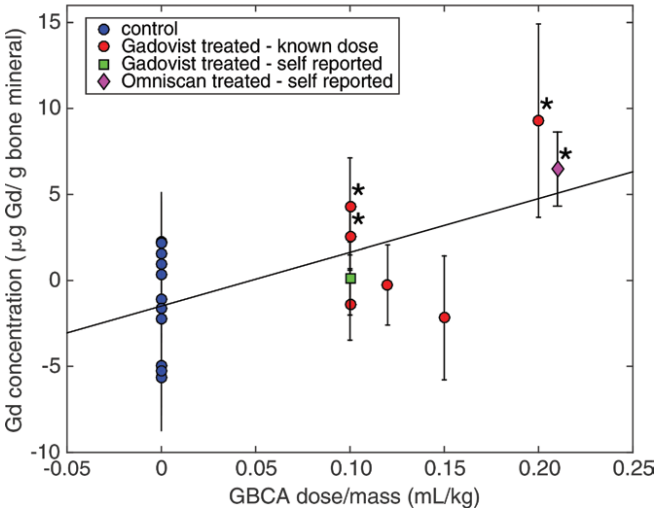

Figure 5: Regression analysis was performed to investigate the relationship between GBCA dose per mass of the subject and gadolinium concentration in bone. A significant positive slope of 28.2 μg Gd/g bone mineral ± 11.7 ($P = .03$) describes the increase in gadolinium bone concentration for the volume of injected GBCA (gadobutrol) per mass of the subject (in kilograms). The value of this slope does not change, and the significance of this slope increases ($P = .005$) with the addition of a data point from a subject who received two doses of gadodiamide. The coefficient of determination for this relationship is $R^2 = 0.37$. ∗ = Gadolinium concentration is significantly higher ($P < .05$) than the control group mean.

Figure 6

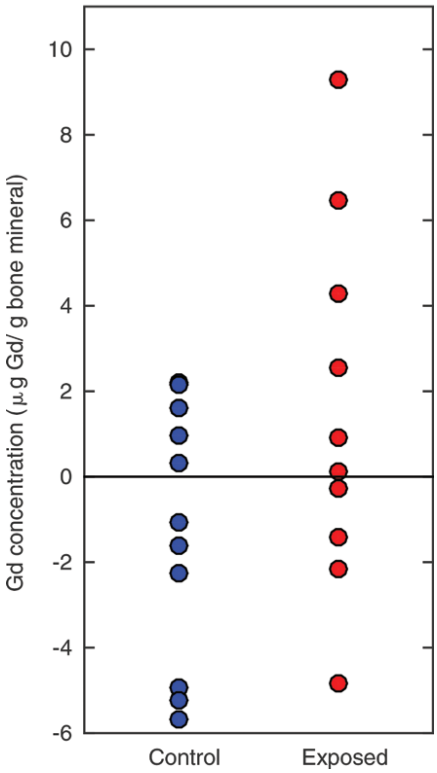

Figure 6: Visual representation of gadolinium concentration in the tibia in the control group versus that in the exposed group. Only 10 data points are visible for the exposed group, as two exposed subjects had a gadolinium concentration of −0.26 μg Gd/g bone mineral. A one-tailed Student *t* test enabled us to confirm that gadolinium concentration in the exposed group is significantly higher than that in the control group ($P = .05$). With inverse variance weighting, gadolinium concentration on the exposed group is also determined to be significantly higher than this in the control group but with greater confidence ($P = .01$). Error bars (ie, individual measurement uncertainty) were omitted for clarity.

may suggest that bone may act as a long-term storage site for gadolinium in the body. Overall, our results indicate that our XRF system enables detection of gadolinium in our small pilot study.

Reproducibility measurements were not performed in humans, as the Hamilton Integrated Research Ethics Board approved only one measurement per subject in this pilot study. However, reproducibility measurements performed on anthropomorphic hydroxyapatite phantoms led to the conclusion that there is no evidence of variability in the measurement beyond that predicted by the measurement uncertainty derived from the spectral analysis. Reproducibility for an autopsy sample from an individual who had received GBCAs showed no evidence of variability in excess of that predicted from the measurement uncertainty. Accuracy of an XRF measurement with our system was tested by using a cross-validation study with inductively coupled plasma (ICP) mass spectrometry (MS) and seven autopsy samples. This previously published study resulted in comparable gadolinium concentrations with both techniques (30), suggesting that the XRF technique and ICP MS yield similar values when measuring gadolinium level in bone.

Other measurements of gadolinium in bone to date have been performed with ICP MS and have been invasive, coming from either femoral heads removed during hip replacement surgery (18–20) or from autopsy samples (21). Murata et al (21) recently reported ICP MS measurements of 5.28 and 2.38 μg Gd/g bone, which are within our range of detected gadolinium levels. The other reported values are below our detection limit, as ICP MS is a more sensitive technique with which to measure gadolinium level. Although the XRF system in our study is not capable of measuring gadolinium concentration values as low as those that can be measured with ICP MS, to our knowledge, there are currently no methods to measure gadolinium level noninvasively in vivo, which sets our XRF measurements apart from other reported measurements of gadolinium in bone.

Our study had limitations. The statistical limitations of the XRF system lead to a minimum detection limit. The phantom minimum detection limit is the minimum concentration of gadolinium that can be detected with our system and is defined as two times the uncertainty of the gadolinium concentration of a zero-concentration phantom

in units of concentration. This value is calculated through a series of hydroxyapatite phantom measurements fit to a linear regression, as described in detail by Lord et al (29). The minimum detection limit worsens with time, as the ^{109}Cd source is constantly decaying and becoming less active. The measurement uncertainty can be worse in people than in phantoms because of factors such as patient motion or overlying tissue thickness. For example, it can be difficult to measure small amounts of gadolinium in individuals with large amounts of overlaying tissue. Our minimum detection limit at the time of the experiments was 2.3 μg Gd/g bone mineral (30). Thus, gadolinium concentrations under this level could not be detected with our system and were indistinguishable from statistical noise.

We have attributed observation of gadolinium in bone to administration of GBCAs. Recently, the issue of ingesting gadolinium through local water supplies raises questions about alternative sources of gadolinium deposition in bone. While anthropogenic gadolinium has been detected in the water supply (35), gadolinium concentrations in water are eight orders of magnitude lower than the gadolinium concentration received in one GBCA administration and are therefore not likely to contribute substantially to gadolinium concentration measured with this XRF system.

The small size of the population, the range of contrast agents used, the differing intervals between exposure and measurement in our self-reported group, and the limited medical data on the measured subjects makes it difficult to draw any clinical conclusions from the XRF measurements. A larger population study would yield more information on the clinical side of gadolinium deposition, as well as on the performance of the XRF system. The broad technique of XRF allows any research group with a ^{109}Cd source and a high-purity germanium detector to perform these measurements. However, it is important to have a control group for comparison in studies to account for any potential bias created when using mathematic models and techniques to extract gadolinium data from the observed x-ray continuum.

In conclusion, we have conducted noninvasive in vivo XRF measurements of gadolinium in the tibia in 11 subjects who were previously administered GBCAs and in 11 control subjects by using a biomedical device. We conclude that this XRF-based device is a tool that can be used to measure gadolinium deposition in bone noninvasively in vivo. We also conclude that gadolinium is retained in the bone for years after one dose of a GBCA in healthy volunteers. This low-risk painless in vivo gadolinium measurement technology has the potential to be used to assess gadolinium deposition in studies investigating the potential health effect of gadolinium deposition in the bones and to hopefully help understand the frequency and clinical importance of gadolinium deposition in the bones of patients receiving these contrast agents.

Disclosures of Conflicts of Interest: M.L.L. disclosed no relevant relationships. **D.R.C.** disclosed no relevant relationships. **J.L.G.** disclosed no relevant relationships. **M.D.N.** Activities related to the present article: disclosed no relevant relationships. Activities not related to the present article: received lecture honoraria from GE Healthcare Canada. Other relationships: disclosed no relevant relationships. **F.E.M.** disclosed no relevant relationships.

References

1. Medical Imaging. Data highlights. Canadian Institute for Health Information. https://www.cihi.ca/en/medical-imaging#_Highlights. Published February 12, 2013. Accessed December 1, 2016.
2. Weinmann HJ, Brasch RC, Press WR, Wesbey GE. Characteristics of gadolinium-DTPA complex: a potential NMR contrast agent. AJR Am J Roentgenol 1984;142(3):619–624.
3. Carr DH, Brown J, Bydder GM, et al. Gadolinium-DTPA as a contrast agent in MRI: initial clinical experience in 20 patients. AJR Am J Roentgenol 1984;143(2):215–224.
4. Caravan P, Ellison JJ, McMurry TJ, Lauffer RB. Gadolinium(III) chelates as MRI contrast agents: structure, dynamics, and applications. Chem Rev 1999;99(9):2293–2352.
5. Hao D, Ai T, Goerner F, Hu X, Runge VM, Tweedle M. MRI contrast agents: basic chemistry and safety. J Magn Reson Imaging 2012;36(5):1060–1071.
6. Joffe P, Thomsen HS, Meusel M. Pharmacokinetics of gadodiamide injection in patients with severe renal insufficiency and patients undergoing hemodialysis or continuous ambulatory peritoneal dialysis. Acad Radiol 1998;5(7):491–502.
7. Noseworthy MD, Ackerley C, Qi X, Wright GA. Correlating subcellular contrast agent location from dynamic contrast-enhanced magnetic resonance imaging (dMRI) and analytical electron microscopy. Acad Radiol 2002; 9(2,Suppl 2):S514–S518.
8. Huckle JE, Altun E, Jay M, Semelka RC. Gadolinium deposition in humans: when did we learn that gadolinium was deposited in vivo? Invest Radiol 2016;51(4):236–240.
9. Grobner T. Gadolinium: a specific trigger for the development of nephrogenic fibrosing dermopathy and nephrogenic systemic fibrosis? Nephrol Dial Transplant 2006; 21(4):1104–1108.
10. Marckmann P, Skov L, Rossen K, et al. Nephrogenic systemic fibrosis: suspected causative role of gadodiamide used for contrast-enhanced magnetic resonance imaging. J Am Soc Nephrol 2006;17(9):2359–2362.
11. Thomsen HS, Morcos SK, Dawson P. Is there a causal relation between the administration of gadolinium based contrast media and the development of nephrogenic systemic fibrosis (NSF)? Clin Radiol 2006; 61(11):905–906.
12. Altun E, Martin DR, Wertman R, Lugo-Somolinos A, Fuller ER 3rd, Semelka RC. Nephrogenic systemic fibrosis: change in incidence following a switch in gadolinium agents and adoption of a gadolinium policy: report from two U.S. universities. Radiology 2009;253(3):689–696.
13. Kanda T, Ishii K, Kawaguchi H, Kitajima K, Takenaka D. High signal intensity in the dentate nucleus and globus pallidus on unenhanced T1-weighted MR images: relationship with increasing cumulative dose of a gadolinium-based contrast material. Radiology 2014;270(3):834–841.
14. Errante Y, Cirimele V, Mallio CA, Di Lazzaro V, Zobel BB, Quattrocchi CC. Progressive increase of T1 signal intensity of the dentate nucleus on unenhanced magnetic resonance images is associated with cumulative doses of intravenously administered gadodiamide in patients with normal renal function, suggesting dechelation. Invest Radiol 2014;49(10): 685–690.
15. McDonald RJ, McDonald JS, Kallmes DF, et al. Intracranial gadolinium deposition after

contrast-enhanced MR imaging. Radiology 2015;275(3):772–782.

16. Quattrocchi CC, Mallio CA, Errante Y, et al. Gadodiamide and dentate nucleus T1 hyperintensity in patients with meningioma evaluated by multiple follow-up contrast-enhanced magnetic resonance examinations with no systemic interval therapy. Invest Radiol 2015;50(7):470–472.
17. Kanda T, Fukusato T, Matsuda M, et al. Gadolinium-based contrast agent accumulates in the brain even in subjects without severe renal dysfunction: evaluation of autopsy brain specimens with inductively coupled plasma mass spectroscopy. Radiology 2015; 276(1):228–232.
18. White GW, Gibby WA, Tweedle MF. Comparison of Gd(DTPA-BMA) (Omniscan) versus Gd(HP-DO3A) (ProHance) relative to gadolinium retention in human bone tissue by inductively coupled plasma mass spectroscopy. Invest Radiol 2006;41(3):272–278.
19. Gibby WA, Gibby KA, Gibby WA. Comparison of Gd DTPA-BMA (Omniscan) versus Gd HP-DO3A (ProHance) retention in human bone tissue by inductively coupled plasma atomic emission spectroscopy. Invest Radiol 2004;39(3):138–142.
20. Darrah TH, Prutsman-Pfeiffer JJ, Poreda RJ, Ellen Campbell M, Hauschka PV, Hannigan RE. Incorporation of excess gadolinium into human bone from medical contrast agents. Metallomics 2009;1(6):479–488.
21. Murata N, Gonzalez-Cuyar LF, Murata K, et al. Macrocyclic and other non–group 1 gadolinium contrast agents deposit low levels of gadolinium in brain and bone tissue: preliminary results from 9 patients with normal renal function. Invest Radiol 2016;51(7):447–453.
22. Sherry AD, Caravan P, Lenkinski RE. Primer on gadolinium chemistry. J Magn Reson Imaging 2009;30(6):1240–1248.
23. Thakral C, Alhariri J, Abraham JL. Long-term retention of gadolinium in tissues from nephrogenic systemic fibrosis patient after multiple gadolinium-enhanced MRI scans: case report and implications. Contrast Media Mol Imaging 2007;2(4):199–205.
24. Ramalho J, Ramalho M, Semelka RC. Gadolinium deposition and toxicity: a global concern. Curr Radiol Rep 2016;4:59.
25. Semelka RC, Ramalho M, AlObaidy M, Ramalho J. Gadolinium in humans: a family of disorders. AJR Am J Roentgenol 2016;207(2):229–233.
26. Semelka RC, Commander CW, Jay M, Burke LM, Ramalho M. Presumed gadolinium toxicity in subjects with normal renal function: a report of 4 cases. Invest Radiol 2016;51(10):661–665.
27. Roberts DR, Lindhorst SM, Welsh CT, et al. High levels of gadolinium deposition in the skin of a patient with normal renal function. Invest Radiol 2016;51(5):280–289.
28. Burke LM, Ramalho M, AlObaidy M, Chang E, Jay M, Semelka RC. Self-reported gadolinium toxicity: a survey of patients with chronic symptoms. Magn Reson Imaging 2016;34(8):1078–1080.
29. Lord ML, McNeill FE, Gräfe JL, Noseworthy MD, Chettle DR. A phantom-based feasibility study for detection of gadolinium in bone in-vivo using X-ray fluorescence. Appl Radiat Isot 2016;112:103–109.
30. Lord ML, McNeill FE, Gräfe JL, et al. Confirming improved detection of gadolinium in bone using in vivo XRF. Appl Radiat Isot 2017;120:111–118.
31. Gräfe JL, McNeill FE, Noseworthy MD, Chettle DR. Gadolinium detection via in vivo prompt gamma neutron activation analysis following gadolinium-based contrast agent injection: a pilot study in 10 human participants. Physiol Meas 2014;35(9):1861–1872.
32. Nie H, Chettle D, Luo L, O'Meara J. Dosimetry study for a new in vivo x-ray fluorescence (XRF) bone lead measurement system. Nucl Instrum Methods Phys Res B 2007;263(1):225–230.
33. Keldani Z, Lord ML, McNeill FE, Chettle DR, Gräfe JL. Coherent normalization for in vivo measurements of gadolinium in bone. Physiol Meas 2017;38(10):1848–1858.
34. Chamberlain M, Gräfe JL, Byun SH, et al. The feasibility of in vivo quantification of bone-fluorine in humans by delayed neutron activation analysis: a pilot study. Physiol Meas 2012;33(2):243–257.
35. Kulaksız S, Bau M. Anthropogenic gadolinium as a microcontaminant in tap water used as drinking water in urban areas and megacities. Appl Geochem 2011;26(11): 1877–1885.

Chapter 7

Paper V: Self-identified gadolinium toxicity: comparison of gadolinium in bone and urine to healthy gadolinium-based contrast agent exposed volunteers

M. L. Lord, F. E. McNeill, J. L. Gräfe, M. D. Noseworthy and D. R. Chettle. Physiol. Meas.

The work in this paper is an extension of Paper IV. Additional Gd bone measurements were performed with the cloverleaf XRF detection system, as well Gd urine measurements. Following the publication of Paper IV, I was contacted by a patient advocacy group, consisting of individuals self-reporting symptoms of Gd toxicity as a result of receiving GBCAs. These individuals had been monitoring Gd content in their body through a series of 24-hour urine measurements. Since bone is another potential marker to correlate retained Gd to potential toxicity symptoms, I wanted to perform Gd bone measurements on these individuals and compare concentrations of

Gd in bone to Gd in urine. The purpose of this work was to: (1) report additional Gd bone and urine data to contribute to gaps in knowledge with respect to Gd retention in the body, and (2) investigate the potential relationship between Gd retention in bone and Gd excretion in urine for individuals exhibiting symptoms of Gd toxicty.

I received ethics approval from the Hamilton Integrated Research Board to conduct additional Gd bone measurements on 4 of these self-reporting symptomatic exposed individuals, and well as 4 more controls. Bone measurements were carried out with identical measurement and analysis protocol as presented in Paper IV. In addition to bone measurements, I was granted permission to perform Gd urine measurements on 4 control and 4 non-symptomatic exposed subjects from the pilot study, and to receive Gd urine data from the 4 self-reported symptomatic exposed subjects, who provided us with their most recent 24-hour Gd urine levels. Urine samples were collected on McMaster University campus and shipped to Mayo Medical Laboratories in Rochester, MN for their standard 24-hour Gd urine test. One-tailed t tests and linear regressions were performed on Gd bone and urine concentrations to investigate the difference between groups (control, symptomatic exposed, non-symptomatic exposed), and the relationship between Gd retention and GBCA dose, respectively. Additionally, the possible relationship between Gd concentration in bone and Gd concentration in urine was investigated with a linear regression.

Gd bone concentration analyses resulted in similar conclusions as in Paper IV, a significant difference in Gd bone concentration was found between exposed and control groups ($p < 0.0001$). Additionally, a significant difference was found within the exposed group between the symptomatic and non-symptomatic groups ($p < 0.01$). Gd urine concentrations in both control and non-symptomatic exposed subjects were significantly lower than symptomatic exposed subjects ($p = 0.02$ and $p = 0.05$, respectively). The only subjects that had detectable levels of gadolinium in their urine were those who had received multiple doses of GBCAs. Subjects who had only received a single dose of GBCA had an undetectable amount of gadolinium in their urine. There was a strong correlation between Gd urine concentrations and GBCA dose ($p < 0.000001$), yet no relationship was found between Gd concentrations excreted in

urine and measured Gd bone concentrations, suggesting there is another large storage site of Gd in the body, other than bone.

This project was proposed by David Chettle, Fiona McNeill, and myself, following the interest of a patient advocacy group in receiving Gd bone measurements with the XRF detection system. I wrote the additional ethics reports to receive approval to perform 8 additional Gd bone measurements, and collect urine from 8 existing study participants. All statistical analyses of collected data were performed by myself, with the help of David Chettle and Fiona McNeill. James Gräfe and Mike Noseworthy provided additional expert guidance throughout the project. I wrote the first draft of the manuscript, which was then edited by all authors.

IOP Publishing Physiol. Meas. 39 (2018) 115008 (10pp) https://doi.org/10.1088/1361-6579/aaedc6

Physiological Measurement

IPEM Institute of Physics and Engineering in Medicine

PAPER

Self-identified gadolinium toxicity: comparison of gadolinium in bone and urine to healthy gadolinium-based contrast agent exposed volunteers

RECEIVED
4 September 2018

REVISED
30 October 2018

ACCEPTED FOR PUBLICATION
2 November 2018

PUBLISHED
27 November 2018

Michelle L Lord[1], Fiona E McNeill[2], James L Gräfe[3], Michael D Noseworthy[4,5] and David R Chettle[2]

[1] Interdisciplinary Graduate Program in Radiation Sciences, McMaster University, 1280 Main St. W., Hamilton, ON L8S 4L8, Canada
[2] Department of Physics and Astronomy, McMaster University, 1280 Main St. W., Hamilton, ON L8S 4L8, Canada
[3] Department of Physics, Ryerson University, 350 Victoria St., Toronto, ON M5B 2K3, Canada
[4] McMaster School of Biomedical Engineering, McMaster University, 1280 Main St. W., Hamilton, ON L8S 4L8, Canada
[5] Department of Electrical and Computer Engineering, McMaster University, 1280 Main St. W., Hamilton, ON L8S 4L8, Canada

E-mail: lordml@mcmaster.ca

Keywords: gadolinium-based contrast agents, gadolinium retention, gadolinium toxicity, MRI contrast

Supplementary material for this article is available online

Abstract

Objective: To report additional gadolinium bone and urine data that can contribute to gaps in knowledge with respect to gadolinium uptake and retention in the body. *Approach*: *In vivo* measurements of gadolinium retention in the tibia bone were performed on individuals self-identified as exhibiting symptoms of gadolinium toxicity as a result of receiving GBCA, as well as on control individuals. Gadolinium urine measurements for controls, symptomatic exposed, and non-symptomatic exposed were conducted through Mayo Medical Laboratories. *Main results*: Gadolinium bone concentration in the exposed group is significantly higher than the control group ($p < 0.01$), with a significant difference between symptomatic and non-symptomatic ($p < 0.01$), using a one-tailed t test on variance-weighted means. Gadolinium urine levels in both control subjects and non-symptomatic exposed subjects are significantly lower than symptomatic exposed subjects ($p \leq 0.05$). A linear regression analysis for gadolinium urine levels and GBCA dose resulted in a positive linear relationship ($R^2 = 0.91, p < 0.01$). Gadolinium levels in urine and gadolinium concentration in bone were found to have a non-significant relationship ($R^2 = 0.11, p = 0.3$). *Significance*: Significant differences in gadolinium levels in bone and urine are observed between individuals experiencing symptoms of gadolinium toxicity and for those who are not exhibiting symptoms. No correlation was observed between gadolinium in bone and gadolinium excreted in urine, suggesting that the retention of gadolinium in the body is complicated, involving multiple long-term storage sites.

1. Introduction

Gadolinium-based contrast agents (GBCAs) are incredibly effective for diagnostic MR imaging, and as such are commonly used in imaging centers worldwide. Developed in the 1980s, GBCAs were thought to be completely safe and excreted from the body within hours of administration (Carr *et al* 1984, Weinmann *et al* 1984, Caravan *et al* 1999). The advent of adverse effects in individuals with renal disease, known as nephrogenic systemic fibrosis (NSF) (Grobner 2006, Marckmann *et al* 2006, Thomsen *et al* 2006), led to a change in protocol for administration of GBCAs for individuals with impaired renal function, followed by a restored confidence in the use of GBCAs for individuals with normal renal function (Altun *et al* 2009). However, at approximately the same time as the discovery of NSF, evidence of gadolinium retention in bone was found in healthy individuals with normal renal function (Gibby *et al* 2004, White *et al* 2006).

Recently, the issue of gadolinium retention in healthy individuals has sparked a great deal of discussion, as many studies have reported gadolinium retention in brain (Errante *et al* 2014, Kanda *et al* 2014, 2015,

2016, McDonald *et al* 2015, Quattrocchi *et al* 2015, Radbruch *et al* 2015), as well as other organs, such as bone (Darrah *et al* 2009, Murata *et al* 2016). Additionally, several reports have been published presenting individuals with self-reported symptoms of gadolinium toxicity following administration of GBCAs, for both linear and macrocyclic agents (Burke *et al* 2016, Ramalho *et al* 2016, Roberts *et al* 2016, Semelka *et al* 2016a). The retention of gadolinium in healthy individuals with normal renal function, resulting in adverse effects, has been referred to as 'gadolinium deposition disease' in some reports (Semelka *et al* 2016b). The symptoms described by individuals are similar; the most common symptoms are central torso pain, peripheral arm and leg pain, brain fog, and skin thickening (Burke *et al* 2016, Ramalho *et al* 2016, Semelka *et al* 2016a, 2016b).

Unlike other trace elements, which can be acquired from drinking water or work exposures, the predominant source of gadolinium retention in the body is from GBCA administered for MRI. Ingestion of anthropogenic gadolinium through drinking water has recently been investigated as a potential contributor to gadolinium retention in the body (Kulaksız and Bau 2011). However, it was found that gadolinium concentrations in drinking water are 8 orders of magnitude lower than the concentration in a single administration of GBCA, and are therefore unlikely to contribute to any gadolinium retention in the body.

With little known about the clinical repercussions of gadolinium in the body, the radiology community is faced with a conflict between using these effective diagnostic agents or considering their safety, in fear of possible GBCA-related symptoms. There are limited data and many gaps in knowledge with respect to gadolinium uptake and retention in the body. Gadolinium excreted in urine is often used as a biomarker by self-identified symptomatic individuals to monitor their potential gadolinium toxicity (Semelka *et al* 2016b). We propose that another potential marker to correlate gadolinium levels and possible gadolinium-related symptoms could be gadolinium concentration in bone. However, to our knowledge, it is currently unknown what the expected levels of gadolinium in urine and bone at various time points should be for healthy asymptomatic individuals following GBCA administration, and further whether there are differences in self-reported symptomatic individuals.

Our research group previously reported gadolinium concentrations in bones of healthy individuals who had received GBCAs (Lord *et al* 2017a). These measurements were performed with a non-invasive *in vivo* biomedical device using the technique of x-ray fluorescence (XRF) (Lord *et al* 2016, 2017b). A significant difference in gadolinium concentration in bone was observed between the control group and GBCA exposed group, and the biomedical device was shown to measure gadolinium in bone in a small population. The purpose of this study is to report additional gadolinium bone and urine data that can contribute to gaps in knowledge with respect to gadolinium uptake and retention in the body. This article reports the findings of gadolinium in bone and urine for three groups of individuals: control, self-reported symptomatic exposed, and asymptomatic exposed.

2. Methods

2.1. Study population

Our original prospective pilot study measuring gadolinium in bone consisted of 11 healthy control subjects, and 11 healthy subjects who had previously received GBCA, whom were referred to as 'exposed' subjects (Lord *et al* 2017a). For this study extension, permission was granted by the Hamilton integrated research board (HiREB) to measure gadolinium in bone for an additional four control subjects, and four exposed subjects. The four additional exposed subjects were self-identified as exhibiting symptoms of gadolinium toxicity, where the 11 original exposed subjects were healthy individuals who did not report symptoms of gadolinium toxicity. In addition to bone measurements, permission was granted to perform gadolinium urine measurements on four control and four non-symptomatic exposed subjects, and to receive gadolinium urine data from the four self-reported symptomatic exposed subjects, who provided us with their most recent 24 h gadolinium urine levels (as measured by the Mayo Medical Laboratories or Genova Diagnostics). All participant demographics can be found in supplementary tables E1–E3 (stacks.iop.org/PM/39/115008/mmedia).

2.2. XRF bone measurement

XRF bone (tibia) measurements took place between June and August 2017 on the additional four control and four self-reported symptomatic exposed subjects, using an identical measurement and analysis protocol and the same biomedical device presented in the original pilot study (Lord *et al* 2017a). A Cd-109 activation source was mounted to the face of a high-purity germanium detector (GL0210R/S; Canberra Industries, Concord, Ontario, Canada) to create an approximately 180° measurement geometry. Subjects were asked to sit for a period of 30 min, placing their leg directly in front of the Cd-109 source, and remaining still throughout the measurement. The gamma rays emitted by the Cd-109 source excited any present gadolinium in the tibia bone, which in turn produced x-rays characteristic of gadolinium. The characteristic x-rays were measured and analyzed further to calculate the tibial concentration of gadolinium. Subjects received an equivalent dose of 357 μSv to the tibia and an effective dose of 0.13 μSv for a 30 min measurement. Detailed methods regarding the use of the XRF bone system, as well as reproducibility measurements, can be found in the original pilot study

(Lord *et al* 2017a). The results of the XRF bone measurements can be found in supplementary tables E1 and E2. It is important to note that gadolinium measurements reported as negative values do not physically represent negative gadolinium concentrations. Negative values are the result of measuring low levels of gadolinium with statistical variation in the x-ray scatter background. When measuring gadolinium, the x-ray scatter background beneath the gadolinium peaks is estimated by fitting an appropriate mathematical function to an energy region that includes the gadolinium peaks plus 'background' regions of immediately lower and higher energies than the gadolinium peaks. Since we are detecting very low levels of gadolinium, the estimated background subtracted from the gadolinium peaks can sometimes be higher than the peaks themselves, resulting in a negative value for gadolinium concentration.

2.3. 24 h urine measurement

Urine tests on the four control and four asymptomatic exposed subjects were carried out in December 2017 and January 2018 using the standardized Mayo Medical Laboratories (Rochester, MN) 24 h gadolinium urine test (Test ID: GDU), which uses the technique of inductively coupled plasma mass spectrometry to detect gadolinium as described by Leung *et al* (2009). The eight subjects were given containers and 24 h urine collection instructions. Each urine sample was transferred into a 10 ml tube and sent to the Mayo Clinic for analysis. The four symptomatic exposed subjects had been monitoring their gadolinium urine levels over time, and provided us with their most recent test data, all of which were completed through standardized tests at either the Mayo Clinic or Genova Diagnostics (Asheville, NC). Since three of the four self-reported symptomatic exposed subjects had received multiple chelation therapies in attempts to remove gadolinium from the body, we used their 'unprovoked' levels (gadolinium urine levels prior to chelation). Information regarding the date and results of the urine tests can be found in supplementary table E3.

2.4. Half life correction

As with other heavy metal accumulation in bone, such as lead, we assume gadolinium to have a unique half life in bone (Chettle 2005). We tested therefore, a half life correction to determine whether the time between the date of GBCA administration and the date of XRF bone measurements was a factor in differences in bone gadolinium level between subjects. Correcting for the half-life of gadolinium in bone determines the concentration of gadolinium in bone 'shortly' after GBCA administration (on a scale of weeks to months). This is assumed because the timescale of gadolinium accumulation into bone is not clear. Gadolinium concentration in bone shortly after GBCA administration was calculated with a simple exponential model shown in equation (1):

$$[\mathrm{Gd}] = [\mathrm{Gd}_0]e^{-\frac{\ln 2}{t_{1/2}}t} \tag{1}$$

where [Gd] is the gadolinium concentration at the time of the XRF measurement, [Gd_0] is the gadolinium concentration following GBCA administration, $t_{1/2}$ is the half life of gadolinium in bone, and t is the time between GBCA administration and the XRF measurement. Half lives of 2, 3, 4, and 5 years were tested to determine whether time provided additional explanation to gadolinium bone concentrations. Both positive and negative Gd concentrations were corrected for half-life using equation (1).

2.5. Statistical analysis

A one-tailed t test was used to test gadolinium concentration in the exposed group against the control group. In the previous study measuring gadolinium in bone, both control and exposed groups were not found to deviate significantly from a normal distribution (Lord *et al* 2017a). Thus, normal statistics were used to test for differences in gadolinium concentration between the groups. One-tailed t tests were performed on arithmetic means, as well as inverse variance-weighted means, since inverse variance weighting the data accounts for individual measurement uncertainty and weights the mean towards the more precise measurement values (Chamberlain *et al* 2012). To test for any differences in gadolinium concentration between GBCA exposed groups, a one-tailed t test was performed on the self-reported symptomatic subjects against the asymptomatic subjects, as well as on the variance-weighted means.

A linear regression was performed for gadolinium bone measurements of 15 control subjects, four self-identified symptomatic exposed subjects, and nine non-symptomatic exposed subjects, to test for a possible relationship between gadolinium concentration in bone and cumulative GBCA dose. For all linear regression analyses in this study, Matlab software (MathWorks, Natick, Mass) was used to carry out a linear least-squares regression, the p-value of the slope was used to assess the significance of the regression, and an R^2 value was used to evaluate correlation. In our original pilot study, two individuals could not provide an estimated GBCA dose and were not included in the regression analysis (exposed subjects 9 and 11). Exposed subject 2 was excluded from the linear regression in the original pilot study due to lack of information regarding GBCA dose. Since publication, the individual was able to provide data on approximate doses for previous GBCA administrations and is

now included in the regression analysis. Linear regressions were tested for each half life correction of 2, 3, 4, and 5 years.

Gadolinium urine levels were compared between the four control, four self-reported symptomatic exposed, and four asymptomatic exposed subjects using a one-tailed t test on the groups. Some 24 h urine tests resulted in a non-detectable amount of gadolinium, which the Mayo Clinic defines as having urine levels less than 0.1 μg/24 h. For these individuals, their levels were set as 0.05 μg/24 h for the one-tailed t test. One-tailed t tests with variance weighting could not be carried out for urine analysis since measurement uncertainties were not reported by the Mayo Clinic.

Linear regression analysis was performed on urinary gadolinium data from the four control, four symptomatic exposed, and four non-symptomatic exposed subjects to test for a relationship between gadolinium levels in urine and cumulative GBCA dose. Lastly, linear regression was performed on gadolinium bone concentrations and urinary gadolinium levels to test for a possible relationship between the amount of gadolinium stored in bone and the amount excreted in urine.

3. Results

3.1. Gadolinium concentration in bone of control, symptomatic exposed, and non-symptomatic exposed groups

As shown in figure 1, the arithmetic mean of gadolinium concentration in the exposed group was calculated to be 1.66 ± 1.25 μg Gd g^{-1} bone mineral, which proves to be significantly higher than the arithmetic mean of the control group, -1.20 ± 0.85 μg Gd g^{-1} bone mineral ($p = 0.03$). The variance-weighted means for the exposed and control group were found to be 2.33 ± 0.59 and -0.97 ± 0.57 μg Gd g^{-1} bone mineral, respectively, resulting in a significant difference between concentrations in the two groups with greater confidence ($p = 0.000\,027$). A more detailed assessment within the exposed group showed a non-significant difference between the arithmetic means for the symptomatic and non-symptomatic subgroups ($p = 0.40$). However, a significant difference was found when performing a one-tailed t test on variance-weighted means of the symptomatic and non-symptomatic subgroups ($p = 0.0042$). All arithmetic and variance-weighted means are summarized in table 1.

3.2. Linear regression for gadolinium concentration in bone and cumulative GBCA dose

Linear regression of gadolinium concentration in bone and cumulative GBCA dose for the 15 control and 13 exposed subjects showed that bone gadolinium concentration increases by 0.042 ± 0.020 μg Gd g^{-1} bone mineral per 1 ml of GBCA administered ($p = 0.046$, $R^2 = 0.14$), with a y-intercept of -0.43 ± 0.83 μg Gd g^{-1} bone mineral (figure 2). A half life correction of 3 years for gadolinium in bone results in the highest correlation coefficient ($R^2 = 0.57$) compared to the other half life corrections of 2, 4, and 5 years ($R^2 = 0.52$, $R^2 = 0.53$, $R^2 = 0.46$, respectively). The linear regression of predicted gadolinium concentration in bone shortly after GBCA administration and cumulative GBCA dose, assuming a half life of 3 years, resulted in a positive slope, suggesting that gadolinium concentration in bone (at a short time after administration) increases by 0.49 ± 0.09 μg Gd g^{-1} bone mineral per 1 ml of GBCA administered ($p = 0.000\,0078$), with a y-intercept of -3.53 ± 3.49 μg Gd g^{-1} bone mineral (figure 3).

3.3. Gadolinium in urine of control, symptomatic exposed, and non-symptomatic exposed groups

Gadolinium levels in urine for the symptomatic exposed group were visibly higher compared to the non-symptomatic exposed and control group (figure 4). Mean urinary gadolinium levels for control, symptomatic exposed, and non-symptomatic exposed subjects were 0.05 ± 0.0, 0.45 ± 0.26, and 0.09 ± 0.07 μg/24 h, respectively. Urinary levels between control subjects and non-symptomatic exposed subjects were not significantly different ($p = 0.20$). Urinary gadolinium levels in both control and non-symptomatic exposed subjects were significantly lower than symptomatic exposed subjects ($p = 0.02$ and $p = 0.05$, respectively).

3.4. Linear regression for gadolinium in urine and cumulative GBCA dose

Linear regression analysis for urinary gadolinium levels and GBCA dose in 12 subjects (figure 5) resulted in a positive linear relationship of 0.0047 ± 0.0004 μg/24 h per 1 ml of GBCA administered ($R^2 = 0.91$, $p = 0.000\,000\,98$), with a y-intercept of 0.0158 ± 0.0635 μg/24 h.

3.5. Relationship between gadolinium in urine and gadolinium in bone

Gadolinium levels in urine and current bone gadolinium concentration had a non-significant relationship of 6.5 ± 5.9 μg/24 h per μg Gd g^{-1} bone mineral through a linear regression analysis ($R^2 = 0.11$, $p = 0.3$).

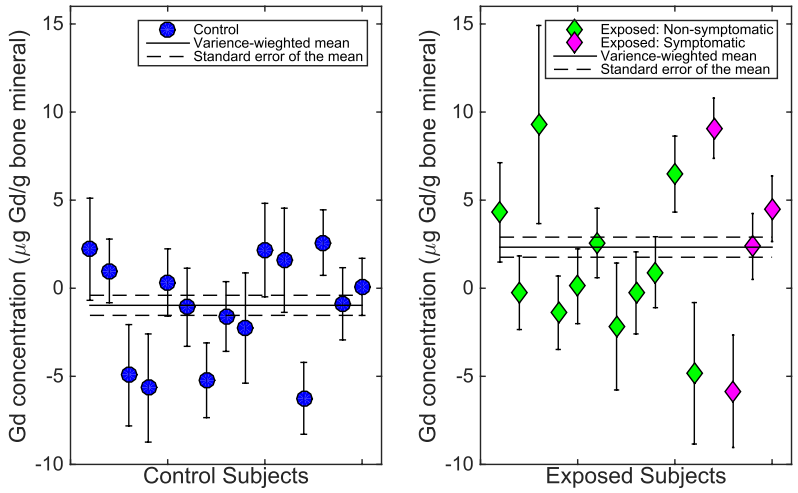

Figure 1. Gadolinium concentration in bone for control and exposed groups: 15 control subjects, 11 non-symptomatic exposed subjects, and four symptomatic exposed subjects. A one-tailed *t* test on the arithmetic means confirms gadolinium concentration in the exposed group is significantly higher than the control group ($p = 0.03$), with inverse variance weighting the data resulting in the same outcome with superior confidence ($p = 0.000027$). A one-tailed *t* test on the arithmetic means of gadolinium concentration for the symptomatic and non-symptomatic exposed subgroups showed an insignificant difference between groups ($p = 0.40$). Inverse variance weighting the data resulted in a significantly higher gadolinium concentration in symptomatic exposed subjects ($p = 0.0042$). Error bars represent individual Gd measurement uncertainties. The variance-weighted means for control and exposed groups are represented by a solid black line, with the corresponding standard error of the mean represented by a black dashed line.

Table 1. Summary of arithmetic and variance-weight means for control and exposed groups, as well as non-symptomatic and symptomatic exposed subgroups. *P*-values from one tailed *t* tests are included to show the significance between the control and exposed groups, as well as the non-symptomatic and symptomatic exposed subgroups.

	Control (μg Gd g^{-1} bone mineral)	Exposed (μg Gd g^{-1} bone mineral)	*p*-value
Arithmetic mean	-1.20 ± 0.85	1.66 ± 1.25	0.03
Variance-weighted mean	-0.97 ± 0.57	2.33 ± 0.59	0.000 027
	Exposed: non-symptomatic (μg Gd g^{-1} bone mineral)	Exposed: symptomatic (μg Gd g^{-1} bone mineral)	*p*-value
Arithmetic mean	1.34 ± 1.35	2.53 ± 4.42	0.40
Variance-weighted mean	1.19 ± 0.73	4.44 ± 0.99	0.0042

4. Discussion

4.1. Gadolinium in bone

Data in figure 1 visually display a difference in present day gadolinium bone concentration between control and exposed population groups, which was previously seen by Lord *et al* in the original pilot study with 11 control and 11 exposed subjects (Lord *et al* 2017a). The addition of four control and 4 symptomatic exposed subjects to the original study population distinguishes the difference in gadolinium concentrations between the exposed and control groups with greater confidence (from $p = .01$ to $p < 0.0001$ for a one-tailed *t* test using variance-weighted means). Additional data increases confidence in the reporting that gadolinium is retained in bone following exposure to GBCAs. There was no statistically significant difference when comparing bone gadolinium concentration between symptomatic and non-symptomatic subjects, based on a one-tailed *t* test ($p = 0.40$). However, when performing a one-tailed *t* test on variance-weighted means, bone gadolinium concentration in symptomatic exposed subjects was significantly higher than non-symptomatic exposed subjects ($p = 0.0042$). Our research group prefers to use variance-weighted means when comparing two populations since bone gadolinium measurements have variable measurement uncertainty that depends on factors such as leg shape, size, mass and subject motion. The use of variance-weighted means places more value on the more precise measurements taken during an experiment (Chamberlain *et al* 2012).

In the original pilot study, linear regression analysis of gadolinium concentration in bone and GBCA dose showed a significant positive correlation ($R^2 = 0.42, p = 0.01$). The addition of four control and four symptomatic exposed subjects to this study decreased the significance of the relationship between gadolinium concentration in bone and GBCA dose ($R^2 = 0.14, p = 0.046$). Applying a half life correction accounts for the varying

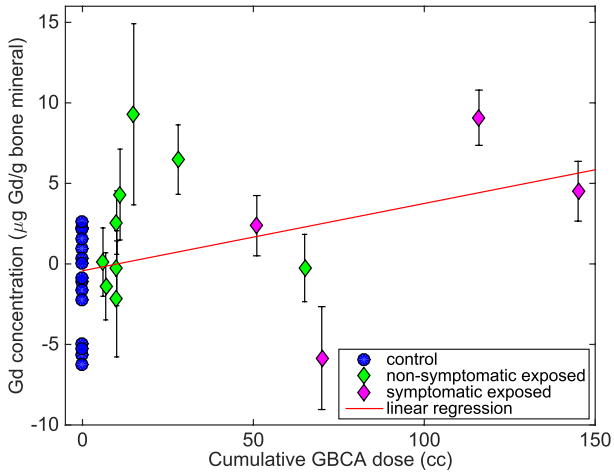

Figure 2. Gadolinium concentration in bone versus cumulative GBCA dose (various brands) for control and exposed groups: 15 control subjects, four symptomatic exposed subjects, and nine non-symptomatic exposed subjects. A positive relationship of $0.042 \pm 0.020\ \mu g\ Gd\ g^{-1}$ bone mineral per 1 ml of GBCA administered is shown ($p = 0.046$, $R^2 = 0.14$), with a y-intercept of $-0.43 \pm 0.83\ \mu g\ Gd\ g^{-1}$ bone mineral. Error bars represent the standard deviation of the calculated gadolinium concentration.

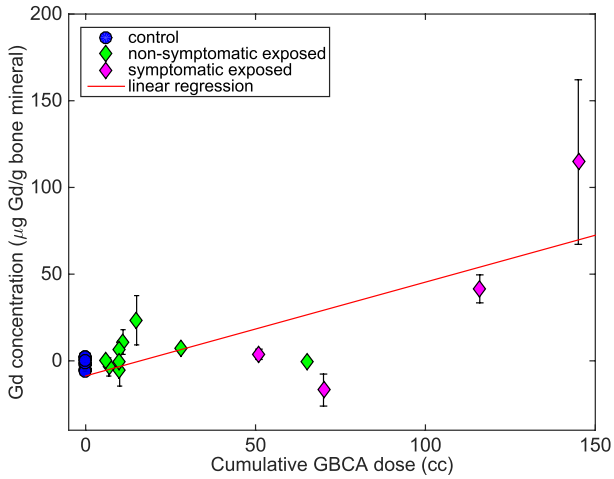

Figure 3. Linear regression analysis repeated for gadolinium concentration in bone shortly after GBCA administration versus cumulative GBCA dose for control and exposed groups, assuming a 3-year half life for gadolinium in bone. A positive relationship of $0.49 \pm 0.09\ \mu g\ Gd\ g^{-1}$ bone mineral per 1 ml of GBCA administered is shown ($p = 0.000\,0078$, $R^2 = 0.57$), with a y-intercept of $-3.53 \pm 3.49\ \mu g\ Gd\ g^{-1}$ bone mineral. Error bars represent the standard deviation of the calculated gadolinium concentration.

amount of time between the most recent GBCA administration and the XRF bone measurement between subjects. Time between bone Gd measurement and GBCA administration in this group of subjects varied from 5 to 15 years, whereas in the initially reported study the variability in time was significantly less. For example, one additional self-reported symptomatic exposed subject (number 12) had not received any contrast agent since 2002, and a substantial amount of gadolinium initially accumulated in the bone after receiving GBCA could have depleted during the time between administration and the XRF bone measurement. A half life correction of 3 years resulted in the strongest correlation between gadolinium concentration in bone and cumulative GBCA dose, increasing the correlation coefficient from $R^2 = 0.14$ to $R^2 = 0.57$, suggesting a relatively short half-life of a few years. While this correction gives a significant improvement in the regression analysis, it is only a first order correction. It may not be true that the same half life applies to each subject in this study, given the wide range of GBCAs used and the variation in age and sex of the participants. In addition, the improved significance in the regression analysis heavily relies on the two highest data points, one of which has the largest uncertainty. A half life of 3 years is a suggested starting point for further assessment of gadolinium in bone. This, however, deserves further study to see how bone gadolinium half life may drive urinary and blood levels.

All linear regression analyses performed in this study include control data to avoid any potential bias. However, the inclusion of 11 control data points with zero dose has the potential to give an uneven weight to the

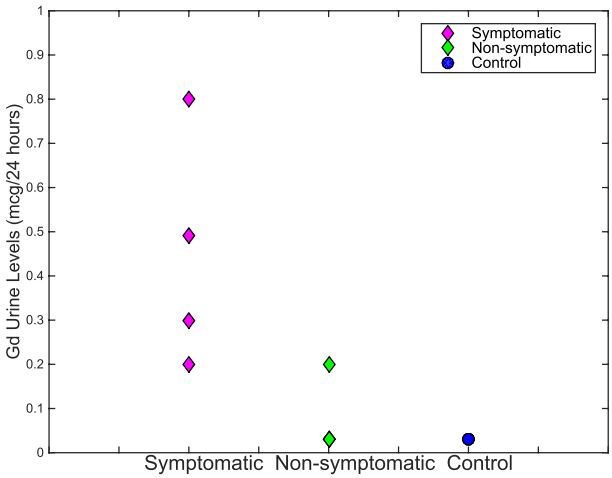

Figure 4. Gadolinium urine levels for control and exposed groups: four control subjects, four self-identified symptomatic exposed subjects, and four non-symptomatic exposed subjects; with mean gadolinium urine levels being 0.05, 0.45, and 0.09 μg/24 h, respectively. Urine levels for symptomatic exposed subjects are significantly higher than both control and non-symptomatic subjects ($p = 0.02$ and $p = 0.05$, respectively).

regression. For this reason, we repeated the linear regression analyses of gadolinium concentration in bone and GBCA dose, excluding the control data. Repeating the regression analysis for the relationship in figure 2 results in an insignificant relationship between gadolinium concentration in bone and GBCA dose ($p = 0.45$). Therefore, the addition of the control data to the regression analysis causes the significance of this relationship. However, repeating the regression analysis without control data for the relationship in figure 3 results in the relationship between gadolinium concentration in bone and GBCA dose with the 3-year half-life correction remaining highly significant ($p < 0.01$).

Due to limitations with our study samples groups (discussed below), further investigation with fewer variables is required to better understand the relationship between bone gadolinium, GBCA dose, and time since administration.

4.2. Gadolinium in urine

The symptomatic exposed group demonstrated the highest mean urinary gadolinium level, being significantly higher than both control and non-symptomatic exposed groups. This suggests either (a) there is a difference in gadolinium excretion between symptomatic and asymptomatic individuals, or (b) self-reported symptomatic individuals received a higher initial GBCA dose which has been retained in a long-term body compartment that does not appear to be bone. The only subjects to have detectable levels of gadolinium in their urine are those who have received multiple doses of GBCAs. Subjects who had only received a single dose of GBCA have an undetectable amount of gadolinium in their urine. A noteworthy discrepancy in this data is the range of time elapsed between the last GBCA administration and the date of urine collection in the subjects, which ranges from 1.5 to 14 years. The presence of gadolinium in urine is assumed to come from various long term storage sites in which gadolinium is distributed throughout the body.

The biodistribution of gadolinium in the body is complex, with little known about storage compartments in humans. Since the majority of administered GBCA is excreted within the first 24 h, the long term excretion of gadolinium in urine suggests long term storage sites in the body.

Over the past 5 years there has been a large focus on gadolinium retention in the brain, as multiple studies have detected gadolinium in the brain, either through high T1-weighted signal intensities or inductively coupled plasma mass spectrometry of autopsy samples (Errante *et al* 2014, Kanda *et al* 2014, 2015, 2016, McDonald *et al* 2015, Quattrocchi *et al* 2015, Radbruch *et al* 2015, Murata *et al* 2016). Robert *et al* compared long-term brain elimination kinetics after repeated injections of GBCAs, and found a large fraction of administered gadolinium retained in the brain after one year for linear GBCAs (Robert *et al* 2018). However, in a set of autopsy samples, Murata *et al* found gadolinium concentration in bone samples to be 23 times larger than gadolinium concentration in brain, suggesting that brain is not the main storage site for gadolinium in the body (Murata *et al* 2016).

As briefly mentioned in the introduction, bone is another organ in which gadolinium has been found to accumulate in higher concentrations (Gibby *et al* 2004, White *et al* 2006, Darrah *et al* 2009, Murata *et al* 2016). In our pilot study, which used XRF to measure gadolinium in bone, we were able to detect gadolinium up to 5 years following the administration of GBCA (Lord *et al* 2017a). In this study, we were able to detect gadolinium

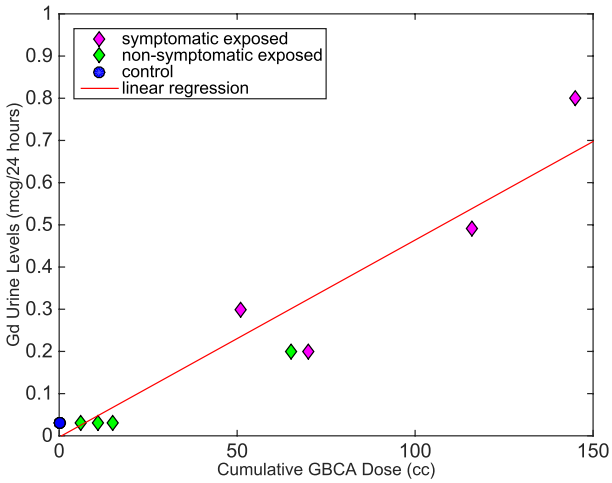

Figure 5. Gadolinium levels in urine versus cumulative GBCA dose (various brands) for control and exposed groups: four control subjects, four symptomatic exposed subjects, and four non-symptomatic exposed subjects. A positive relationship of 0.0047 ± 0.0004 μg/24 h per 1 ml of GBCA administered is shown ($R^2 = 0.91, p = 0.000\,000\,98$), with a y-intercept of 0.0158 ± 0.0635 μg/24 h.

in bone in an individual (exposed subject 12) who last received contrast 8 years prior to the XRF measurement, and an individual (exposed subject 15) who last received contrast 15 years prior to the XRF measurement, suggesting that the retention of gadolinium in bone is long-term. In addition to observation of long-term retention, gadolinium is one of the greatest competitive inhibitors for calcium ions (Ca^{2+}) and is therefore likely to replace calcium in bone (Sherry *et al* 2009).

Since (a) there is a correlation between gadolinium levels in urine and GBCA dose and (b) there is not a correlation between gadolinium in urine and current gadolinium in bone, there is an implication that bone is not the only significant long term storage site for Gd in the body. Other organs that have been reported to retain significant levels of gadolinium are the liver and kidneys (Tweedle *et al* 1995, Aime and Caravan 2009, Maximova *et al* 2016, Bussi *et al* 2018). However, there is limited information on gadolinium storage for these organs in the human body, as the majority of biodistribution studies have been carried out in animal populations. Therefore, the source of gadolinium in urine is complex, and a first order correction cannot be applied to account for the difference in time between GBCA administration and urine collection, as was previously done for gadolinium in bone.

The strong correlation between gadolinium levels in urine and cumulative GBCA dose in 12 subjects (four control, four symptomatic exposed, and four non-symptomatic exposed) indicates that gadolinium content in urine increases linearly as the total dose of GBCA increases. The regression analysis for the relationship between gadolinium levels in urine and GBCA dose was repeated excluding control data to investigate if multiple zero dose data points caused an uneven weight to the regression. Excluding control data from the linear regression did not cause a significant change in the relationship, as $p < 0.01$ with or without the control data.

4.3. Relationship between gadolinium in bone and gadolinium in urine

No apparent relationship was observed between current gadolinium levels in urine and current gadolinium concentration in bone. The fact that urine levels do not correlate with bone concentration could be a result of limitations from the study population, differing biokinetics and/or pharmacokinetics for each group, or the fact that there could be another major storage site for gadolinium other than bone. Further study is required to investigate the long term storage of gadolinium in the body.

4.4. Study limitations

This study has limitations due to both the XRF technology and the study population. As discussed in detail in the previously published pilot study, statistical limitations of the XRF system lead to a minimum detection limit, which is the minimum bone gadolinium concentration that can be detected with the XRF system. Our Cd-109 activation source is constantly decaying with a half-life of 461 d, resulting in larger concentrations of gadolinium in bone being undetectable, over time. Our original pilot study had a minimum detection limit of 2.3 μg Gd g^{-1} bone mineral for the original 11 control and 11 non-symptomatic exposed subjects, which increased to 2.6 μg Gd g^{-1} bone mineral for the additional four control and four symptomatic exposed subjects. Therefore, gadolinium concentrations less than 2.6 μg Gd g^{-1} bone mineral were not detected for the additional measurements completed in this study.

All statistical tests were carried out on a small population: 15 control, four self-reported symptomatic exposed, and 11 non-symptomatic exposed, for gadolinium in bone; four control, four self-reported symptomatic exposed, and four non-symptomatic exposed, for gadolinium in urine. In addition to a small study population, subjects are a mixed sample population having received various brands and doses of GBCA at different times. Some self-reported individuals reported the brand and date of administration for GBCA received, but did not have access to their dose. Since recommended clinical practise is to inject GBCAs on a per weight basis, we estimated dose from these patients based on their mass and recommended dose for the particular GBCA brand used. Obviously, this would assume there was no significant deviation in their weight from the time they were injected to the time we performed our measurements. For the symptomatic-exposed group, there may be a selection bias since the self-identified symptomatic individuals have self-reported themselves as having symptoms corresponding to having received GBCA and potentially may have used observation of Gd in urine in that self assessment. A large population with fewer variables with respect to GBCA brand, dose, and time of administration is required in future studies to draw any significant clinical conclusions about gadolinium retention.

5. Conclusion

In conclusion, additional *in vivo* XRF measurements of bone gadolinium, and urinary gadolinium measurements have been conducted for control, self-identified symptomatic exposed, and non-symptomatic exposed individuals. Although the group sample sizes were small, significant differences in gadolinium levels in bone and urine were observed between individuals who report symptoms of gadolinium toxicity and those who do not. Differences may be attributable to the initial GBCA dose. From these data, there seems to be no relationship between gadolinium in bone and gadolinium excreted in urine, suggesting that the retention of gadolinium in the body is complicated, involving multiple long-term storage sites. To truly understand gadolinium retention in the body, a large scale study with less variability in GBCA dose, brand, and time of administration, is required. We believe *in vivo* XRF measurements of gadolinium in bone, as well as urinary gadolinium measurements, have the potential to provide data to fill important knowledge gaps with respect to the clinical significance of gadolinium uptake and retention.

Acknowledgments

The Natural Science and Engineering Council of Canada is acknowledged for financial support in the development of the technology for this study.

ORCID iDs

Michelle L Lord https://orcid.org/0000-0002-7222-4826
James L Gräfe https://orcid.org/0000-0001-8309-0088
Michael D Noseworthy https://orcid.org/0000-0003-1464-159X

References

Aime S and Caravan P 2009 Biodistribution of gadolinium-based contrast agents, including gadolinium deposition *J. Magn. Reson. Imaging* **30** 1259–67

Altun E, Martin D R, Wertman R, Lugo-Somolinos A, Fuller E R III and Semelka R C 2009 Nephrogenic systemic fibrosis: change in incidence following a switch in gadolinium agents and adoption of a gadolinium policy: report from two U.S. universities *Radiology* **253** 689–96

Burke L M, Ramalho M, AlObaidy M, Chang E, Jay M and Semelka R C 2016 Self-reported gadolinium toxicity: a survey of patients with chronic symptoms *Magn. Reson. Imaging* **34** 1078–80

Bussi S, Coppo A, Botteron C, Fraimbault V, Fanizzi A, De Laurentiis E, Colombo Serra S, Kirchin M A, Tedoldi F and Maisano F 2018 Differences in gadolinium retention after repeated injections of macrocyclic MR contrast agents to rats *J. Magn. Reson. Imaging* **47** 746–52

Caravan P, Ellison J J, McMurry T J and Lauffer R B 1999 Gadolinium(III) chelates as MRI contrast agents: structure, dynamics, and applications *Chem. Rev.* **99** 2293–352

Carr D H *et al* 1984 Gadolinium-DTPA as a contrast agent in MRI: initial clinical experience in 20 patients *Am. J. Roentgenol.* **143** 215–24

Chamberlain M *et al* 2012 The feasibility of *in vivo* quantification of bone-fluorine in humans by delayed neutron activation analysis: a pilot study *Physiol. Meas.* **33** 243–57

Chettle D R 2005 Three decades of *in vivo* x-ray fluorescence of lead in bone *X-Ray Spectrom.* **34** 446–50

Darrah T H, Prutsman-Pfeiffer J J, Poreda R J, Ellen Campbell M, Hauschka P V and Hannigan R E 2009 Incorporation of excess gadolinium into human bone from medical contrast agents *Metallomics* **1** 479–88

Errante Y, Cirimele V, Mallio C A, Di Lazzaro V, Zobel B B and Quattrocchi C C 2014 Progressiveincrease of T1 signal intensity of the dentate nucleus on unenhanced magnetic resonance images is associated with cumulative doses of intravenously administered gadodiamide in patients with normal renal function, suggesting dechelation *Invest. Radiol.* **49** 685–90

Gibby W A, Gibby K A and Gibby W A 2004 Comparison of Gd DTPA-BMA (Omniscan) versus Gd HP-DO3A (ProHance) retention in human bone tissue by inductively coupled plasma atomic emission spectroscopy *Invest. Radiol.* **39** 138–42
Grobner T 2006 Gadolinium: a specific trigger for the development of nephrogenic fibrosing dermopathy and nephrogenic systemic fibrosis? *Nephrol. Dial. Transplant.* **21** 1104–8
Kanda T, Ishii K, Kawaguchi H, Kitajima K and Takenaka D 2014 High signal intensity in the dentate nucleus and globus pallidus on unenhanced T1-weighted MR images: relationship with increasing cumulative dose of a gadolinium-based contrast material *Radiology* **270** 834–41
Kanda T, Oba H, Toyoda K and Furui S 2016 Recent advances in understanding gadolinium retention in the brain *Am. J. Neuroradiol.* **37** E1–2
Kanda T *et al* 2015 Gadolinium-based contrast agent accumulates in the brain even in subjects without severe renal dysfunction: evaluation of autopsy brain specimens with inductively coupled plasma mass spectroscopy *Radiology* **276** 228–32
Kulaksız S and Bau M 2011 Anthropogenic gadolinium as a microcontaminant in tap water used as drinking water in urban areas and megacities *Appl. Geochem.* **26** 1877–85
Leung N, Pittelkow M R, Lee C U, Good J A, Hanley M M and Moyer T P 2009 Chelation of gadolinium with deferoxamine in a patient with nephrogenic systemic fibrosis *NDT Plus* **2** 309–11
Lord M L, Chettle D R, Gräfe J L, Noseworthy M D and McNeill F E 2017a Observed deposition of gadolinium in bone using a new noninvasive *in vivo* biomedical device: results of a small pilot feasibility study *Radiology* **287** 96–103
Lord M L, McNeill F E, Gräfe J L, Noseworthy M D and Chettle D R 2016 A phantom-based feasibility study for detection of gadolinium in bone *in vivo* using x-ray fluorescence *Appl. Radiat. Isot.* **112** 103–9
Lord M L *et al* 2017b Confirming improved detection of gadolinium in bone using *in vivo* XRF *Appl. Radiat. Isot.* **120** 111–8
Marckmann P *et al* 2006 Nephrogenic systemic fibrosis: suspected causative role of gadodiamide used for contrast-enhanced magnetic resonance imaging *J. Am. Soc. Nephrol.* **17** 2359–62
Maximova N, Gregori M, Zennaro F, Sonzogni A, Simeone R and Zanon D 2016 Hepatic gadolinium deposition and reversibility after contrast agent-enhanced MR imaging of pediatric hematopoietic stem cell transplant recipients *Radiology* **281** 418–26
McDonald R J *et al* 2015 Intracranial gadolinium deposition after contrast-enhanced MR imaging *Radiology* **275** 772–82
Murata N, Murata K, Gonzalez-Cuyar L F and Maravilla K R 2016 Gadolinium tissue deposition in brain and bone *J. Magn. Reson. Imaging* **34** 1359–65
Quattrocchi C C *et al* 2015 Gadodiamide and dentate nucleus T1 hyperintensity in patients with meningioma evaluated by multiple follow-up contrast-enhanced magnetic resonance examinations with no systemic interval therapy *Invest. Radiol.* **50** 470–2
Radbruch A, Weberling L D, Kieslich P J, Eidel O, Burth S, Kickingereder P, Heiland S, Wick W, Schlemmer H P and Bendszus M 2015 Gadolinium retention in the dentate nucleus and globus pallidus is dependent on the class of contrast agent *Radiology* **275** 783–91
Ramalho J, Ramalho M and Semelka R C 2016 Gadolinium deposition and toxicity: a global concern *Curr. Radiol. Rep.* **4** 59
Robert P *et al* 2018 One-year retention of gadolinium in the brain: comparison of gadodiamide and gadoterate meglumine in a rodent model *Radiology* **288** 424–33
Roberts D R *et al* 2016 High levels of gadolinium deposition in the skin of a patient with normal renal function *Invest. Radiol.* **51** 280–9
Semelka R C, Commander C W, Jay M, Burke L M and Ramalho M 2016a Presumed gadolinium toxicity in subjects with normal renal function: a report of 4 cases *Invest. Radiol.* **51** 661–5
Semelka R C, Ramalho M, AlObaidy M and Ramalho J 2016b Gadolinium in humans: a family of disorders *Am. J. Roentgenol.* **207** 229–33
Sherry A D, Caravan P and Lenkinski R E 2009 Primer on gadolinium chemistry *J. Magn. Reson. Imaging* **30** 1240–8
Thomsen H S, Morcos S K and Dawson P 2006 Is there a causal relation between the administration of gadolinium based contrast media and the development of nephrogenic systemic fibrosis (NSF)? *Clin. Radiol.* **61** 905–6
Tweedle M F, Wedeking P and Kumar K 1995 Biodistribution of radiolabeled, formulated gadopentetate, gadoteridol, gadoterate, and gadodiamide in mice and rats *Invest. Radiol.* **30** 372–80
Weinmann H J, Brasch R C, Press W R and Wesbey G E 1984 Characteristics of gadolinium-DTPA complex: a potential NMR contrast agent *Am. J. Roentgenol.* **142** 619–24
White G W, Gibby W A and Tweedle M F 2006 Comparison of Gd(DTPA-BMA) (Omniscan) versus Gd(HP-DO3A) (ProHance) relative to gadolinium retention in human bone tissue by inductively coupled plasma mass spectroscopy *Invest. Radiol.* **41** 272–8

Chapter 8

Conclusions and future outlook

In the work comprising this thesis, I have developed and applied an XRF-based detection system to detect Gd in bones of individuals who had previously received GBCAs. The thesis begins with studies which encompass the development of a feasible XRF system in Papers I, II & III. A series of phantom measurements and a cross-validation study on autopsy bones were carried out in Papers I & II, which deemed the XRF system feasible for human measurements. In preparation for *in vivo* measurements, the work completed in Paper III validated the technique of coherent normalization to correct for interpatient variability.

The last segment of this thesis work became more clinically oriented, as Papers IV & V summarized studies comprising human measurements. The first non-invasive *in vivo* measurements of Gd in bone were conducted using the XRF system in Paper IV. The results presented in this paper were both technical and clinical: the XRF system was shown to be capable of performing *in vivo* measurements of Gd in bone, and Gd concentrations in the group of individuals who had previously received GBCAs were significantly higher than the control group. The retention of Gd in bone was explored further in Paper V by investigating Gd in bone and urine of individuals self-reporting symptoms of Gd toxicity. Results from Paper V suggested that symptomatic individuals are storing and excreting more Gd compared to non-symptomatic individuals. In addition, the study raised the possibility of an additional storage site for Gd existing in the body since Gd levels in bone and urine were not correlated. While results

presented in Papers IV and V point to interesting suggestions regarding the clinical significance of Gd in bone, no clinical conclusions could be made due to the small population size of the studies.

This thesis work has begun to answer many of the burning questions around Gd toxicity. However, some of these questions remain unanswered and demand further attention, in part due to the limited size of the studies. Moreover, this work has uncovered further pieces of the puzzle that remain unsolved. The following section describes several avenues of future research worthy of exploring to improve the XRF detection system and resolve the open questions around Gd retention in the body.

8.1 Gadolinium retention in kidney and liver

The presented results in Paper V show no correlation between Gd concentrations in bone and urine, suggesting there are other Gd storage sites in the body contributing to the excretion of Gd in urine. Multiple animal-based biodistribution studies have reported the kidney and liver as organs retaining high levels of Gd [29, 34, 104–106]. Currently, there is little known about the retention of Gd in the kidney and liver in humans, making these two organs potential *in vivo* measurement locations for investigating Gd retention in the body.

8.1.1 Neutron activation analysis

As mentioned in section 1.1, Gd has the largest thermal neutron capture cross section of all the stable elements, meaning its nucleus has a high probability of absorbing a neutron. Therefore, Gd is an excellent candidate for detection using neutron activation analysis (NAA) - a measurement technique that has been used for *in vivo* trace element analysis for decades. NAA involves bombarding a sample with neutrons and measuring the resultant γ-ray emissions from neutron absorption and neutron inelastic scattering. The interaction that occurs between a neutron and target nucleus depends on the energy of the neutron and the structure of the nucleus.

Inelastic scattering involves the transfer of kinetic energy from the neutron to target nucleus upon collision. A fraction of the neutron energy is transferred to the nucleus, creating an excited nuclear state. The excited nucleus releases energy in the form of a γ-ray to return to a stable state. Neutron absorption involves the target nucleus absorbing the incident neutron, creating an isotope of A+1, where A is the atomic mass. The additional neutron causes the nucleus to be in an excited state, which then de-excites through a variety emissions such as photons, charged particles, or more neutrons. Neutron irradiation of naturally occurring isotopes Gd-155 and Gd-157 produce the excited states of Gd-156* and Gd-158* through neutron absorption, which then immediately de-excite through the emission of "prompt" γ-rays. Similar to the detection of Gd Kα x-rays in this thesis work, prompt γ-rays can be detected using a HPGe detector system, and can be used to identify any present Gd in a measured sample.

8.1.2 Source-based system

The *in vivo* detection of Gd retention in humans using prompt gamma neutron activation analysis (PGNAA) has been investigated previously as a PhD thesis in our research group at McMaster University [107], in which the technique of PGNAA and a source-based system were found to measure Gd in muscle *in vivo* successfully, following the administration of GBCA [7]. The source-based system used in this work consisted of a Pu-238/Be source producing a high energy spectrum of neutrons, a neutron shielding box, and a HPGe detector. Due to the high energy of the neutrons emitted from the Pu/Be source (up to 11 MeV), a considerable amount of neutron moderation was required to reduce the neutron kinetic energy in order for neutron absorption to occur. The feasibility of using this system for *in vivo* measurements was investigated through a series of phantom-based experiments, as well as Monte Carlo simulations. Minimum detection limits for a 2000 s (33.3 min) measurement time on the source-based system were found to be 2.33 ppm for the kidneys, and 0.74 ppm for the liver. In addition, a dosimetry study resulted in an effective dose of 74 μSv/hr for kidney measurements, and 48 μSv/hr for liver measurements [108]. Therefore, a 30-minute human measurement of the kidney or liver would result in effective doses

significantly less than a typical chest x-ray (100 μSv). The relatively low detection limits, as well as the low-risk measurement dose, make *in vivo* measurements using the previously developed source-based PGNAA system for Gd retention in liver and kidney a possible route of exploration for future work.

8.1.3 Accelerator-based system

While there is opportunity to carry out *in vivo* measurements of Gd in kidney and liver with the well-established source-based PGNAA system, an accelerator-based system may provide multiple advantages over the source-based system.

The "KN" accelerator system at McMaster University produces neutrons via the ^{7}Li(p,n) reaction with average energies orders of magnitude lower than the source-based system. Lower energy neutrons would result in a lower dose delivered to the measurement subject per neutron absorption event. Therefore, a higher neutron fluence could be applied by increasing the accelerator current, resulting in more prompt γ-rays from Gd to be detected [109]. Since only thermal neutrons contribute to absorption events, the elimination of fast neutrons is desired to decrease background in the acquired spectra. This can be accomplished on the "KN" accelerator system by pulsing the accelerator beam. Turning the beam on for 10 μs (i.e. the time for a fast neutron to be thermalized in human tissue), then counting the sample for 100 μs (i.e. the time for diffusion of thermal neutrons in human tissue) would allow for only thermal neutrons to be present during the counting period, eliminating background from fast neutrons [110].

8.2 Detector electronics

The results presented in Paper IV proved that the XRF system developed in this thesis work is capable of measuring Gd in bone in a small population. While this is promising for *in vivo* measurements of Gd in bone, the system is not yet capable of reporting Gd concentrations on an individual basis. For successful individual measurements to take place, the MDL would need to be lowered further, which would

require a higher input count rate (i.e. rate of radiation events detected) to detect more Gd Kα x-rays. However, as the input count rate increases, so does the system dead time, which will decrease the output count rate (i.e. rate of radiation events processed and recorded). Therefore, the input count rate and system dead time must be optimized to produce a maximum output count rate, and allow for more Gd Kα x-ray events to be recorded on spectra. Additionally, a higher output count rate allows for much shorter data collection times, which are desirable for human measurements.

A traditional preamplifier in a HPGe detector system uses RC feedback, which consists of a resistor and capacitor. The feedback capacitor (C_f) establishes the output voltage from the collected charge through the relationship:

$$V_0 = Q_{in}/C_f$$

where V_0 is output voltage, and Q_{in} is the charge collected on the feedback capacitor. The feedback resistor (R_f) discharges the feedback capacitor with a time constant of $\tau = C_f R_f$. As described in section 2.3.2, each output voltage pulse rides on the exponential decay of the previous pulse. With a high enough count rate, the preamplifier will saturate at the maximum allowable voltage, and no longer output pulses. The feedback resistor R_f and the time constant τ can be reduced to allow a higher count rate to be processed. However, this introduces noise and leads to poor resolution. In a transistor reset preamplifier (TRP), the feedback resistor is eliminated. The output of the preamplifier steps in a random staircase, with each step representing a separate pulse, until the maximum voltage is met and a transistor switch resets the preamplifier abruptly (Figure 8.1). Therefore, a TRP is a non-saturating preamplifier.

In February 2016, a newly purchased HPGe detector with a TRP was compared to a single element HPGe detector with an RC preamplifier by placing the Cd-109 source in front of the detectors and observing the resultant input count rates and dead times. Both detectors behaved similarly until the source was brought closer than 20 cm from the face of the detector. At this point, the RC preamplifier was found to

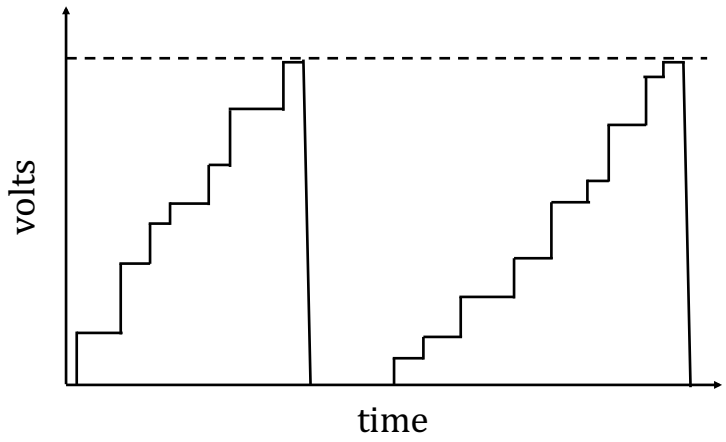

Figure 8.1: Output voltage pulses in a transistor reset preamplifier (TRP) represented by steps on a staircase. Once the maximum allowable voltage it met, a transistor switch resets the preamplifier.

saturate at an input count rate of 6.2×10^4 counts per second, where the TRP was able to handle a much higher rate of 1.0×10^5 counts per second, although with a high system dead time of approximately 75%. Overall, when used with the current DSA1000 pulse processing electronics, TRPs would not result in a significantly improved MDL for the XRF system. However, if paired with the appropriate pulse restoration electronics, TRPs have the potential to allow for a higher count rate to be processed, leading to a lower MDL.

8.2.1 Quantum Xspress3 digital pulse processing system

In December of 2016, a representative from Quantum Detectors visited our lab at McMaster University to test the Xspress3 digital pulse processing system on the HPGe detector with a TRP. Xspress3 is a digital readout system designed to maximize the output count rate of detectors by restoring pulses, rather than rejecting them.

Multiple spectra were acquired using the DSA1000 unit from Canberra, as well as the Xspress3 unit. Example spectra for both Xspress3 and DSA1000 are displayed in Figure 8.2, where it is apparent that the DSA1000 resolution (FWHM of the 88

keV coherent peak) is superior to the Xspress3 resolution. An output count rate of 2.2 $\times$ 10^4 was achieved with a dead time of 65% using the DSA1000 unit. The output count rate was increased and the system dead time was decreased by using the Xspress3 unit: an output count rate of 1.14 $\times$ 10^6 was achieved with a dead time of only 29%. A reasonable "figure of merit" for comparing the resolution and output count rates of the pulse processing systems, is $F = \sqrt{\text{FWHM/OCR}}$, where FWHM is the resolution, and OCR is the output count rate. The closer F is to zero, the better the performance of the pulse processing system. The lowest value of F (0.00167) was achieved by the Xspress3 system for an output count rate of 1.14 $\times$ 10^6 and dead time of 29%. This suggests that despite the poor resolution, the high output count rates of the Xspress3 unit should result in a lower MDL for the XRF system, and is a possible route of exploration for improving Gd bone measurements.

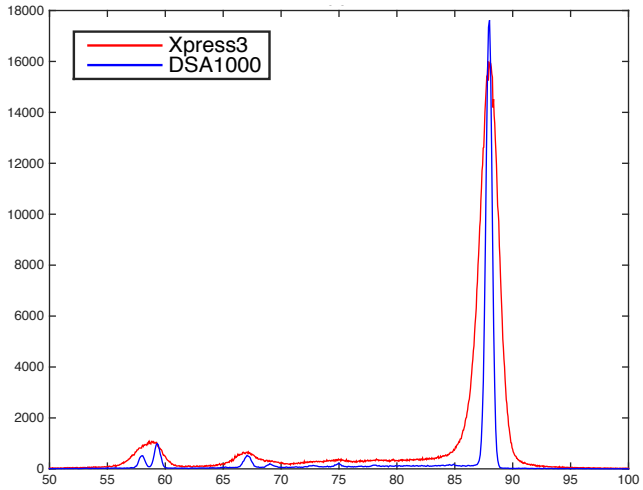

Figure 8.2: Spectra for the DSA1000 and Xspress3 pulse processing systems for an input count rate of approximately 1.0 $\times$ 10^5 counts per second.

8.2.2 XIA FalconX digital pulse processing system

In May of 2014, a representative from XIA visited McMaster University to perform a short series of experiments using the FalconX pulse pileup recognition and restoration system. The Cd-109 source was shone directly at one of the four cloverleaf detectors.

The resolution (FWHM) of the 88 keV coherent peak was observed for varying input count rates. The FalconX allowed high input count rates up to 914,000 counts per second with a maximum dead time of 12%. However, the resolution of the 88 keV peak using the FalconX ranged from 745 - 1127 eV, where the DSA1000 typically results in a resolution of approximately 500 eV. Similar to the Xspress3 system, the FalconX shows promise of reducing the MDL by allowing a higher count rate to be processed, but has worsened resolution compared to the DSA1000. Overall, the FalconX system should be retested with the HPGe transistor reset detector, for a direct comparison with the Xspress3 digital pulse processing system by Quantum.

8.3 Monte Carlo benchmarked model

Another possible extension of this thesis work would be the use of Monte Carlo simulations to investigate how various geometries and measurement setups would affect the MDL of the XRF system developed in this thesis work. Having an accurate benchmarked model of the XRF system would be useful for further optimization of the system. I have completed basic preliminary work for a benchmarked model using MCNP6, which was adapted from an existing MCNP6 model developed by Zaid Keldani for Paper III. The original MCNP model described in Paper III successfully simulated the experimental spectra for the purpose of testing the feasibility of coherent normalisation. However, the simulated spectra were not an exact match to the experimental spectra and needed some fine tuning before being used as a benchmarked model.

The first step in creating a benchmarked model for the XRF system for detecting Gd in bone is to match the the simulated spectra to the experimental. For an MCNP model, this is accomplished by defining the source accurately, as well as matching the detector efficiency and energy resolution.

8.3.1 Source definition

At the end of this thesis work, I began to create a benchmarked MCNP model of the XRF system by defining the Cd-109 source. In the original MCNP model used in Paper III, the source was defined as a 3 mm × 5 mm cylindrical gap within the collimator, with a point source situated near the back of the space. The source gap was resized to the correct dimensions of 3 mm × 3 mm and source details such as the W plug, Ti capsule, and active Cd-109 volume (as shown in Figure 2.4, Section 2.2.1) were added to the model. In addition to source details, the collimator material in the MCNP code was changed from W to Ag, since we are aiming at eliminating W and its resultant scatter behind the Gd Kα peaks. These small changes resulted in the simulated spectra matching the experimental spectra visually(Figure 8.3). Even though the spectra appear to match in Figure 8.3, the detector efficiency and energy resolution must be matched to complete this benchmarked MCNP model. These will be discussed briefly in the following subsection 8.3.2.

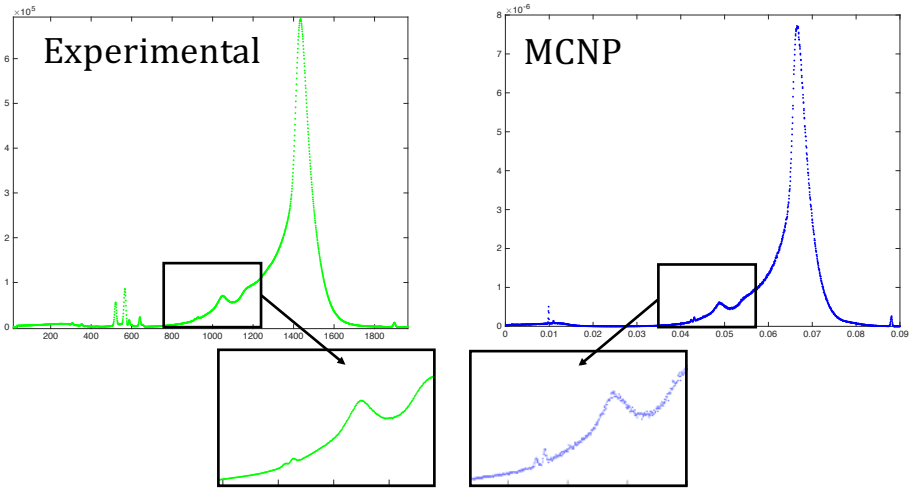

Figure 8.3: Experimental and simulated spectra for a 120 μg Gd/g PoP phantom. The general features of the spectra are matched, however the efficiency and resolution are not.

An additional aspect of source definition explored was eliminating W from the source to inspect how the background around the Gd Kα peaks would change visually. A spectrum without the presence of W was simulated by replacing the W plug

with a Ag plug (Figure 8.4). This produced a visual of how the background would be reduced, but did not tell us anything about how the MDL would improve. Multiple runs of the MCNP model should be completed for all phantom concentrations to calculate the MDL for a W-free source.

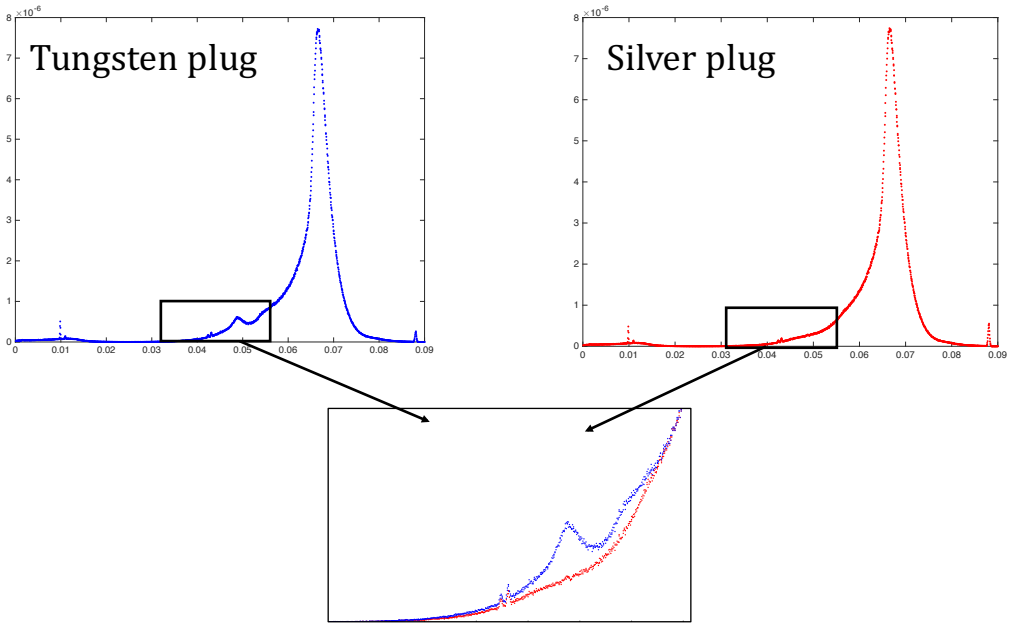

Figure 8.4: Simulated spectra for a source with and without W. The elimination of W visually reduces the background behind the Gd Kα peaks. However, further simulations must be run to determine the MDL using a source without W.

8.3.2 Future improvements to MCNP model

Detector efficiency

Detector efficiency is the probability of detection for a single radiation event. A complete MCNP model of the XRF system should be able to simulate the efficiency of the HPGe detector accurately. To compare simulated and experimental detector efficiencies, a series of γ sources with known activities can be shone at the detector. The peak efficiency can then be calculated by dividing the measured γ peak counting rate by the expected emission rate of the γ source. If simulation and experimental

detector efficiencies are significantly different, this suggests that the accuracy of the physical dimensions of the detector or the position of the detector is incorrect, and the detector dimensions in the MCNP model need to be re-evaluated [111].

Gaussian energy broadening

Currently, the energy resolution of the benchmarked MCNP model does not match the experimental energy resolution completely. This can be modified by using Gaussian Energy Broadening (GEB), which is a special treatment for tallies in MCNP where the tallied energy is broadened by sampling from a Gaussian. The FWHM of a Gaussian for a radiation detector can be described as:

$$\text{FWHM} = a + b(E + cE^2)^{1/2}$$

where E is energy, and a, b, and c are constants. The constants a, b, and c can be determined for the HPGe detector by performing a series of measurements with various γ sources to determine the FWHM over a range of energies. The constants are then entered in the GEB card of MCNP input file [112].

8.3.3 Proposed use for MCNP model

Once the detector efficiency and energy resolution of simulated spectra have been matched to experimental spectra, there are a number of proposed projects that the MCNP model can be used to carry out. The main goal of using the MCNP model, is to optimize the XRF system. Factors such as source-to-subject distance, excitation source energy, and detector size can be varied through Monte Carlo simulations to determine how the MDL would be affected. The technique of measuring both tibia bones simultaneously with two separate XRF systems could also be investigated as a potential measurement technique though this MCNP model. Overall, a benchmarked MCNP model of the XRF system for measuring Gd in bone would allow for numerous variations in measurement technique to be explored through simulation, rather than

experiment, which can be time consuming and costly.

8.4 Clinical studies

One of the main questions of concern with Gd retention is whether it causes any adverse affects in the human body. To answer this big question, multiple large-scale clinical studies would need to be carried out. While individuals who had previously received GBCAs were measured in Papers IV & V, study limitations did not allow us to make any clinical conclusions with respect to Gd retention and potential health effects.

8.4.1 Study limitations

The results presented in Paper IV formed the conclusion that the XRF detection system developed in this thesis work was successful in measuring Gd in bone in a small population. With this non-invasive technology, I showed that there is a significant difference in Gd bone concentration between groups of healthy exposed and control volunteers. However, the small population size, the lack of medical data on the measured volunteers, as well as the many uncontrolled variables such as GBCA brand and dose, did not allow us to make any significant clinical conclusions. Paper V reported additional Gd bone concentrations as well as Gd urine concentrations for healthy (i.e. non-symptomatic) exposed, symptomatic exposed, and control groups. The results presented in this paper showed that Gd bone and urine levels are significantly higher for a group of exposed individuals experiencing symptoms of Gd toxicity. This suggests that individuals exhibiting symptoms of Gd toxicity may be storing more Gd compared to individuals not exhibiting symptoms. Similar to Paper IV, due to the small study size and uncontrolled variables, these clinical conclusions could not be made. It was concluded that a large population study with fewer variables with respect to GBCA brand and dose are required to draw any significant clinical conclusions.

8.4.2 Routes of clinical investigation

Many questions remain about Gd retention in bone, and even more, the bigger picture of Gd retention in the body. The XRF technology developed in this thesis work could be used to investigate a number of these remaining questions. For example, a possible route of investigation is to look at the difference in Gd retention in bone between NSF patients and healthy individuals who have received similar doses and brands of GBCA. Another route of investigation is to compare Gd retention in bone between various doses and brands of GBCAs. Additionally, serial measurements in patients could give some insight as to how Gd retention in bone changes over time. The National Institutes of Health 2018 meeting on GBCAs concluded that the greatest priorities in GBCA research are to determine: (1) if GBCA retention adversely affects human tissue, (2) if retention is associated with clinical symptoms of Gd toxicity, and (3) if vulnerable populations are at greater risk of experiencing symptoms of Gd toxicity [20].

8.4.3 Potential future study

An example of a potential larger-scale study to look at the differences in Gd retention between 2 brands of GBCAs would involve 25 volunteers who have received a dose of "brand A" GBCA, and 25 volunteers who have received a dose of "brand B" GBCA. All volunteers would have not received any GBCAs prior to this study. The main purpose of this study would be to evaluate the retention of Gd in the body between brands A and B. The methods of evaluation would include: the XRF detection system to evaluate Gd concentration in bone, T1 MRI brain mapping to examine Gd retention in the brain, and Gd urine analysis to look at the excretion of Gd from the body. Volunteers would be recruited prior to their initial MRI scan, and the 3 methods of evaluation for Gd retention would be performed 1 month following the scan. A time period of 1 month was chosen to allow Gd to be incorporated into the bone, while allowing Gd to clear from short term storage sites such as muscle [107].

8.5 Conclusions

Gadolinium retention in the human body following the administration of GBCAs is currently a rapidly developing area of research, with new findings being released frequently. The extensive research conducted on Gd retention in the body over the past few years has raised serious concerns in the radiology community with respect to the safety of GBCAs. Radiologists are now faced with the tough decision of using these highly effective contrast agents and risking potential symptoms of toxicity, or not using these contrast agents and missing important diagnoses.

One of the biggest concerns regarding GBCA safety is the fact that some individuals are self-reporting symptoms similar to NSF, such as central torso pain, peripheral arm and leg pain, brain fog and skin thickening. The increasing number of reports of Gd toxicity following administration of GBCAs leads to the question of why certain individuals are experiencing symptoms, while some do not. Results presented in Paper V suggest that symptomatic individuals are storing more Gd in bone compared to non-symptomatic individuals. However, larger studies with more controlled variables must be carried out before clinical conclusions can be made. The question remains, if symptomatic individuals are in fact storing more Gd, then what causes those individuals to retain more Gd in the first place?

It is clear that we have only just started unravelling the mystery of Gd retention in the body, and the work carried out in this thesis has the potential to play an important role as this story unfolds. The developed XRF technology is able to perform non-invasive measurements of Gd in bone following the administration of GBCAs and should be exploited to address some of the remaining questions and fill the gaps in knowledge around Gd retention and GBCA safety.

Bibliography

[1] JH Hubbell. Photon cross sections, attenuation coefficients and energy absorption coefficients. *National Bureau of Standards Report NSRDS-NBS29, Washington DC*, 1969.

[2] William M Haynes. *CRC handbook of chemistry and physics*. CRC press, 2014.

[3] A Dean Sherry, Peter Caravan, and Robert E Lenkinski. Primer on gadolinium chemistry. *Journal of Magnetic Resonance Imaging: An Official Journal of the International Society for Magnetic Resonance in Medicine*, 30(6):1240–1248, 2009.

[4] MB Chadwick, M Herman, P Obložinskỳ, Michael E Dunn, Y Danon, AC Kahler, Donald L Smith, B Pritychenko, Goran Arbanas, R Arcilla, et al. Endf/b-vii. 1 nuclear data for science and technology: cross sections, covariances, fission product yields and decay data. *Nuclear data sheets*, 112(12):2887–2996, 2011.

[5] ME Bartolini, J Pekar, DR Chettle, F McNeill, A Scott, J Sykes, FS Prato, and GR Moran. An investigation of the toxicity of gadolinium based MRI contrast agents using neutron activation analysis. *Magnetic resonance imaging*, 21(5):541–544, 2003.

[6] JL Gräfe, FE McNeill, SH Byun, DR Chettle, and MD Noseworthy. The feasibility of in vivo detection of gadolinium by prompt gamma neutron activation

analysis following gadolinium-based contrast-enhanced MRI. *Applied Radiation and Isotopes*, 69(1):105–111, 2011.

[7] JL Gräfe, FE McNeill, MD Noseworthy, and DR Chettle. Gadolinium detection via in vivo prompt gamma neutron activation analysis following gadolinium-based contrast agent injection: a pilot study in 10 human participants. *Physiological measurement*, 35(9):1861, 2014.

[8] AR Spowart. Neutron radiography. *Journal of physics E: Scientific instruments*, 5(6):497, 1972.

[9] Hiroyuki Tokumitsu, Hideki Ichikawa, and Yoshinobu Fukumori. Chitosan-gadopentetic acid complex nanoparticles for gadolinium neutron-capture therapy of cancer: preparation by novel emulsion-droplet coalescence technique and characterization. *Pharmaceutical research*, 16(12):1830–1835, 1999.

[10] Zhaoda Zhang, Shrikumar A Nair, and Thomas J McMurry. Gadolinium meets medicinal chemistry: MRI contrast agent development. *Current medicinal chemistry*, 12(7):751–778, 2005.

[11] M Helena Mendonça-Dias, Elena Gaggelli, and Paul C Lauterbur. Paramagnetic contrast agents in nuclear magnetic resonance medical imaging. In *Seminars in nuclear medicine*, volume 13, pages 364–376. Elsevier, 1983.

[12] RC Brasch. Work in progress: methods of contrast enhancement for NMR imaging and potential applications. a subject review. *Radiology*, 147(3):781–788, 1983.

[13] Val M Runge, JA Clanton, CM Lukehart, CL Partain, and AE James Jr. Paramagnetic agents for contrast-enhanced NMR imaging: a review. *American journal of roentgenology*, 141(6):1209–1215, 1983.

[14] IR Young, GJ Clarke, DR Baffles, JM Pennock, FH Doyle, and GM Bydder. Enhancement of relaxation rate with paramagnetic contrast agents in NMR imaging. *Journal of Computed Tomography*, 5(6):543–547, 1981.

[15] Jacques Reuben. Gadolinium (III) as a paramagnetic probe for proton relaxation studies of biological macromolecules. binding to bovine serum albumin. *Biochemistry*, 10(15):2834–2838, 1971.

[16] Hanns-Joachim Weinmann, Robert C Brasch, Wolf-R Press, and George E Wesbey. Characteristics of gadolinium-DTPA complex: a potential NMR contrast agent. *American Journal of Roentgenology*, 142(3):619–624, 1984.

[17] Artur Palasz and Piotr Czekaj. Toxicological and cytophysiological aspects of lanthanides action. *Acta Biochimica Polonica*, 47(4):1107–1114, 2000.

[18] Seishiro Hirano and Kazuo T Suzuki. Exposure, metabolism, and toxicity of rare earths and related compounds. *Environmental health perspectives*, 104(Suppl 1):85, 1996.

[19] Vladimir Torchilin. Tumor delivery of macromolecular drugs based on the epr effect. *Advanced drug delivery reviews*, 63(3):131–135, 2011.

[20] Robert J McDonald, Deborah Levine, Jeffrey Weinreb, Emanuel Kanal, Matthew S Davenport, James H Ellis, Paula M Jacobs, Robert E Lenkinski, Kenneth R Maravilla, Martin R Prince, et al. Gadolinium retention: A research roadmap from the 2018 NIH/ACR/RSNA workshop on gadolinium chelates. *Radiology*, page 181151, 2018.

[21] DH Carr, J Brown, GM Bydder, RE Steiner, HJ Weinmann, U Speck, AS Hall, and IR Young. Gadolinium-DTPA as a contrast agent in MRI: initial clinical experience in 20 patients. *American Journal of Roentgenology*, 143(2):215–224, 1984.

[22] Michael D Noseworthy, Cameron Ackerley, Xuiling Qi, and Graham A Wright. Correlating subcellular contrast agent location from dynamic contrast-enhanced magnetic resonance imaging (dMRI) and analytical electron microscopy. *Academic radiology*, 9(2):S514–S518, 2002.

[23] James E Huckle, Ersan Altun, Michael Jay, and Richard C Semelka. Gadolinium deposition in humans: when did we learn that gadolinium was deposited in vivo? *Investigative radiology*, 51(4):236–240, 2016.

[24] Peter Caravan, Jeffrey J Ellison, Thomas J McMurry, and Randall B Lauffer. Gadolinium (III) chelates as MRI contrast agents: structure, dynamics, and applications. *Chemical reviews*, 99(9):2293–2352, 1999.

[25] Petr Hermann, Jan Kotek, Vojtěch Kubíček, and Ivan Lukeš. Gadolinium (III) complexes as MRI contrast agents: ligand design and properties of the complexes. *Dalton Transactions*, (23):3027–3047, 2008.

[26] Jean-Marc Idée, Marc Port, Caroline Robic, Christelle Medina, Monique Sabatou, and Claire Corot. Role of thermodynamic and kinetic parameters in gadolinium chelate stability. *Journal of Magnetic Resonance Imaging: An Official Journal of the International Society for Magnetic Resonance in Medicine*, 30(6):1249–1258, 2009.

[27] Andre S Merbach. *The chemistry of contrast agents in medical magnetic resonance imaging*. John Wiley & Sons, 2013.

[28] P Wedeking, K Kumar, and MF Tweedle. Dissociation of gadolinium chelates in mice: relationship to chemical characteristics. *Magnetic resonance imaging*, 10(4):641–648, 1992.

[29] Michael F Tweedle, Paul Wedeking, and Krishan Kumar. Biodistribution of radiolabeled, formulated gadopentetate, gadoteridol, gadoterate, and gadodiamide in mice and rats. *Investigative radiology*, 30(6):372–380, 1995.

[30] Claire Corot, Jean-Marc Idee, Anne-Marie Hentsch, Robin Santus, Catherine Mallet, Valérie Goulas, Bruno Bonnemain, and Dominique Meyer. Structure-activity relationship of macrocyclic and linear gadolinium chelates: Investigation of transmetallation effect on the zinc-dependent metallopeptidase angiotensin-converting enzyme. *Journal of Magnetic Resonance Imaging*, 8(3):695–702, 1998.

[31] N Rao Puttagunta, Wendell A Gibby, and Vijaya L Puttagunta. Comparative transmetallation kinetics and thermodynamic stability of gadolinium-DTPA bis-glucosamide and other magnetic resonance imaging contrast media. *Investigative radiology*, 31(10):619–624, 1996.

[32] Wendell A Gibby, Krissa A Gibby, and W Andrew Gibby. Comparison of Gd DTPA-BMA (Omniscan) versus Gd HP-DO3A (ProHance) retention in human bone tissue by inductively coupled plasma atomic emission spectroscopy. *Investigative radiology*, 39(3):138–142, 2004.

[33] Gregory W White, Wendell A Gibby, and Michael F Tweedle. Comparison of Gd (DTPA-BMA)(Omniscan) versus Gd (HP-DO3A)(ProHance) relative to gadolinium retention in human bone tissue by inductively coupled plasma mass spectroscopy. *Investigative radiology*, 41(3):272–278, 2006.

[34] Robert J McDonald, Jennifer S McDonald, Daying Dai, Dana Schroeder, Mark E Jentoft, David L Murray, Ramanathan Kadirvel, Laurence J Eckel, and David F Kallmes. Comparison of gadolinium concentrations within multiple rat organs after intravenous administration of linear versus macrocyclic gadolinium chelates. *Radiology*, 285(2):536–545, 2017.

[35] Nozomu Murata, Luis F Gonzalez-Cuyar, Kiyoko Murata, Corinne Fligner, Russell Dills, Daniel Hippe, and Kenneth R Maravilla. Macrocyclic and other non–group 1 gadolinium contrast agents deposit low levels of gadolinium in brain and bone tissue: preliminary results from 9 patients with normal renal function. *Investigative radiology*, 51(7):447–453, 2016.

[36] William P Cacheris, Steven C Quay, and Scott M Rocklage. The relationship between thermodynamics and the toxicity of gadolinium complexes. *Magnetic resonance imaging*, 8(4):467–481, 1990.

[37] Sophie Laurent, Luce Vander Elst, and Robert N Muller. Comparative study of the physicochemical properties of six clinical low molecular weight gadolinium contrast agents. *Contrast media & molecular imaging*, 1(3):128–137, 2006.

[38] SK Morcos. Extracellular gadolinium contrast agents: differences in stability. *European journal of radiology*, 66(2):175–179, 2008.

[39] Thomas Frenzel, Philipp Lengsfeld, Heiko Schirmer, Joachim Hütter, and Hanns-Joachim Weinmann. Stability of gadolinium-based magnetic resonance

imaging contrast agents in human serum at 37C. *Investigative radiology*, 43(12):817–828, 2008.

[40] Dapeng Hao, Tao Ai, Frank Goerner, Xuemei Hu, Val M Runge, and Michael Tweedle. MRI contrast agents: basic chemistry and safety. *Journal of Magnetic Resonance Imaging*, 36(5):1060–1071, 2012.

[41] JL Abraham, C Thakral, L Skov, K Rossen, and P Marckmann. Dermal inorganic gadolinium concentrations: evidence for in vivo transmetallation and long-term persistence in nephrogenic systemic fibrosis. *British journal of dermatology*, 158(2):273–280, 2008.

[42] Steven A Greenberg. Zinc transmetallation and gadolinium retention after MR imaging: case report. *Radiology*, 257(3):670–673, 2010.

[43] A Sonesson. On the complex chemistry of the tervalent rare earth ions. i. the acetate systems of lanthanum, cerium, neodymium, and gadolinium. *Acta Chemica Scandinavica (Denmark) Divided into Acta Chem. Scand., Ser. A and Ser. B*, 12, 1958.

[44] Marc Port, Jean-Marc Idée, Christelle Medina, Caroline Robic, Monique Sabatou, and Claire Corot. Efficiency, thermodynamic and kinetic stability of marketed gadolinium chelates and their possible clinical consequences: a critical review. *Biometals*, 21(4):469–490, 2008.

[45] Michael F Tweedle, Emanuel Kanal, and Robert Muller. Considerations in the selection of a new gadolinium-based contrast agent. *Appl Radiol*, 43(5 Suppl):1–11, 2014.

[46] Shawn E Cowper, Lyndon D Su, Jag Bhawan, Howard S Robin, and Philip E LeBoit. Nephrogenic fibrosing dermopathy. *The American journal of dermatopathology*, 23(5):383–393, 2001.

[47] Thomas Grobner. Gadolinium–a specific trigger for the development of nephrogenic fibrosing dermopathy and nephrogenic systemic fibrosis? *Nephrology Dialysis Transplantation*, 21(4):1104–1108, 2006.

[48] Peter Marckmann, Lone Skov, Kristian Rossen, Anders Dupont, Mette Brimnes Damholt, James Goya Heaf, and Henrik S Thomsen. Nephrogenic systemic fibrosis: suspected causative role of gadodiamide used for contrast-enhanced magnetic resonance imaging. *Journal of the American Society of Nephrology*, 17(9):2359–2362, 2006.

[49] HS Thomsen, SK Morcos, and P Dawson. Is there a causal relation between the administration of gadolinium based contrast media and the development of nephrogenic systemic fibrosis (nsf)? *Clinical radiology*, 61(11):905–906, 2006.

[50] Preben Joffe, Henrik S Thomsen, and Monika Meusel. Pharmacokinetics of gadodiamide injection in patients with severe renal insufficiency and patients undergoing hemodialysis or continuous ambulatory peritoneal dialysis. *Academic radiology*, 5(7):491–502, 1998.

[51] Whitney A High, Reed A Ayers, John Chandler, Gary Zito, and Shawn E Cowper. Gadolinium is detectable within the tissue of patients with nephrogenic systemic fibrosis. *Journal of the American Academy of Dermatology*, 56(1):21–26, 2007.

[52] Alan S Boyd, John A Zic, and Jerrold L Abraham. Gadolinium deposition in nephrogenic fibrosing dermopathy. *Journal of the American Academy of Dermatology*, 56(1):27–30, 2007.

[53] Ersan Altun, Diego R Martin, Rebecca Wertman, Aida Lugo-Somolinos, Edwin R Fuller 3rd, and Richard C Semelka. Nephrogenic systemic fibrosis: change in incidence following a switch in gadolinium agents and adoption of a gadolinium policyreport from two us universities. *Radiology*, 253(3):689–696, 2009.

[54] Tomonori Kanda, Kazunari Ishii, Hiroki Kawaguchi, Kazuhiro Kitajima, and Daisuke Takenaka. High signal intensity in the dentate nucleus and globus pallidus on unenhanced T1-weighted MR images: relationship with increasing cumulative dose of a gadolinium-based contrast material. *Radiology*, 270(3):834–841, 2013.

[55] Yuri Errante, Vincenzo Cirimele, Carlo Augusto Mallio, Vincenzo Di Lazzaro, Bruno Beomonte Zobel, and Carlo Cosimo Quattrocchi. Progressive increase of T1 signal intensity of the dentate nucleus on unenhanced magnetic resonance images is associated with cumulative doses of intravenously administered gadodiamide in patients with normal renal function, suggesting dechelation. *Investigative radiology*, 49(10):685–690, 2014.

[56] Carlo Cosimo Quattrocchi, Carlo Augusto Mallio, Yuri Errante, Vincenzo Cirimele, Luciano Carideo, Antonella Ax, and Bruno Beomonte Zobel. Gadodiamide and dentate nucleus T1 hyperintensity in patients with meningioma evaluated by multiple follow-up contrast-enhanced magnetic resonance examinations with no systemic interval therapy. *Investigative radiology*, 50(7):470–472, 2015.

[57] Robert J McDonald, Jennifer S McDonald, David F Kallmes, Mark E Jentoft, David L Murray, Kent R Thielen, Eric E Williamson, and Laurence J Eckel. Intracranial gadolinium deposition after contrast-enhanced MR imaging. *Radiology*, 275(3):772–782, 2015.

[58] Tomonori Kanda, Toshio Fukusato, Megumi Matsuda, Keiko Toyoda, Hiroshi Oba, Junichi Kotoku, Takahiro Haruyama, Kazuhiro Kitajima, and Shigeru Furui. Gadolinium-based contrast agent accumulates in the brain even in subjects without severe renal dysfunction: evaluation of autopsy brain specimens with inductively coupled plasma mass spectroscopy. *Radiology*, 276(1):228–232, 2015.

[59] Nozomu Murata, Kiyoko Murata, Luis F Gonzalez-Cuyar, and Kenneth R Maravilla. Gadolinium tissue deposition in brain and bone. *Magnetic resonance imaging*, 34(10):1359–1365, 2016.

[60] Soma Sanyal, Peter Marckmann, Susanne Scherer, and Jerrold L Abraham. Multiorgan gadolinium (gd) deposition and fibrosis in a patient with nephrogenic systemic fibrosisan autopsy-based review. *Nephrology Dialysis Transplantation*, 26(11):3616–3626, 2011.

[61] Charu Thakral, Jihad Alhariri, and Jerrold L Abraham. Long-term retention of gadolinium in tissues from nephrogenic systemic fibrosis patient after multiple gadolinium-enhanced MRI scans: case report and implications. *Contrast media & molecular imaging*, 2(4):199–205, 2007.

[62] Jerrold L Abraham and Charu Thakral. Tissue distribution and kinetics of gadolinium and nephrogenic systemic fibrosis. *European journal of radiology*, 66(2):200–207, 2008.

[63] Thomas H Darrah, Jennifer J Prutsman-Pfeiffer, Robert J Poreda, M Ellen Campbell, Peter V Hauschka, and Robyn E Hannigan. Incorporation of excess gadolinium into human bone from medical contrast agents. *Metallomics*, 1(6):479–488, 2009.

[64] Joana Ramalho, Miguel Ramalho, and Richard C Semelka. Gadolinium deposition and toxicity: A global concern. *Current Radiology Reports*, 4(11):59, 2016.

[65] Richard C Semelka, Miguel Ramalho, Mamdoh AlObaidy, and Joana Ramalho. Gadolinium in humans: A family of disorders. *American Journal of Roentgenology*, pages W1–W5, 2016.

[66] Richard C Semelka, Clayton W Commander, Michael Jay, Lauren MB Burke, and Miguel Ramalho. Presumed gadolinium toxicity in subjects with normal renal function: a report of 4 cases. *Investigative Radiology*, 51(10):661–665, 2016.

[67] Donna R Roberts, Scott M Lindhorst, Cynthia T Welsh, Kenneth R Maravilla, Mary N Herring, K Adam Braun, Bruce H Thiers, and W Clay Davis. High levels of gadolinium deposition in the skin of a patient with normal renal function. *Investigative radiology*, 51(5):280–289, 2016.

[68] Lauren MB Burke, Miguel Ramalho, Mamdoh AlObaidy, Emily Chang, Michael Jay, and Richard C Semelka. Self-reported gadolinium toxicity: A survey of patients with chronic symptoms. *Magnetic resonance imaging*, 34(8):1078–1080, 2016.

[69] Michael F L'Annunziata. *Radioactivity: introduction and history, from the quantum to quarks*. Elsevier, 2016.

[70] James E Turner. Atoms, radiation, and radiation protection. *Atoms, Radiation, and Radiation Protection, 2nd Edition, by James E. Turner, pp. 576. ISBN 0-471-59581-0. Wiley-VCH, April 1995.*, page 576, 1995.

[71] Claude Cohen-Tannoudji, Jacques Dupont-Roc, and Gilbert Grynberg. Atom-photon interactions: basic processes and applications. *Atom-Photon Interactions: Basic Processes and Applications, by Claude Cohen-Tannoudji, Jacques Dupont-Roc, Gilbert Grynberg, pp. 678. ISBN 0-471-29336-9. Wiley-VCH, March 1998.*, page 678, 1998.

[72] Glenn F Knoll. *Radiation detection and measurement*. John Wiley & Sons, 2010.

[73] Manne Siegbahn. Relations between the K and L series of the high-frequency spectra. *Nature*, 96(2416):676, 1916.

[74] Rene Van Grieken and Andrzej Markowicz. *Handbook of X-ray Spectrometry*. CRC press, 2001.

[75] Walter Bambynek, Bernd Crasemann, RW Fink, H-U Freund, Hans Mark, CD Swift, RE Price, and P Venugopala Rao. X-ray fluorescence yields, Auger, and Coster-Kronig transition probabilities. *Reviews of modern physics*, 44(4):716, 1972.

[76] Burkhard Beckhoff, Birgit Kanngießer, Norbert Langhoff, Reiner Wedell, and Helmut Wolff. *Handbook of practical X-ray fluorescence analysis*. Springer Science & Business Media, 2007.

[77] Joris Dik, Koen Janssens, Geert Van Der Snickt, Luuk van der Loeff, Karen Rickers, and Marine Cotte. Visualization of a lost painting by Vincent van Gogh using synchrotron radiation based x-ray fluorescence elemental mapping. *Analytical chemistry*, 80(16):6436–6442, 2008.

[78] C Shenberg and M Boazi. Rapid qualitative determination of main components in archeological samples by radioisotope-excited x-ray fluorescence analysis. *Journal of Radioanalytical Chemistry*, 27(2):457–463, 1975.

[79] D Papadopoulou, A Sakalis, N Merousis, and NC Tsirliganis. Study of decorated archeological ceramics by micro x-ray fluorescence spectroscopy. *Nuclear Instruments and Methods in Physics Research Section A: Accelerators, Spectrometers, Detectors and Associated Equipment*, 580(1):743–746, 2007.

[80] R Klockenämper, Alex von Bohlen, Luc Moens, and Wim Devos. Analytical characterization of artists' pigments used in old and modern paintings by total-reflection x-ray fluorescence. *Spectrochimica Acta Part B: Atomic Spectroscopy*, 48(2):239–246, 1993.

[81] Lillian J Somervaille, David R Chettle, and Malcolm C Scott. In vivo measurement of lead in bone using x-ray fluorescence. *Physics in Medicine & Biology*, 30(9):929, 1985.

[82] Lars Ahlgren and Soren Mattsson. Cadmium in man measured in vivo by x-ray fluorescence analysis. *Physics in Medicine & Biology*, 26(1):19, 1981.

[83] A Pejović-Milić, IM Stronach, J Gyorffy, CE Webber, and DR Chettle. Quantification of bone strontium levels in humans by in vivo x-ray fluorescence. *Medical physics*, 31(3):528–538, 2004.

[84] E Schönfeld and R Dersch. 109cd–comments on evaluation of decay data. *Table of Radionuclides–(Comments on evaluation), Bé et al.(Eds.), Monographie BIPM-5, BIPM, Seevres*, pages 167–173, 1996.

[85] Miles N Wernick and John N Aarsvold. *Emission tomography: the fundamentals of PET and SPECT*. Elsevier, 2004.

[86] Simon R Cherry, James A Sorenson, and Michael E Phelps. *Physics in nuclear medicine e-Book*. Elsevier Health Sciences, 2012.

[87] Doug Reilly, Norbert Ensslin, Hastings Smith Jr, and Sarah Kreiner. Passive nondestructive assay of nuclear materials. Technical report, Nuclear Regulatory

Commission, Washington, DC (United States). Office of Nuclear Regulatory Research; Los Alamos National Lab., NM (United States), 1991.

[88] Gopal B Saha. Scintillation and semiconductor detectors. In *Physics and Radiobiology of Nuclear Medicine*, pages 81–107. Springer, 2006.

[89] Gordon Gilmore. *Practical gamma-ray spectroscopy*. John Wiley & Sons, 2011.

[90] Ian Rittersdorf. Gamma ray spectroscopy. *Nuclear Engineering & Radiological Sciences*, pages 18–20, 2007.

[91] Rıdvan Durak and Yusuf Şahin. Measurement of k-shell fluorescence yields of selected elements from Cs to Pb using radioisotope x-ray fluorescence. *Physical Review A*, 57(4):2578, 1998.

[92] Eugene P Bertin. *Principles and practice of X-ray spectrometric analysis*. Springer Science & Business Media, 2012.

[93] S Fine and CF Hendee. X-ray critical-absorption and emission energies in kev. *Nucleonics (US) Ceased publication*, 13, 1955.

[94] Z Keldani, ML Lord, FE McNeill, DR Chettle, and JL Gräfe. Coherent normalization for in vivo measurements of gadolinium in bone. *Physiological measurement*, 38(10):1848, 2017.

[95] Huiling Nie, David Chettle, Liqiang Luo, and Joanne OMeara. Dosimetry study for a new in vivo x-ray fluorescence (XRF) bone lead measurement system. *Nuclear Instruments and Methods in Physics Research Section B: Beam Interactions with Materials and Atoms*, 263(1):225–230, 2007.

[96] William P Cawthorn and Erica L Scheller. Bone marrow adipose tissue: formation, function, and impact on health and disease. *Frontiers in endocrinology*, 8:112, 2017.

[97] R Bruce Martin, David B Burr, Neil A Sharkey, et al. *Skeletal tissue mechanics*, volume 190. Springer, 1998.

[98] Mir Sadat-Ali, Ezzat Elshaboury, Abdallah S Al-Omran, Md Quamar Azam, Anjum Syed, and Abid Hussain Gullenpet. Tibial cortical thickness: A dependable tool for assessing osteoporosis in the absence of dual energy x-ray absorptiopmetry. *International Journal of Applied and Basic Medical Research*, 5(1):21, 2015.

[99] AC Todd. Coherent scattering and matrix correction in bone-lead measurements. *Physics in Medicine & Biology*, 45(7):1953, 2000.

[100] AC Todd. Contamination of in vivo bone-lead measurements. *Physics in Medicine & Biology*, 45(1):229, 2000.

[101] Eric Da Silva, Brian Kirkham, Darrick V Heyd, and Ana Pejovic-Milic. Pure hydroxyapatite phantoms for the calibration of in vivo x-ray fluorescence systems of bone lead and strontium quantification. *Analytical chemistry*, 85(19):9189–9195, 2013.

[102] A Pejović-Milić, JA Brito, J Gyorffy, and DR Chettle. Ultrasound measurements of overlying soft tissue thickness at four skeletal sites suitable for in vivo x-ray fluorescence. *Medical physics*, 29(11):2687–2691, 2002.

[103] Philip R Bevington, D Keith Robinson, J Morris Blair, A John Mallinckrodt, and Susan McKay. Data reduction and error analysis for the physical sciences. *Computers in Physics*, 7(4):415–416, 1993.

[104] Silvio Aime and Peter Caravan. Biodistribution of gadolinium-based contrast agents, including gadolinium deposition. *Journal of Magnetic Resonance Imaging: An Official Journal of the International Society for Magnetic Resonance in Medicine*, 30(6):1259–1267, 2009.

[105] Natalia Maximova, Massimo Gregori, Floriana Zennaro, Aurelio Sonzogni, Roberto Simeone, and Davide Zanon. Hepatic gadolinium deposition and reversibility after contrast agent–enhanced MR imaging of pediatric hematopoietic stem cell transplant recipients. *Radiology*, 281(2):418–426, 2016.

[106] Simona Bussi, Alessandra Coppo, Catherine Botteron, Valérie Fraimbault, Antonello Fanizzi, Elisa De Laurentiis, Sonia Colombo Serra, Miles A Kirchin,

Fabio Tedoldi, and Federico Maisano. Differences in gadolinium retention after repeated injections of macrocyclic MR contrast agents to rats. *Journal of Magnetic Resonance Imaging*, 47(3):746–752, 2018.

[107] James L Gräfe. *In vivo detection of gadolinium by prompt gamma neutron activation analysis: An investigation of the potential toxicity of gadolinium-based contrast agents used in MRI*. PhD thesis, 2012.

[108] JL Gräfe, FE McNeill, DR Chettle, and SH Byun. Characteristic x ray emission in gadolinium following neutron capture as an improved method of in vivo measurement: A comparison between feasibility experiment and Monte–Carlo simulation. *Nuclear Instruments and Methods in Physics Research Section B: Beam Interactions with Materials and Atoms*, 281:21–25, 2012.

[109] W Matysiak, WV Prestwich, and SH Byun. Precise measurements of the thick target neutron yields of the 7Li (p, n) reaction. *Nuclear Instruments and Methods in Physics Research Section A: Accelerators, Spectrometers, Detectors and Associated Equipment*, 643(1):47–52, 2011.

[110] KV Ettinger, HC Biggin, NS Chen, DR Chettle, JH Fremlin, TC Harvey, WD Morgan, R Nowotny, BJ Thomas, and D Vartsky. In vivo neutron activation analysis of nitrogen using capture gamma rays. *Kerntechnik*, 17(2):89–92, 1975.

[111] RG Helmer, JC Hardy, VE Iacob, M Sanchez-Vega, RG Neilson, and J Nelson. The use of Monte Carlo calculations in the determination of a Ge detector efficiency curve. *Nuclear Instruments and Methods in Physics Research Section A: Accelerators, Spectrometers, Detectors and Associated Equipment*, 511(3):360–381, 2003.

[112] J Kenneth Shultis and Richard E Faw. An MCNP primer. Technical report, 2011.